PFC/RR-82-13 DOE/ET-51013-44

# STUDY OF RESISTIVE MHD INSTABILITIES IN ALCATOR C

Robert Seth Granetz

Plasma Fusion Center
Massachusetts Institute of Technology
Cambridge, MA 02139

April 1982

This work was supported by the U.S. Department of Energy Contract No. DE-AC02-78ET51013. Reproduction, translation, publication, use and disposal, in whole or in part by or for the United States government is permitted.

# STUDY OF RESISTIVE MHD INSTABILITIES IN ALCATOR C

by

ROBERT SETH GRANETZ

S.B., M.I.T.
(1977)
S.M., M.I.T.
(1977)

SUBMITTED TO THE DEPARTMENT OF
PHYSICS IN PARTIAL
FULFILLMENT OF THE
REQUIREMENTS FOR THE
DEGREE OF

DOCTOR OF SCIENCE IN PHYSICS

at the

MASSACHUSETTS INSTITUTE OF TECHNOLOGY

June 1982



Signature of Author Robert S. Granetz
Department of Physics
April 23, 1982

Certified by Peter H. Politzer
Dr. Peter Politzer
Thesis Supervisor

Accepted by G. F. Koster
Prof. G.F. Koster
Chairman, Graduate Committee

TABLE OF CONTENTS

# STUDY OF RESISTIVE MHD INSTABILITIES

# IN ALCATOR C

by

ROBERT SETH GRANETZ

Submitted to the Department of Physics
on April 23, 1982 in partial fulfillment of the
requirements for the Degree of Doctor of Science in
Physics

## ABSTRACT

An experimental study of MHD activity has been carried out on the Alcator C tokamak. A novel instrument, the $m$-spectrum analyzer, was designed to process signals from magnetic pickup coils and continuously yield the amplitudes of low mode number instabilities in real time. These measurements of magnetic fluctuations arising from resistive MHD modes reveal unexpected behavior in Alcator C. After the plasma current has risen to its steady state level, no significant MHD activity is observed unless the electron density is above a threshold value, $\overline{n}_c$. For a given toroidal field, $\overline{n}_c$ is remarkably repeatable. It is found that $\overline{n}_c$ is proportional to $B^2$ and independent of $I_p$. This threshold phenomenon plays a role in major disruptions; however, confinement time is not observed to be affected by MHD activity.

The resistive MHD theory of tearing modes explains the lack of instabilities at low densities, provided certain theoretical modifications are included in the elementary model. However, the threshold and high density phenomena cannot be accounted for. A subtle dependence of the current profile on plasma density is discussed, but this hypothesis is rejected.

The addition of a radial centripetal force due to an equilibrium rotation could qualitatively account for the observed phenomena, including the scaling of $\overline{n}_c$ with $B$. Recommendations for future work include further study of low- and high-density disruptions, a more complete quantitative analysis of the effects of equilibrium fluid flow on the tearing mode stability, and an experiment to measure plasma rotation.

Thesis Supervisor: Dr. Peter Politzer

Title: Principal Investigator

## I. INTRODUCTION

In recent years, theoretical and experimental studies of magnetically confined plasmas have generated a large body of information on a class of instabilities known collectively as resistive MHD modes. To understand why the attribute of resistivity is so important, it is helpful to review briefly the non-resistive case. Ideal magnetohydrodynamic (MHD) theory combines Maxwell's equations with a set of fluid equations to yield a mathematical model appropriate for describing a perfectly conducting fluid in a magnetic field[1]. Ideal MHD is therefore applicable to plasmas which are of interest in controlled thermonuclear research, where electron temperatures, $T_e$, are on the order of 1–10 keV. The classical resistivity, $\eta_{cl}$, of such plasmas[2] is in the range $10^{-7}$–$10^{-9}$ ohm-m, which makes them better conductors than copper. The ideal MHD model has two primary applications—the solution of the steady-state, equilibrium configuration of a plasma in a given magnetic field, and the solution of time-dependent phenomena, which yields possible instabilities in the equilibrium.

The stability criteria predicted by ideal MHD theory helped to define the required configurations of magnetic fields and currents in order for magnetic fusion experiments to be stable to these modes. Two illustrative examples are the "sausage mode"[3], which demonstrates the need for a strong magnetic field in current-carrying plasmas, and the "kink mode", from which is derived the Kruskal-Shafranov limit[4] on the safety factor, $q$ :

$$q(a) \simeq \frac{aB_t}{RB_\theta(a)} > 1 \tag{1}$$

This particular criterion has the effect of limiting the current a plasma can carry for a given toroidal field, $B_t$, and aspect ratio, $R/a$. In tokamaks, this limit translates into a desire for low aspect ratio (i.e. fat) configurations. These criteria, along with a few others, have necessarily been incorporated into the design of tokamaks so that the elementary ideal MHD modes remain benign. The theory also predicts the possibility of other types of modes, such as interchange modes, which can be important under certain circumstances. However, these do not appear to present problems in the current generation of machines.

Hence, given the parameters of present-day experiments, a tokamak plasma would be

completely stable if its dynamics were constrained to follow the ideal MHD model. But with so much kinetic and magnetic energy confined in a tokamak plasma, it is not surprising to expect that any non-ideal effects which relax some of the constraints will be important.

Resistivity is one such non-ideal effect—it is certainly not the only one. Even though a plasma is a very good conductor, as stated above, its conductivity is still finite. This removes the "frozen-in" constraint on the magnetic field lines which is a consequence of two of the ideal MHD equations:

$$E = -v \times B \qquad \text{(general Ohm's law)} \tag{2}$$

$$\nabla \times E = -\frac{\partial B}{\partial t} \qquad \text{(Faraday induction law)} \tag{3}$$

It is seen that in the frame of the plasma fluid, where $v = 0$, equation (2) implies that $E = 0$. Substituting this into equation (3) dictates that the magnetic field is constant in the frame of the fluid. In effect the field lines are frozen into the fluid. They may be compressed or bent, but they can never touch or cross. In addition, equation (2) stipulates that even in the lab frame there can be no electric fields parallel to the $B$-field lines—they are shorted out by the perfectly conducting plasma.

If a finite resistivity exists, equation (2) is modified slightly:

$$E = -v \times B + \eta J \tag{4}$$

It is simple to see that the above constraints on the plasma are relaxed. Magnetic flux surfaces can now join and/or tear apart. Electric fields aligned with the magnetic field lines are possible, and these $E$-fields can drive perturbed currents parallel to $B$. Therefore the existence of finite resistivity, even if it is very small, allows for the possibility of an additional class of MHD modes.

Whether or not such resistive modes are actually unstable depends upon the change in total energy which results from the perturbed currents and fields associated with these

modes. The first theoretical studies on resistive MHD modes were published by Furth, Killeen, and Rosenbluth in 1963[5]. Callen, Waddell, and others[6,7,8] calculated the perturbations in the equilibrium magnetic field and plasma current due to resistive tearing modes. In cylindrical geometry such modes are defined to have the form:

$$f(r)e^{i(m\theta - k_n z)} \tag{5}$$

where the geometry is as shown in Fig. 1 and $f(r)$ stands for any of the perturbed MHD quantities ($B, E, J, \rho, p, \psi$, etc). Since the cylindrical model is used as a straightened out approximation of a toroidal plasma, its length is usually taken to be $2\pi R$, where $R$ is the major radius of the tokamak. Thus $k_n = \frac{2\pi}{\lambda_n} = \frac{n}{R}$. The integers $m$ and $n$ are known as the poloidal and toroidal mode numbers respectively. Equation (5) describes perturbations which have a helical structure winding around the cylinder (or torus) a rational number of times. For given values of $m$ and $n$ the perturbed current will be exactly parallel to the equilibrium magnetic field lines at the radius where $q(r) = m/n$. The flux surface at this radius, $r_s$, is called the "mode rational surface" and the perturbation is said to be a resonant mode. When the perturbed magnetic fields due to a resonant instability are added to the equilibrium fields, the flux surfaces form "magnetic islands"[9] centered at the resonant surface (Fig. 2). Again it is pointed out that the growth of magnetic islands is not possible in ideal MHD theory, where the field lines must remain in simply nested flux surfaces.

The expected effects of magnetic islands on overall plasma behavior should be important. For example, energy transport should increase in the presence of islands. This is due to the fact that charged particles move along a $B$-field line many orders of magnitude faster than across field lines. Any regions of the plasma which are connected by magnetic field lines (i.e. flux surfaces) are essentially shorted together as far as their temperatures and densities are concerned. Without magnetic islands, thermal energy flowing radially outward must go across field lines, proceeding on a relatively slow collisional timescale. However, when there are magnetic islands present, the inner edge and outer edge of the islands are on the same flux surface, and the energy flow is effectively shunted across the width of the

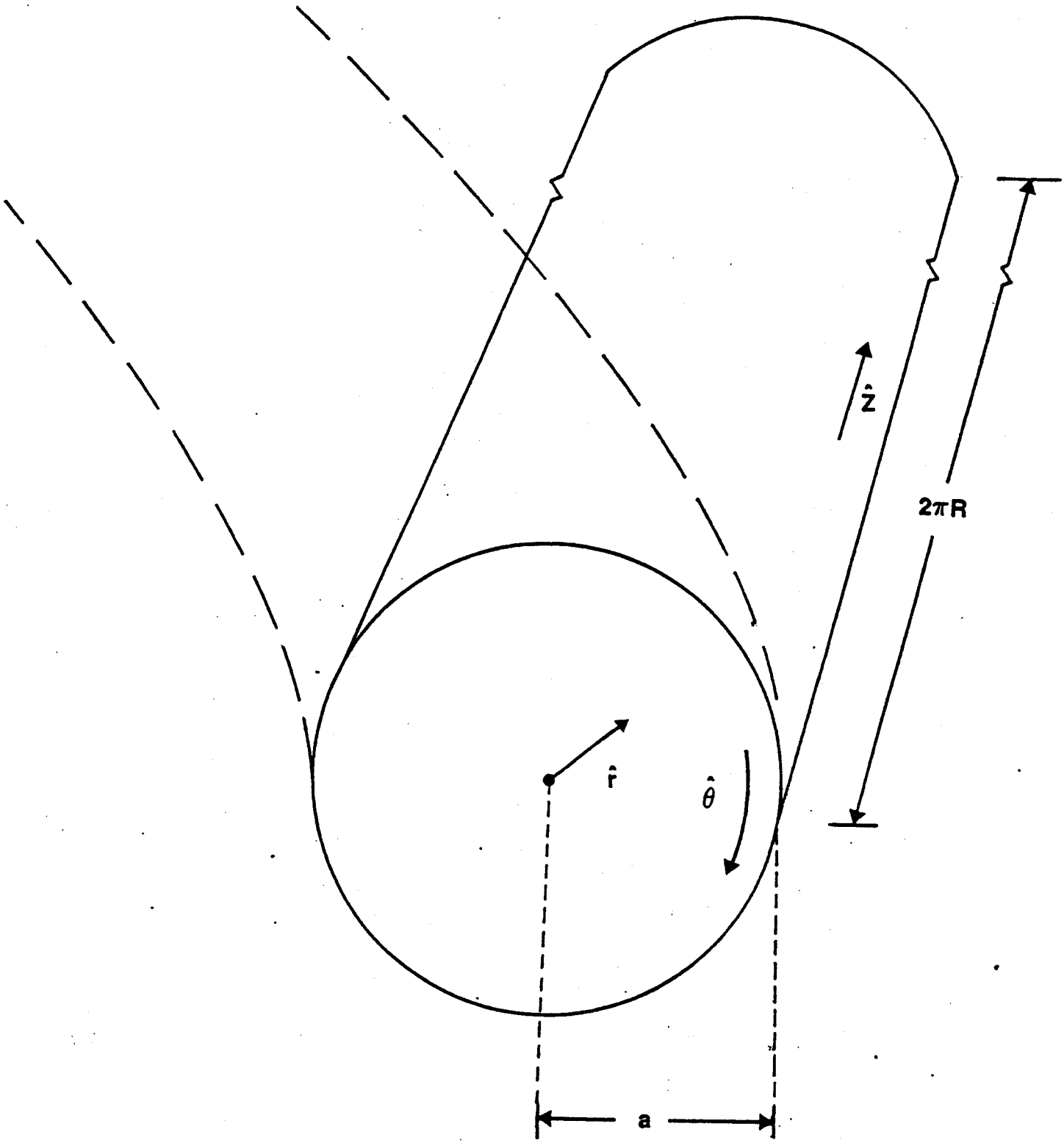


FIG. 1 — Cylindrical coordinate system used to model tokamak geometry.

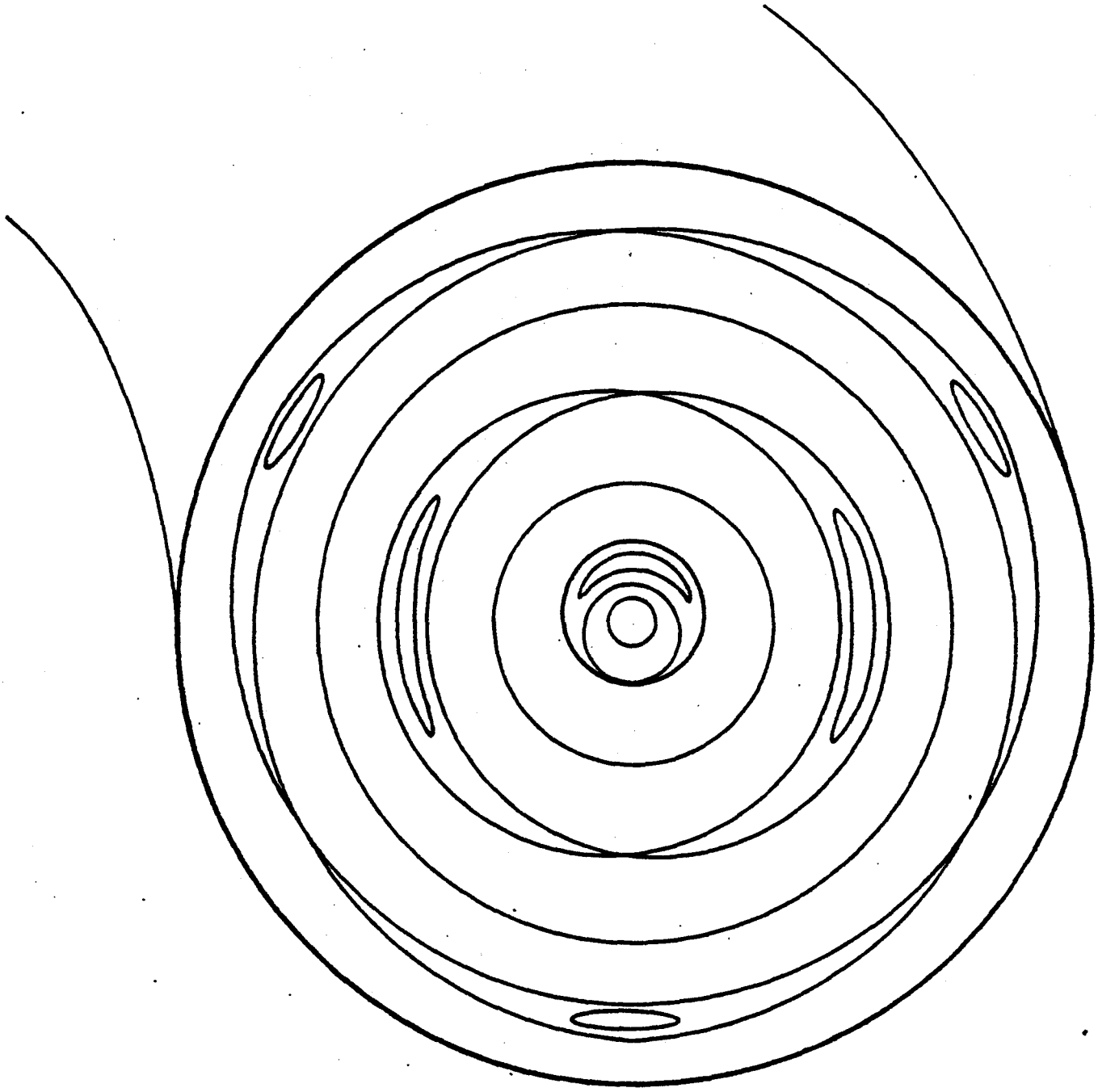

FIG. 2 — Flux surface contours showing $m = 1, 2$ and 3 "magnetic islands" which are theoretically possible in the resistive MHD model.

island. Therefore magnetic islands should decrease confinement times from this classical point of view.

Of course, the situation can get even worse if the magnetic island is very large or if the instability never saturates--most of the plasma volume would then not be confined. Even if these resistive instabilities did saturate at small island widths, poor confinement is still possible since there are an infinite number of $m$ and $n$ mode numbers. Thus islands might exist at many different radii, effectively covering the entire plasma cross-section and totally destroying confinement. A modification of this idea, namely the overlap of magnetic islands of different helicities, has been hypothesized by theorists[10,11,12] in recent years to explain the major disruption.

Substantial experimental evidence of resistive MHD instabilities in tokamaks has been accumulated during the past decade starting with the observations by Mirnov[13]. Using a set of magnetic pickup coils spaced around a poloidal circumference, Mirnov measured the spatial structure of magnetic field oscillations at the vacuum wall. He found that the modes had an apparent rotation which moved roughly at the ion diamagnetic velocity, $v_{Dia} = \frac{B \times \nabla p}{neB^2}$. The fluctuations had the approximate form $e^{im\theta}$, with small values of $m$, but the poloidal mode number decreased as the plasma discharge evolved. This is a consequence of the rising current and the accompanying decrease in the maximum value of $q$ within the plasma. For low $n$, the poloidal mode number, $m$, must decrease in order for an island to be resonant in the plasma.

Another type of diagnostic which has yielded considerable detail on resistive modes is the soft x-ray diode array. Von Goeler et al[14] first used this technique to look at the x-ray flux emitted predominately from the thermal bulk of the electron distribution. The diagnostic is therefore sensitive to changes in both electron temperature and density and also has a fairly high frequency response. Unlike magnetic loops, which can only detect effects external to the plasma, an array of x-ray diodes can image the interior and measurements of the radial structure of modes can be performed. The discovery of sawtoothing x-ray emission and $m = 1/n = 1$ precursor oscillations demonstrated the importance of

the resistive tearing instability even in the absence of a major disruption. The growth of $m = 1/n = 1$ magnetic islands limits the central value of $q$ that can be achieved:

$$\begin{aligned} q_o &= \lim_{r \to 0} \frac{rB_t}{RB_\theta(r)} \\ &= \frac{2B_t}{\mu_o R J_o} \\ &\simeq 1 \end{aligned} \tag{6}$$

thus limiting the central current density. Internal disruptions may also play a major role in the energy loss from the central region of a tokamak plasma.

Primarily using these two diagnostic tools, MHD activity associated with helical resistive instabilities has been studied on a large number of tokamaks. Although this work has been carried out under many different operating regimes and conditions, there are several common conclusions which can be drawn. What follows is a brief summary of the characteristics of MHD activity observed on several prominent tokamak experiments around the world. (One point which should be explained—throughout the thesis I will use the phrase "MHD activity" to denote $m \geq 2$ instabilities, which occur outside the $q = 1$ surface. This does not include the sawtooth behavior often going on in the central region of hot plasmas.)

Shortly after Mirnov's work on T-3 was disclosed, similar measurements on ST were begun at Princeton[15]. Even though this was an early tokamak, ST typically ran with a magnetic field of 34 kG and central electron temperatures and densities near 800 ev and $2 \times 10^{13}$ cm$^{-3}$ respectively. As the $q$-value at the limiter decreased during the current rise, a sequence of modes starting with $m = 6$ and going down to $m = 2$ was observed, with frequencies approximately equal to $\omega_{*e}$, the electron diamagnetic frequency. This is qualitatively similar to the T-3 findings except that the apparent rotation is in the opposite direction. This current rise activity is one of the common features found in all tokamaks—examples of data illustrating this behavior are shown in Fig. 3 (from Alcator A[16]). MHD activity in ST was found to vary considerably even for a fixed set of external parameters, with worse stability observed immediately after a vacuum break. As $q(a)$ was lowered to $\sim$3, a growing $m = 2$ mode was detected. As its amplitude increased, its frequency would

decrease and a disruption usually occurred when $\tilde{B}_\theta/B_\theta \approx 2\%$. It is not known whether these discharges were sawtoothing since soft x-ray detectors were not in use at the time.

An excellent comparison between experiment and elementary resistive MHD theory (which will be detailed in section II) was carried out at Oak Ridge using both Ormak and T-4 data on $\tilde{B}_\theta$ and $T_e(r)$ as a function of $q(a)$. Carreras et al[17] found good agreement with the theoretical predictions of $\tilde{B}_\theta/B_\theta$ at the vacuum wall in both machines. In addition, the experimental data from Ormak showed a strong correlation between the energy confinement time and the amplitude of $m = 2$ perturbations. As $q(a)$ was decreased from 6 to 4, $\tilde{B}_\theta/B_\theta$ increased dramatically while $\tau_E$ was cut in half. Similar agreement between experiment and theory was shown in detail for the JIPP T-II tokamak[18]. In that device, disruptions were apparently caused by either the overlap of an $m = 2/n = 1$ island with an $m = 3/n = 2$, or by just an $m = 2/n = 1$ contacting the limiter. Current profile control was claimed to be successful in reaching a low-$q$ operating regime.

More detailed measurements of the perturbed fields due to tearing modes were carried out in the TOSCA tokamak at Culham[19]. The relatively low temperatures in that device allowed for the insertion of magnetic probes directly into the discharge. For the $m = 3$ mode both $\tilde{B}_r(r)$ and $\tilde{B}_\theta(r)$ were measured over most of the plasma cross-section and found to be in excellent agreement with the radial eigenmode structure predicted by theory. Magnetic island widths were also as expected. Large $m = 3$ and $m = 2$ oscillations were seen on non-sawtoothing shots. These instabilities were greatly reduced or missing on sawtoothing discharges. Perturbations of several percent amplitude were observed prior to disruptions.

The same qualitative result was found in ISX-A[20], where shots which did not sawtooth had lots of MHD activity, poor confinement times and higher impurity levels as measured by $Z_{eff}$. On the other hand, sawtoothing discharges had very low MHD levels ($\tilde{B}_\theta/B_\theta < 0.1\%$), good confinement, low $Z_{eff}$, and higher maximum densities. Pushing the density up usually forced a marginal shot to begin sawtoothing and in that sense, high densities resulted in more stable plasmas.

Soft x-ray imaging arrays are the predominant source of MHD information for both

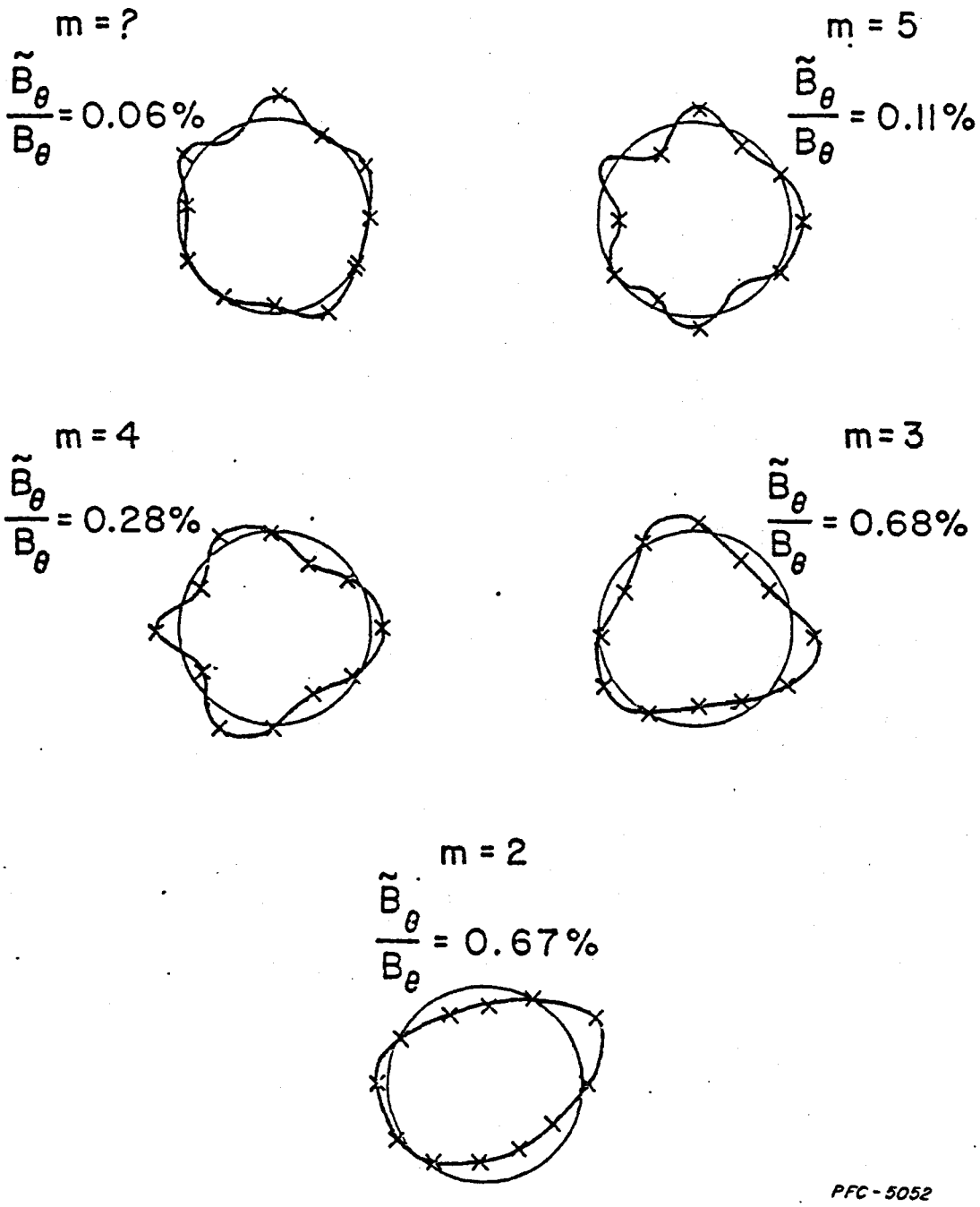


FIG. 3 — Example of magnetic activity measured with Mirnov coils. Note the general decrease in mode number during the current rise. (Reprinted from ref. [16].)

PLT[21] and Doublet-III[22]. Both machines find similar characteristics in their tearing mode activity—non-existent fluctuations during sawtoothing plasmas and large oscillations occurring in dirtier, non-sawtoothing cases. In the latter, Doublet has documented large concentrations of nickel in the center, with large $m = 1/n = 1$ and $q(0)$ remaining greater than unity. Both machines also occasionally see disruptions without any precursors, however, this could perhaps be explained by non-rotating islands. The temperatures and/or inferred current profiles have not been analyzed with the resistive theory. No dependence of MHD activity is observed on the density, as long as the shot is sawtoothing.

The strong relationship with sawtoothing is also clearly seen in the TEXT tokamak[23], which undergoes a "transition period" after the current rise phase. In this portion of the shot, the x-rays are not sawtoothing and large $m = 2$ and 3 modes are detected ($0.1\% \leq \tilde{B}_\theta/B_\theta \leq 1\%$). The discharge then enters a "quiescent period" when sawteeth begin and MHD activity decreases into the noise.

Finally, neutral beam heating has been found to drastically alter MHD behavior on machines such as PDX[24]. These findings will not be discussed here since Alcator C had no auxiliary heating at the time of this thesis study.

Several common features are apparent among the tokamak experimental results discussed here. Non-sawtoothing plasmas tend to have lots of MHD activity and high $Z_{eff}$, while just the opposite is true for sawtoothing shots. Large $m = 2$ and/or $m = 3$ perturbations often (but not always) precede disruptions. Detailed comparison with theory has been carried out with some data, but not for sawtoothing discharges to check the stability criteria. A careful scaling of MHD activity with density, magnetic field, and current independently has not been well-documented in any of these experiments.

If the growth of magnetic islands to large sizes is truly the cause of disruptions, then serious thought should be given to possible stabilization schemes. The theory of resistive tearing modes is presented in the next section, and the factors determining stability will be described there. *If* the theories are correct, it might be possible to prevent the growth of islands to macroscopic size with plausible feedback techniques, thereby preventing the

major disruption.

## II. BASIC TIIEORY OF RESISTIVE TEARING MODES

In this chapter, a physical picture of the tearing mode will be given, as well as a derivation of the stability criteria, growth rates, tearing layer width, and saturated island widths. The elementary theory will be explained first, and then modifications due to non-ideal and other effects will be described. In addition, the theory will be applied to the Alcator C experiment.

The complete set of ideal MHD equations with finite resistivity included (in MKS units) is:

$$\nabla \cdot B = 0 \tag{7}$$

$$\nabla \times E = -\frac{\partial B}{\partial t} \tag{8}$$

$$\nabla \times B = \mu_o J \tag{9}$$

$$E = -v \times B + \eta J \tag{10}$$

$$\rho \frac{dv}{dt} = J \times B - \nabla p \tag{11}$$

$$\frac{d}{dt}\left(\frac{p}{\rho^\Gamma}\right) = 0 \tag{12}$$

$$\frac{d\rho}{dt} + \rho \nabla \cdot v = 0 \tag{13}$$

where $\frac{d}{dt} = \frac{\partial}{\partial t} + v \cdot \nabla$ is the convective derivative, and $\Gamma$ is the ratio of specific heats. The toroidal plasma will be modelled as a straight cylinder, although for the typical aspect ratios of actual tokamaks, this is not a satisfactory approximation for the $m = 1$ mode. First-order effects of toroidicity on tearing modes have been examined numerically[25,26] and the results, which are significant even for $m \geq 2$, will be explained later in this section. Additional approximations are that:

$$B_z(r,t) = B_{z_o} \qquad \text{(i.e. constant)} \tag{14}$$

$$\text{and} \qquad \nabla \cdot v = 0 \tag{15}$$

## II.1 A physical picture

Perturbations in $p$, $\rho$, and $\eta$ will be ignored, so equations (12) and (13) will not be used. The fundamental physical processes involved in island formation are shown in Fig. 4. Start by setting up a radial magnetic field perturbation of the form:

$$\tilde{B}_r(r,t) = \tilde{B}_r(r)e^{i(m\theta - kz)} \tag{16}$$

near the surface $r_s$, where $q(r_s) = m/n$. The poloidal field lines now experience a radial undulation. Those lines close enough to $r_s$ are pulled completely through the singular surface to form the magnetic island structure. If $\tilde{B}_r$ is to grow in time, equation (8) requires there to be an electric field in the parallel direction. In ideal MHD this would be impossible and the mode would remain infinitesimal (i.e. non-existent). But with finite resistivity the $E$-field is permitted and a perturbed current, $\tilde{J}_{||}$, flows along the field lines. As the magnetic island expands radially, the plasma fluid flows with it and forms vortex-type flow patterns. According to equation (11), the perturbed current, $\tilde{J}$, crossed with the equilibrium field can cause the fluid flow to accelerate. This would increase $\tilde{E}_{||}$ by equation (10), driving more $\tilde{J}_{||}$ and the whole process would accelerate—growing exponentially until the fields reach a minimum energy state or until the basic underlying physics changes.

It is important to note that resistivity and $\tilde{J}_{||}$ *are only needed in a thin layer* at $r = r_s$ in order to weld together and tear apart magnetic flux surfaces. Outside of this layer the ideal MHD equations are still assumed to be valid. Resistive MHD can be looked at as a boundary layer problem, where the external ideal solutions must be joined to the complicated solution in the tearing layer. Therefore the exact form of the resistivity isn't critical. (In fact, other non-ideal effects can take the place of resistivity.)

## II.2 Heuristic derivation of the growth rate and tearing layer width

The growth rate of the tearing instability is governed by how fast the resistive diffusion process can tear apart magnetic surfaces within the boundary layer. Since the tearing layer is assumed to be very thin, the physical processes during the initial island growth can be

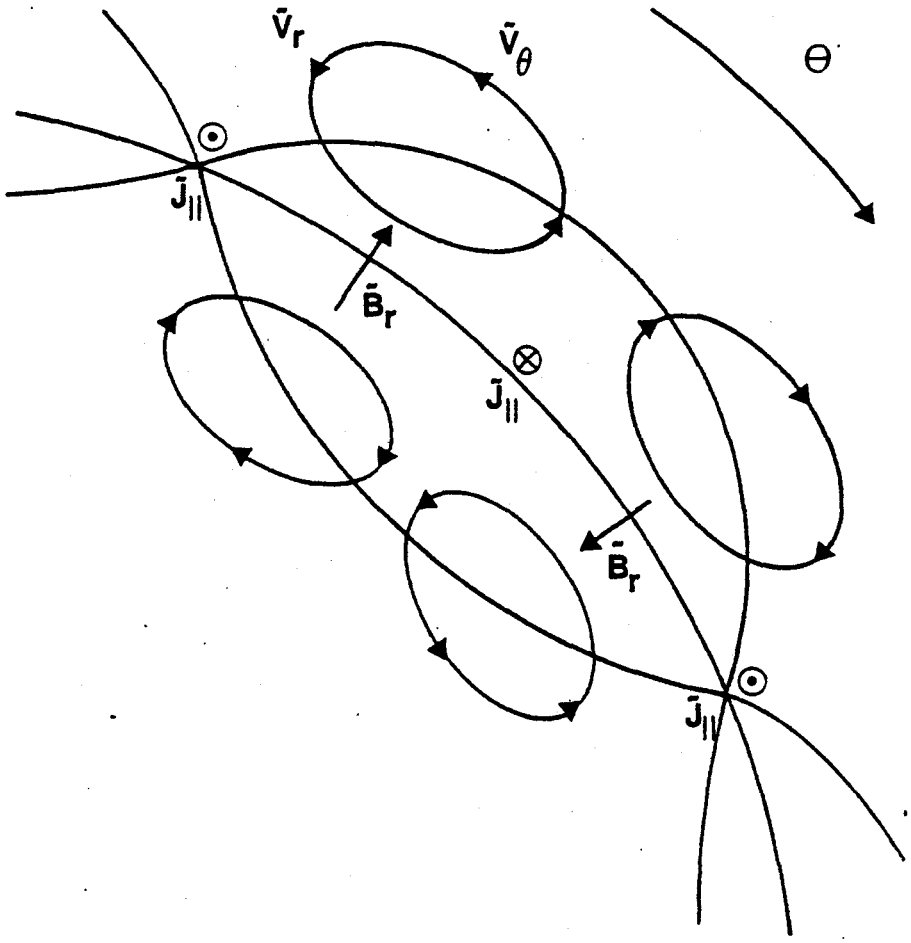


FIG. 4 — Schematic diagram showing the perturbations produced by the resistive tearing mode, and the processes leading to magnetic island formation.

calculated in slab geometry (except for $m = 1$, which involves macroscopic displacement of the plasma center) and then matched to an external ideal solution of any type geometry. Figure 5 shows the coordinate system that will be used here. The $\hat{x}$-direction corresponds to the $\hat{r}$-direction in a cylinder and $\hat{y}$ maps to $\hat{\theta}$.

Assume an equilibrium magnetic field with shear:

$$B_o = B_{y_o}(x)\hat{y} + B_{z_o}\hat{z} \tag{17}$$

Expand the MHD quantities $E$, $B$, $J$, and $v$ into an equilibrium component and a perturbed component. For example:

$$\begin{aligned} B(x,t) &= B_o(x) + \tilde{B}(x)e^{i(k_o x)+\gamma t} \\ &= B_o(x) + \tilde{B}(x)e^{i(k_y y + k_z z)+\gamma t} \end{aligned} \tag{18}$$

For simplicity, set the equilibrium velocity, $v_o = 0$. Plug equation (10) for $E$ into equation (8) to get:

$$\begin{aligned} \frac{\partial B}{\partial t} &= -\nabla \times E = -\nabla \times [-v \times B + \eta J] \\ &= \nabla \times (v \times B) - \frac{\eta}{\mu_o}\nabla \times (\nabla \times B) \\ &= (B \cdot \nabla)v - (v \cdot \nabla)B + \frac{\eta}{\mu_o}\nabla^2 B \end{aligned} \tag{19}$$

Now substitute in the MHD quantities in the form of equation (18) into equation (19) and solve for the first-order perturbed quantities:

$$\frac{\partial \tilde{B}}{\partial t} = (B_o \cdot \nabla)\tilde{v} - (\tilde{v} \cdot \nabla)B_o + \frac{\eta}{\mu_o}\nabla^2 \tilde{B} \tag{20}$$

Single out the $\hat{x}$-component:

$$\frac{\partial \tilde{B}_x}{\partial t} = B_{y_o}\frac{\partial \tilde{v}_x}{\partial y} + B_{z_o}\frac{\partial \tilde{v}_x}{\partial z} + \frac{\eta}{\mu_o}\nabla^2 \tilde{B}_x \tag{21}$$

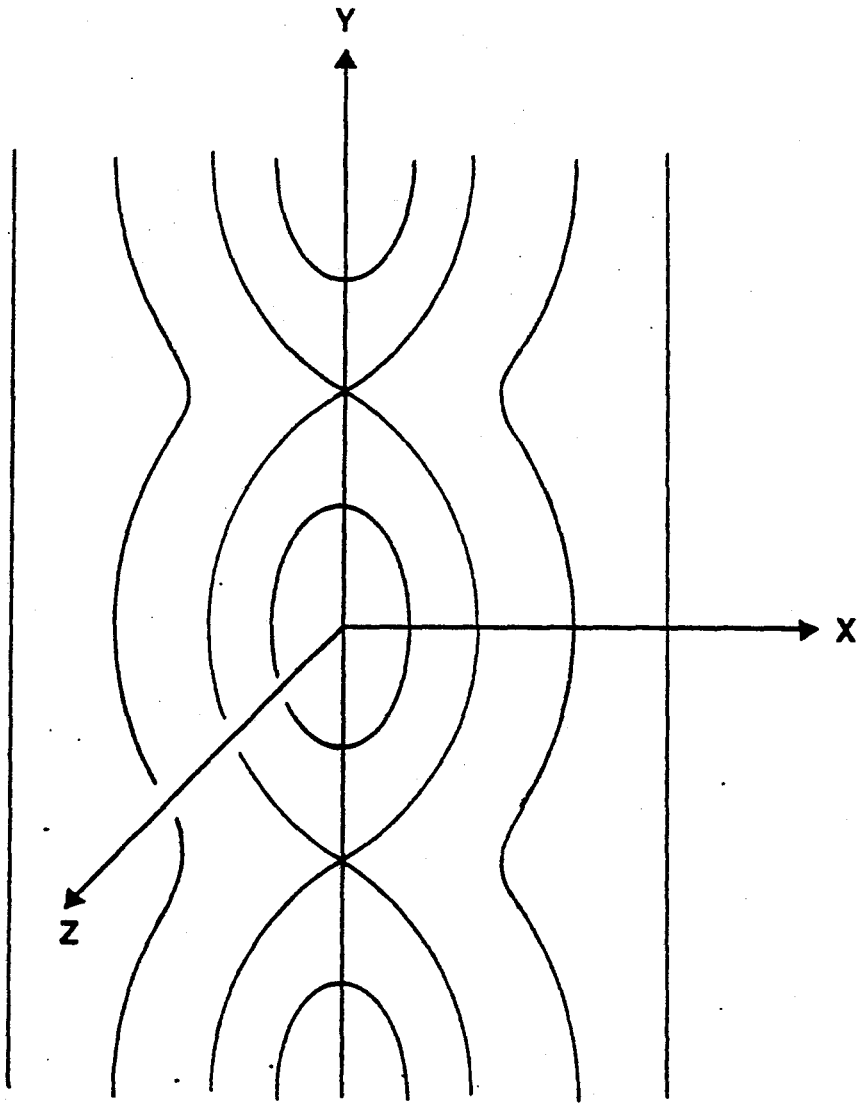


FIG. 5 — Cartesian coordinate system used to model the resistive tearing mode in slab geometry. Flux contours are depicted.

Carry out the differentiation to get:

$$\gamma\tilde{B}_x = ik_y B_{y_o}\tilde{v}_x + ik_z B_{z_o}\tilde{v}_x + \frac{\eta}{\mu_o}\left[\frac{\partial^2\tilde{B}_x}{\partial x^2} - k_y^2\tilde{B}_x - k_z^2\tilde{B}_x\right]$$

$$\gamma\tilde{B}_x = i(\boldsymbol{k}\cdot\boldsymbol{B}_o)\tilde{v}_x + \frac{\eta}{\mu_o}\tilde{B}_x'' - \frac{\eta}{\mu_o}k^2\tilde{B}_x \tag{22}$$

where all quantities are now functions of $x$ only.

Now it is necessary to carefully examine these terms so that some simplification can be done. At the radius where

$$\boldsymbol{k}\cdot\boldsymbol{B}_o = 0 \tag{23}$$

the first right-hand term in equation (22) vanishes, so if the mode is to grow, there must be a finite resistivity here. Obviously away from $\boldsymbol{k}\cdot\boldsymbol{B}_o = 0$, resistivity is not needed. This agrees with the argument mentioned earlier in this section. The radius where $\boldsymbol{k}\cdot\boldsymbol{B}_o = 0$ is, of course, the resonant surface, $x_s$, where the perturbed electric field, $\tilde{\boldsymbol{E}}$, and current, $\tilde{\boldsymbol{J}}$, are exactly parallel to the equilibrium magnetic field lines.

The existence of this very localized perturbed current causes a large change in $\tilde{B}_x'$ within the tearing layer (equation 9). But outside of this narrow region, where there is little perturbed current, $\tilde{B}_x'$ is relatively smooth. Hence, on the scale of the plasma cross-section there appears to be a discontinuity in $\tilde{B}_x'$ at the resonant surface. The second derivative, which is therefore very large near $x = x_s$, is assumed to dominate the other terms within the tearing layer. If the width of this region is $\epsilon$, where:

$$\epsilon \ll a \tag{24}$$

then the second derivative can be approximated as:

$$\tilde{B}_x'' \simeq \left[\frac{\tilde{B}_x'(x_s + \frac{\epsilon}{2}) - \tilde{B}_x'(x_s - \frac{\epsilon}{2})}{\epsilon}\right] \tag{25}$$

The following definition will be made:

$$\Delta' \equiv \left[ \frac{\tilde{B}'_x(x_s + \frac{\epsilon}{2}) - \tilde{B}'_x(x_s - \frac{\epsilon}{2})}{\tilde{B}_x(x_s)} \right] \tag{26}$$

Rewrite equation (25), making use of this parameter.

$$\tilde{B}''_x \simeq \Delta' \frac{\tilde{B}_x}{\epsilon} \tag{27}$$

Substituting this back into equation (22) for the growth rate gives:

$$\gamma \tilde{B}_x \approx \frac{\eta}{\mu_o} \frac{\Delta' \tilde{B}_x}{\epsilon}$$

$$\text{or} \qquad \gamma \approx \frac{\eta \Delta'}{\mu_o \epsilon} \tag{28}$$

It is immediately seen that a necessary condition for instability is:

$$\Delta' > 0 \tag{29}$$

The free parameter $\Delta'$ cannot be determined from these equations inside the tearing layer. However, since the perturbed magnetic field is in reality continuous throughout the plasma, both $\tilde{B}_x$ and $\tilde{B}'_x$ at the surface of the tearing layer must match up with the values in the region outside the layer. Therefore $\Delta'$ *is determined by the ideal MHD equations in the outer, ideal region of the plasma.* This procedure will be detailed shortly.

To calculate the width of the tearing layer, $\epsilon$, is more difficult. Bateman[27] gives a short heuristic derivation which begins by equating the rate of change of kinetic energy in the fluid vortex flow to the work done by the $\tilde{J} \times B_o$ driving force. This relation is obtained by dotting $\tilde{v}^*$ into the force balance equation (11).

$$\rho \tilde{v}^* \cdot \frac{d\tilde{v}}{dt} \simeq \tilde{v}^* \cdot (\tilde{J} \times B_o)$$

$$\frac{1}{2} \rho \gamma (\tilde{v}_x^2 + \tilde{v}_y^2) \simeq \frac{\tilde{v}_x \tilde{J}_z (k \cdot B_o)}{k_y} \tag{30}$$

Since the flow is required to be divergenceless,

$$\frac{|\tilde{v}_y|}{|\tilde{v}_x|} \simeq \frac{\text{poloidal wavelength}}{\text{radial width}}$$

$$\frac{\tilde{v}_y^2}{\tilde{v}_x^2} \simeq \frac{1}{k_y^2\epsilon^2} \gg 1$$

Substitute this into equation (30) and solve for $\tilde{v}_x$:

$$\tilde{v}_x \approx \frac{2k_y\epsilon^2(k\cdot B_o)\tilde{J}_z}{\rho\gamma}$$

From Ampere's law (eq. 9),

$$\tilde{J}_z = \frac{1}{\mu_o}\hat{z}\cdot\nabla\times\tilde{B} = \frac{i}{\mu_o k_y}\left(\frac{\partial^2\tilde{B}_x}{\partial x^2} - k_y^2\tilde{B}_x\right) \approx \frac{i}{\mu_o k_y}\tilde{B}_x''$$

Substituting this into the expression for $\tilde{v}_x$ yields:

$$\tilde{v}_x \approx \frac{2i\epsilon^2(k\cdot B_o)\tilde{B}_x''}{\mu_o\rho\gamma}$$

Now refer back to equation (22) and (rather arbitrarily) postulate that the three dominant terms are of the same order of magnitude at the edge of the tearing layer, $r = r_s \pm \epsilon$. Specifically let

$$i(k\cdot B_o)\tilde{v}_x \sim \frac{\eta}{\mu_o}\tilde{B}_x''$$

$$\text{where} \qquad k\cdot B_o \approx (k\cdot B_o)'\big|_{r_s}\epsilon$$

Substituting in the expression for $\tilde{v}_x$ results in the solution:

$$\frac{2(k\cdot B_o)'^2\epsilon^4}{\gamma\rho} \sim \eta$$

$$\text{or} \qquad \epsilon \sim \left[\frac{\gamma\rho\eta}{2(k\cdot B_o)'^2}\right]^{1/4} \tag{31}$$

The rigorous method of solving for both the tearing layer width and the growth rate is to first derive a pair of coupled differential formulas in cylindrical geometry called the

reduced resistive MHD equations. These involve the introduction of flux and velocity stream functions as follows:

$$\text{since} \qquad \nabla \cdot \boldsymbol{B} = 0$$

$$\boldsymbol{B} \text{ can be written as} \qquad \boldsymbol{B} = \nabla_\perp \psi \times \hat{\boldsymbol{z}} + B_{z_o}\hat{\boldsymbol{z}} \tag{32}$$

where $\psi$ is the poloidal flux function. (A helical flux function can also be used[28] since the perturbations are helically symmetric.) Similarly since

$$\nabla \cdot \boldsymbol{v} = 0$$

$$\boldsymbol{v} \text{ can be written as} \qquad \boldsymbol{v} = \nabla_\perp \phi \times \hat{\boldsymbol{z}} \tag{33}$$

where $\phi$ is known as the velocity stream function.

To derive the first reduced equation, follow the exact same steps used to derive equation (19), except replace $\boldsymbol{B}$ with the flux function expressed in equation (32). The $\hat{\boldsymbol{r}}$-component yields the desired result:

$$\frac{\partial \psi}{\partial t} + (\boldsymbol{v} \cdot \dot{\nabla})\psi = \frac{\eta}{\mu_o}\nabla^2_\perp \psi \tag{34}$$

The second reduced resistive equation is derived by operating on the force equation (eq. 11) with $\hat{\boldsymbol{z}} \cdot \nabla \times$, and also replacing $\boldsymbol{v}$ with the velocity stream function. This yields:

$$\mu_o \rho \frac{\partial}{\partial t}\nabla^2_\perp \phi = -\hat{\boldsymbol{z}} \cdot \left[\nabla_\perp \psi \times \nabla(\nabla^2_\perp \psi)\right] + B_z \frac{\partial}{\partial z}(\nabla^2_\perp \psi) \tag{35}$$

These two equations can then be linearized exactly as before for the first-order perturbed equations involving $\tilde{\psi}(r)$ and $\tilde{\phi}(r)$. Within the tearing layer, the solutions are obtained by using the "constant-$\psi$" approximation; namely $\tilde{\psi}$ is assumed relatively constant but the change in $\tilde{\psi}'$ is not negligible. The coupled equations (34) and (35) reduce to a variant of the Hermite equation with an inhomogeneous driving term, and it can be solved by Green's function techniques[5,29]. The tearing layer width turns out to be:

$$\epsilon \simeq 2a\left(\frac{\gamma \tau_A^2}{\tau_R}\right)^{1/4} \tag{36}$$

where $\tau_A$ is the Alfvén (or ideal MHD) time:

$$\tau_A = \frac{a}{v_A} = \frac{a\sqrt{\mu_o \rho}}{B} \tag{37}$$

and $\tau_R$ is the resistive diffusion time:

$$\tau_R = \frac{\mu_o a^2}{\eta} \tag{38}$$

Note that this is the same as the expression derived heuristically by Bateman if one assumes $(\boldsymbol{k} \cdot \boldsymbol{B}_o)' \sim B/a^2$. If the equation for the tearing layer width is inserted into the intermediate expression for the growth rate (equation 28), we find that:

$$\gamma \simeq 0.6(\Delta' a)^{4/5} \tau_R^{-3/5} \tau_A^{-2/5} \tag{39}$$

In Alcator C at an intermediate radius, typical values of $kT$ and $n_i$ for an 80 kG shot are 500 ev and $2 \times 10^{14}$ cm$^{-3}$ respectively. This gives:

$$\begin{gathered} \tau_A = 1.3 \times 10^{-8} \text{ sec} \\ \tau_R = 0.25 \text{ sec} \\ \gamma \approx 4.5 \text{ kHz} \\ \text{and } \epsilon \approx 0.4 \text{ mm} \end{gathered} \tag{40}$$

(A typical value of $(\Delta' a) = 3$ was assumed and this will be justified shortly.) We see that the linear resistive MHD time scale is about midway between the ideal MHD time and the resistive relaxation time. Also it is noted that equation (24) is certainly well satisfied. Sometimes the growth rate and/or the tearing layer width is expressed in terms of the magnetic Reynolds number, $S$, where:

$$S \equiv \frac{\tau_R}{\tau_A} \gg 1 \tag{41}$$

In Alcator C, $S \approx 2 \times 10^7$. (This high value of $S$ presents difficult numerical stability problems for computational theorists working on the reduced resistive MHD evolution.)

Up to now we have assumed that the tearing mode has been growing exponentially in time and we have used linear theory to describe the physics. But Rutherford[30] has found that the linear theory breaks down when the width of the island becomes of order of the tearing layer thickness. In this non-linear regime, second-order eddy currents develop which produce third-order forces opposing the fluid vortex flow. This has the effect of drastically reducing the growth of the island down to the purely resistive time scale. This is so slow that the fluid inertia (i.e. the left side of equations 11 or 35) becomes unimportant. Therefore in this regime the reduced resistive MHD equations become[31] :

$$\langle \frac{\partial \psi}{\partial t} \rangle = -\langle \eta \rangle J(\psi) \tag{42}$$

$$0 \approx -\hat{z} \cdot \left[ \nabla_\perp \psi \times \nabla_\perp (\nabla^2_\perp \psi) \right] + B_z \frac{\partial}{\partial z} (\nabla^2_\perp \psi) \tag{43}$$

where $\langle \cdots \rangle$ means average over a flux surface. Rutherford solved for the island width, $W$, and found that it grows linearly in time:

$$W \sim \left( \frac{\eta \Delta'}{\mu_o} \right) t \tag{44}$$

More recently, White et al[32] have used a quasi-linear analytical model to extend Rutherford's work. They find that the resistive tearing mode can saturate according to the equation:

$$\frac{dW}{dt} \simeq \frac{1.66 \eta(r_s)}{\mu_o} [\Delta'(W) - aW] \tag{45}$$

where $\Delta'(W)$ is an extension of the use of $\Delta'$ for the thin tearing layer. It is defined to be the discontinuity in the radial magnetic field perturbation from one side of the island to the other:

$$\Delta'(W) \equiv \left[ \frac{\tilde{B}'_r(r_s + \frac{W}{2}) - \tilde{B}'_r(r_s - \frac{W}{2})}{\tilde{B}_r(r_s)} \right] \tag{46}$$

and $a$ is a constant which is determined by matching the perturbations in the outer, non-resistive region to the inner solution at the boundary layer. We see from the definition that $\Delta'(W)$ can change slowly as the non-linear island width increases. Carreras et al[33] argue that when

$$\Delta'(W) = 0 \tag{47}$$

the magnetic island stops growing and settles into a dynamic equilibrium. This assumption is based on the fact that $\Delta'$ is proportional to the change in energy, $\delta W$, effected by the tearing mode[34]. Carreras has demonstrated that the agreement between saturated island sizes calculated by equation (47) and by numerical advancement of the reduced resistive equations is quite good.

II.3 Calculating the width of saturated magnetic islands

With the theory that has been presented here, the saturated size of a magnetic island of mode $(m, n)$ can be calculated in a relatively simple manner (for $m \geq 2$). First, the perturbed flux function, $\tilde{\psi}(r)$, is found by linearizing equation (43) and taking the $\hat{z}$-component as follows:

$$0 = \hat{z}\cdot\left[\nabla_\perp\psi_o \times \nabla_\perp(\nabla_\perp^2\tilde{\psi})\right] + \hat{z}\cdot\left[\nabla_\perp\tilde{\psi} \times \nabla_\perp(\nabla_\perp^2\psi_o)\right] - B_{zo}\frac{\partial}{\partial z}(\nabla_\perp^2\tilde{\psi})$$

However, to better show the ideal MHD nature of the eigenmode, a slightly different approach will be taken here. At marginal stability, the radial magnetic field, $\tilde{B}_r(r)$, obeys the equation:[35]

$$\frac{d}{dr}\left(H\frac{d\tilde{B}_r}{dr}\right) - \left[\frac{g}{F^2} + \frac{1}{F}\frac{d}{dr}\left(H\frac{dF}{dr}\right)\right]\tilde{B}_r = 0 \tag{48}$$

where $$F = \boldsymbol{k}\cdot\boldsymbol{B}_o = \frac{m}{r}B_{\theta o} - kB_{zo}$$

$$H = \frac{r^3}{m^2 + k^2r^2}$$

$$g = \frac{(m^2-1)rF^2}{m^2+k^2r^2} + \frac{k^2r^2}{m^2+k^2r^2}\left(2\frac{dp}{dr} + rF^2 - F\frac{2(krB_{zo} + mB_{\theta o})}{(m^2+k^2r^2)}\right)$$

in the outer region. Since

$$\frac{k^2r^2}{m^2} \simeq \left(\frac{n}{m}\frac{a}{R}\right)^2 \simeq \left(\frac{1}{2}\cdot\frac{1}{4}\right)^2 = \frac{1}{64}$$

the $k^2r^2$ terms can be neglected. This corresponds to neglecting $\tilde{B}_z$. (The $dp/dr$ term is of order $rF^2$ assuming $\beta \sim O(a^2/R^2)$.) The expressions for $H$ and $g$ simplify considerably, and equation (48) becomes:

$$\frac{1}{r}\frac{d}{dr}\left[r\frac{d(r\tilde{B}_r)}{dr}\right] - \frac{m^2}{r^2}(r\tilde{B}_r) = \frac{F'' + \frac{3}{r}F'}{F}(r\tilde{B}_r) \tag{49}$$

Using equation (9), the terms involving derivatives of $F$ can be written in terms of the current profile:

$$F'' + \frac{3}{r}F' = \frac{m}{r}\mu_o\frac{dJ_{zo}}{dr}$$

The denominator, $F$, can be written as:

$$\begin{aligned} F &= \frac{B_{zo}}{R}\left[n - m\left(\frac{RB_{\theta o}}{rB_{zo}}\right)\right] \\ &= \frac{B_{zo}}{R}\left(n - \frac{m}{q(r)}\right) \end{aligned} \tag{50}$$

Also, remembering that $\tilde{\psi}$ is proportional to $r\tilde{B}_r$, equation (49) can be written in its final form:

$$\frac{1}{r}\frac{d}{dr}\left(r\frac{d\tilde{\psi}}{dr}\right) - \frac{m^2}{r^2}\tilde{\psi} = \frac{-\frac{m}{r}\frac{\mu_o R}{B_{zo}}\frac{dJ_{zo}}{dr}}{n - \frac{m}{q(r)}}\tilde{\psi} \tag{51}$$

Equation (51) has a regular singular point at the radius, $r_s$, where $q(r_s) = m/n$. This type of differential equation has a continuous solution everywhere, but the first derivative is discontinuous and leads to the determination of $\Delta'$. By expanding equation (51) around the singular radius, the perturbed flux function can be shown to go as:

$$\tilde{\psi}(r_s \pm \delta) \approx \tilde{\psi}(r_s) \pm C_1\delta\ln\delta \pm C_{\pm}\delta + O(\delta^2) + \cdots \tag{52}$$

where $\delta = |r - r_s|$. It is seen that $\tilde{\psi}(r)$ is indeed finite and continuous across the singular radius, but that $\tilde{\psi}'(r)$ is both discontinuous and possesses a logarithmic singularity at $r = r_s$. Fortunately this infinite term is the same on both sides of $r_s$ and so it drops out in the expression for $\Delta'$ (equation 26), yielding:

$$\Delta' = \frac{C_+ - C_-}{\tilde{\psi}(r_s)} \tag{53}$$

However, the constants $C_+$ and $C_-$ are determined by the boundary conditions at $r = a$ and $r = 0$ respectively. At these large distances, the expansion for $\tilde{\psi}(r)$ is not useful and so the analytic formula for $\Delta'$ (equation 53) is of academic interest only. In addition, since the solution of $\tilde{\psi}$ at the resonant surface depends upon conditions far from $r_s$, the form of the current profile, $J_z(r)$, and $q(r)$ must play an important role in the stability of resistive tearing modes.

For all but the simplest current profiles, equation (51) must be solved by numerical methods for $\tilde{\psi}(r)$. If there is a conducting wall at $r = a$, then one boundary condition is that:

$$B_r(a) = 0$$
$$\text{or} \quad \tilde{\psi}(a) = 0 \quad \text{from equation (32)} \tag{54}$$

The boundary condition at the origin is obtained by solving equation (51) near $r = 0$ where, to first order in $r$:

$$\frac{\partial J_{z_0}}{\partial r} \sim r$$

$$\text{and} \quad q \simeq q_0$$

The two independent solutions are:

$$\tilde{\psi}(r \to 0) \sim r^m, r^{-m} \tag{55}$$

but the divergent case must be thrown out since there is no singularity in the actual plasma current. Starting with these two boundary conditions, one can use a finite difference scheme

$$J_{zo}(r) = J_o e^{-\frac{3r^2}{2a_j^2}} \qquad (58)$$

$$\text{or simply} \qquad J_{zo}(r) = J_o e^{-r^2/a_j^2}$$

where $a_j$ depends only on $q(0)$ and $q(a)$ to within experimental uncertainties. There is a further constraint which can be imposed on $J_o$ from experimental observation of sawtoothing x-ray emission from the center of the plasma column. As stated in the introduction, this behavior, which is seen on virtually all discharges of interest here, limits $q_o$ and therefore $J_o$ (equation 6). Presumably then, in calculating perturbed flux functions and tearing mode stability in Alcator C, the only factor which is available for parameter scans is $q(a)$. From equation (1) we see that there are two independent "knobs" which can be turned to scan $q(a)$, namely the magnetic field, $B_t$, and the plasma current, $I_p$. Both methods are easily and routinely varied during Alcator C operations.

Figs. 6 and 7 show $m = 2/n = 1$ perturbed flux functions for Gaussian current profiles calculated numerically. Note the break in slope at the singular surface. As shown in the lower half of the diagrams, the only difference between the two examples is the width of the current profile, resulting in different values of $q$ at the limiter and different positions of the resonant radius where $q = 2$. Figure 8 shows $\Delta'(W)$ for the two cases. Note that only the narrower current profile is unstable and results in a saturated magnetic island. This is not due so much to the difference in shape, but rather to the fact that the limiter tends to have a stabilizing effect on resistive tearing modes. As the current profile gets broader, the position of the tearing layer moves farther out and therefore closer to the limiter. The effect can be seen quite clearly in Fig. 9, where the saturated widths of $m = 2/n = 1$ islands are plotted against the radial position of their corresponding singular surfaces. Of course, if the plasma current is large enough to give $q(a) < m/n$, then the resistive tearing mode $(m, n)$ can no longer exist in the plasma.

In summary, elementary resistive MHD theory in cylindrical geometry predicts that for Gaussian current profiles with $q_o \simeq 1$ and $q(a) \simeq 3$, $m = 2/n = 1$ islands should exist at macroscopic sizes. As the plasma current is raised, the magnetic islands should first

to get $\tilde{\psi}(r)$ on both sides of $r_s$, iterating arbitrarily close to the singular surface. Matching the inner and outer solutions of $\tilde{\psi}(r)$ at $r = r_s$ is trivial since equation (51) is linear and therefore $\tilde{\psi}$ can be multiplied by any constant. Once the perturbed flux function is known, $\Delta'(W)$ can be calculated from equation (46). If $\Delta'$ is negative, then the particular tearing mode is stable for the given current profile and no magnetic island is formed. If $\Delta'$ is positive, then the elementary theory predicts instability, and the value of W at which $\Delta'(W)$ passes through zero is the final saturated size of the magnetic island.

II.4 Application of formulas to Alcator C

Such computations have been carried out for the parameters and profiles representative of Alcator C. Actual measurements of $J_{zo}(r)$ have not been done yet, but if one assumes classical resistivity and a constant $Z_{eff}$ profile (in reasonable agreement with experimental findings[36]) then:

$$J_{zo}(r) \sim T_e(r)^{3/2} \tag{56}$$

Electron temperature profiles have been measured by cyclotron emission[37] for many values of magnetic field, plasma current and density, and it is found that in almost all cases of sawtoothing discharges the data can be fitted by a Gaussian curve:

$$T_e(r) = T_o e^{-r^2/a_T^2}$$
$$\text{where} \qquad a_T^2 = \frac{3}{2} a^2 \frac{q_o}{q(a)} \tag{57}$$

within the quoted error bars. An important fact which will gain significance later in this paper is that the electron cyclotron emission measurements do not have enough resolution to detect any subtle variation of the temperature profile. Tearing mode activity may be sensitive to such subtle effects, especially near the resonant surface.

From the empirical findings and assumptions that have been made, the current profile can be written:

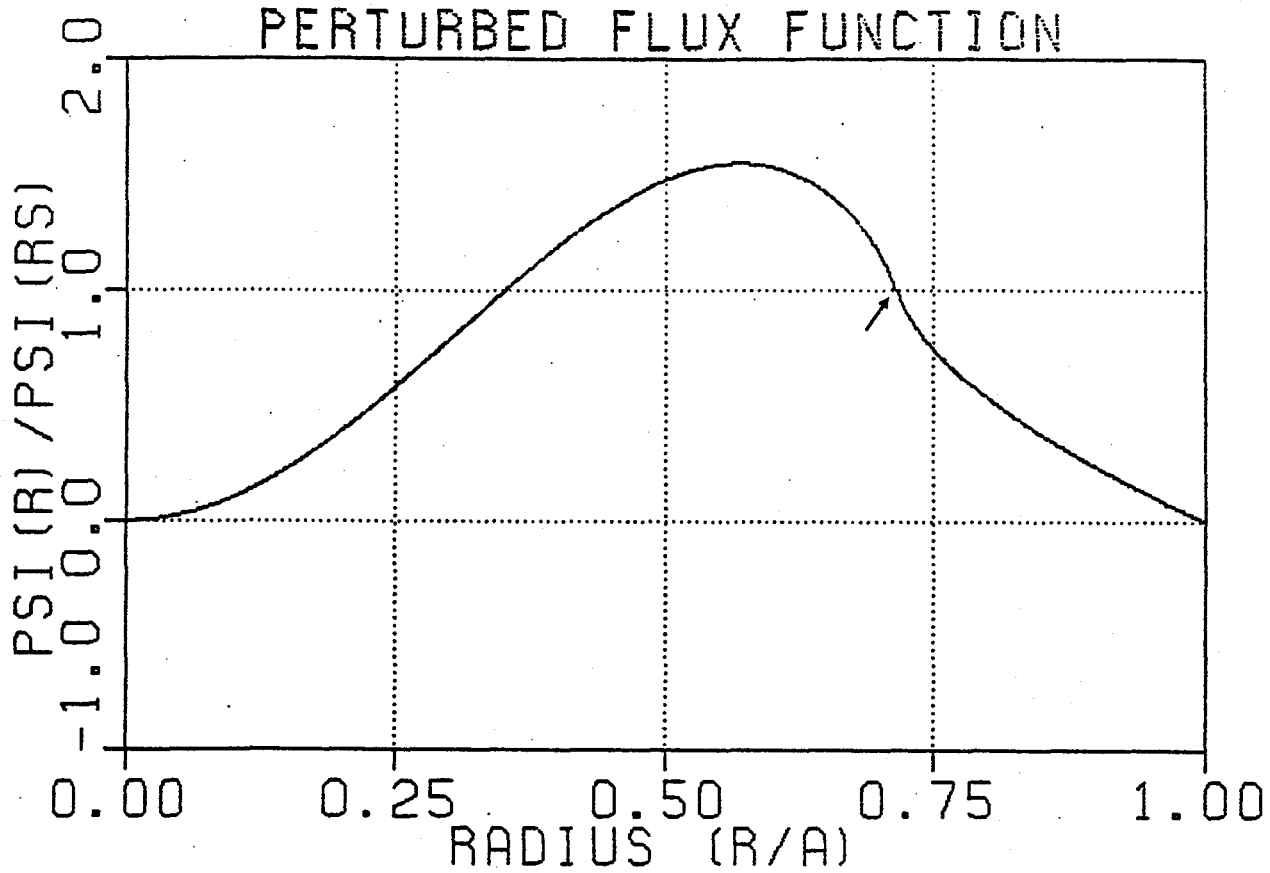


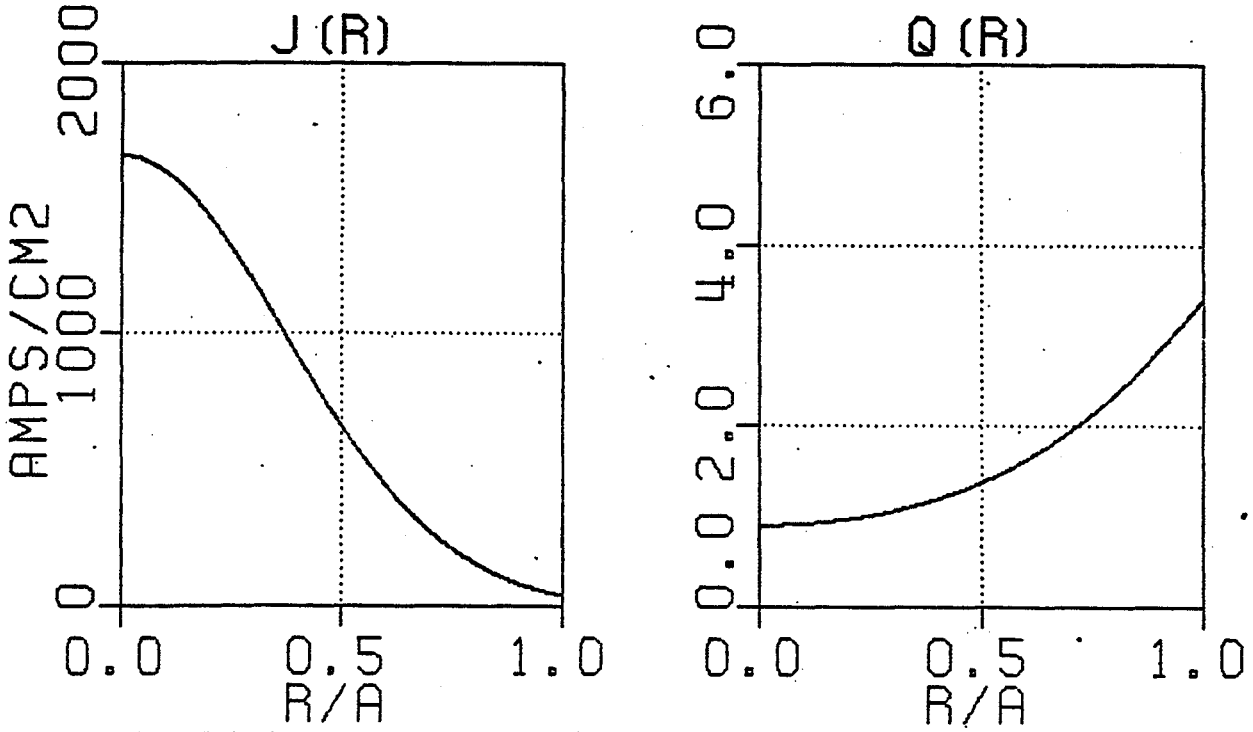


FIG. 6 — Calculated perturbed $m = 2/n = 1$ flux function for a Gaussian current profile. The arrow indicates the position of the resonant surface, where the (slight) break in the first derivative occurs. The $q$ profile is also displayed. Note: $q(a) = 3.4$

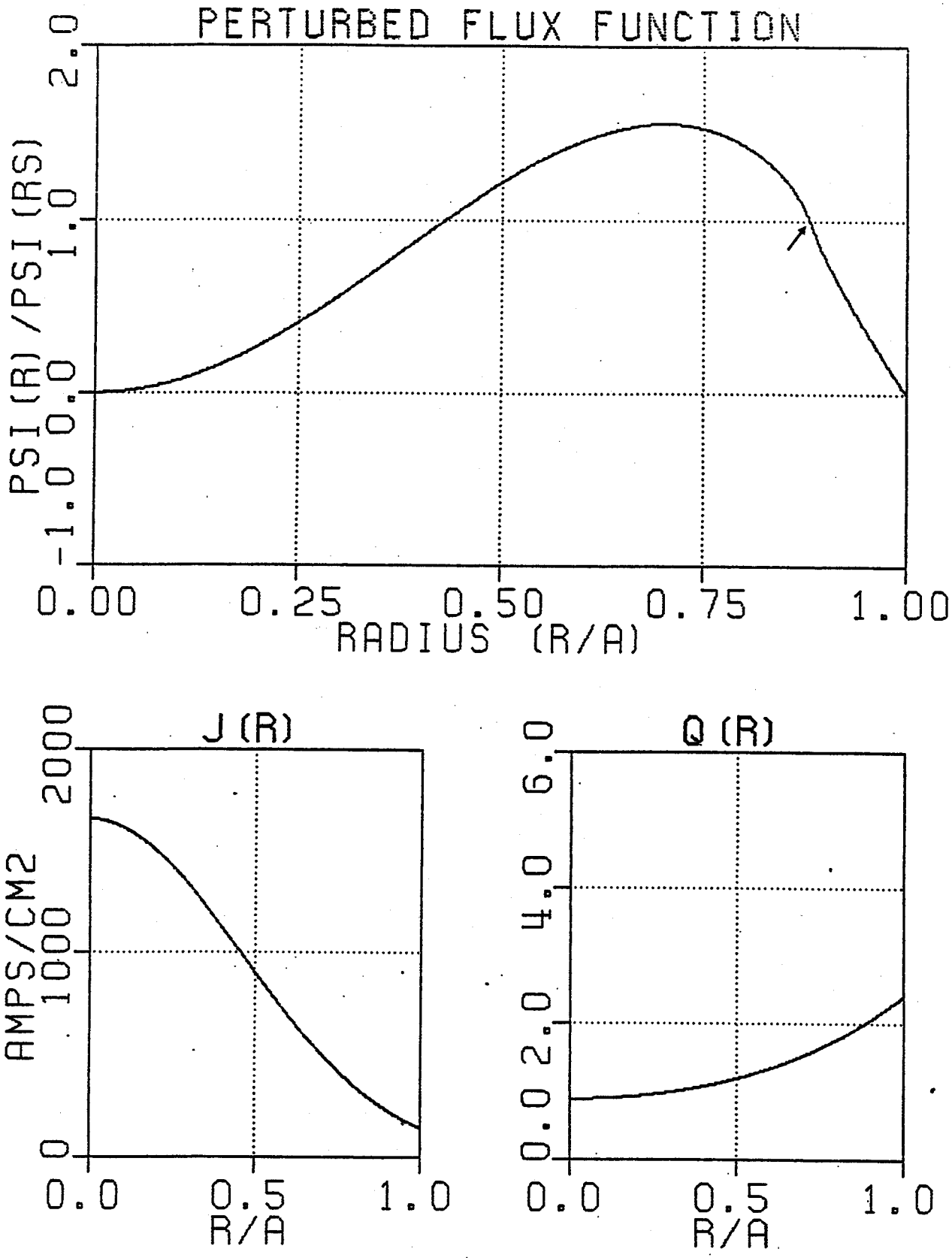


FIG. 7 — Calculated perturbed $m = 2/n = 1$ flux function for a Gaussian current profile. The arrow indicates the position of the resonant surface. The $q$ profile is also displayed. Note: $q(a) = 2.4$

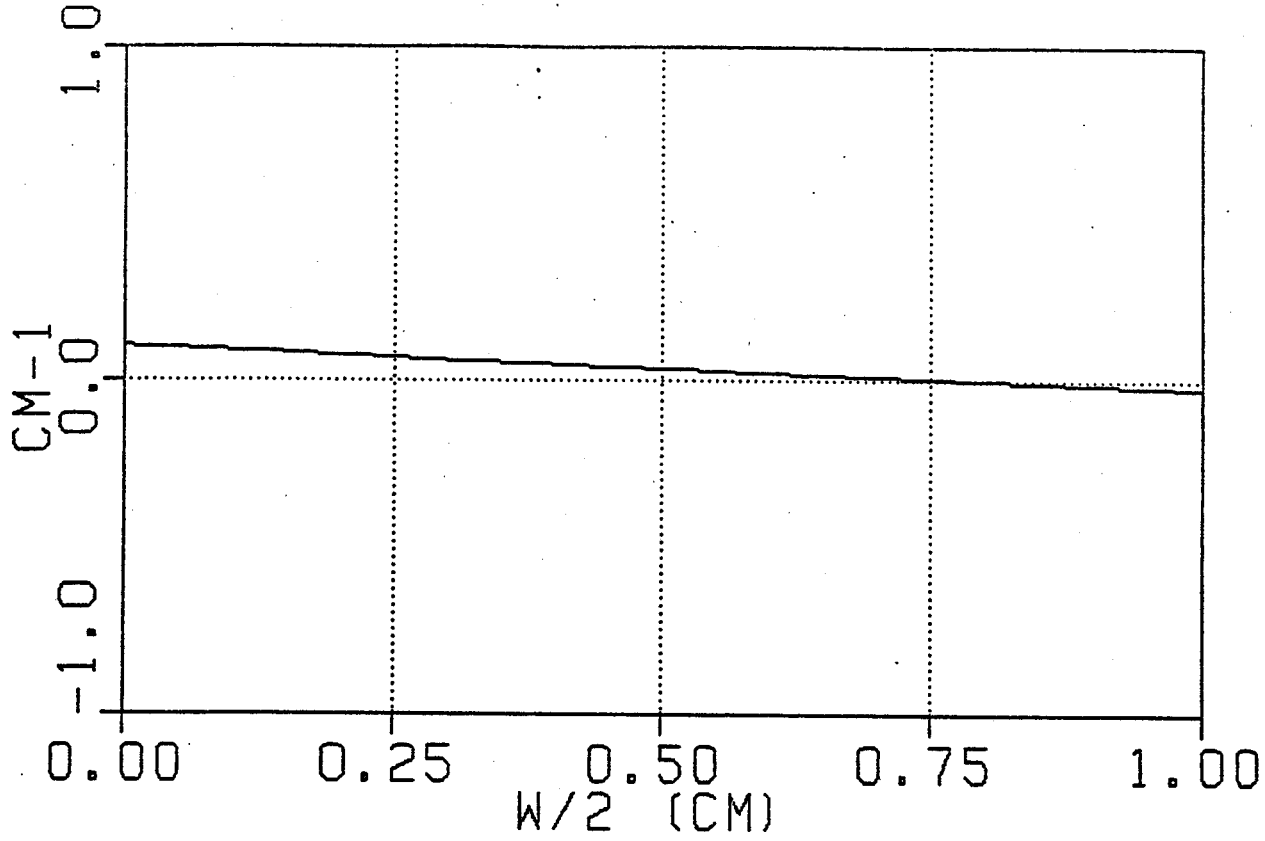


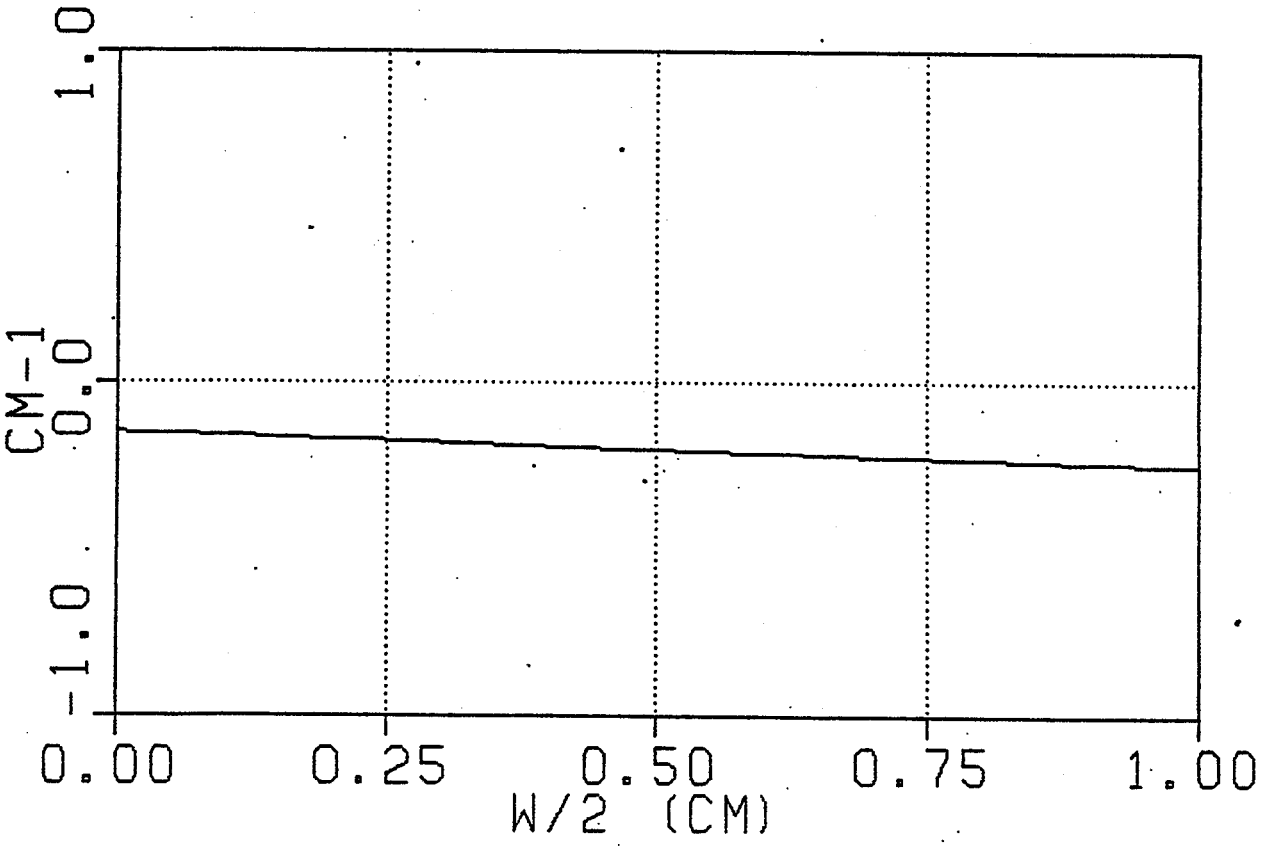


FIG. 8 — $\Delta'(W)$ for the profiles in Figs. 6 and 7 respectively.

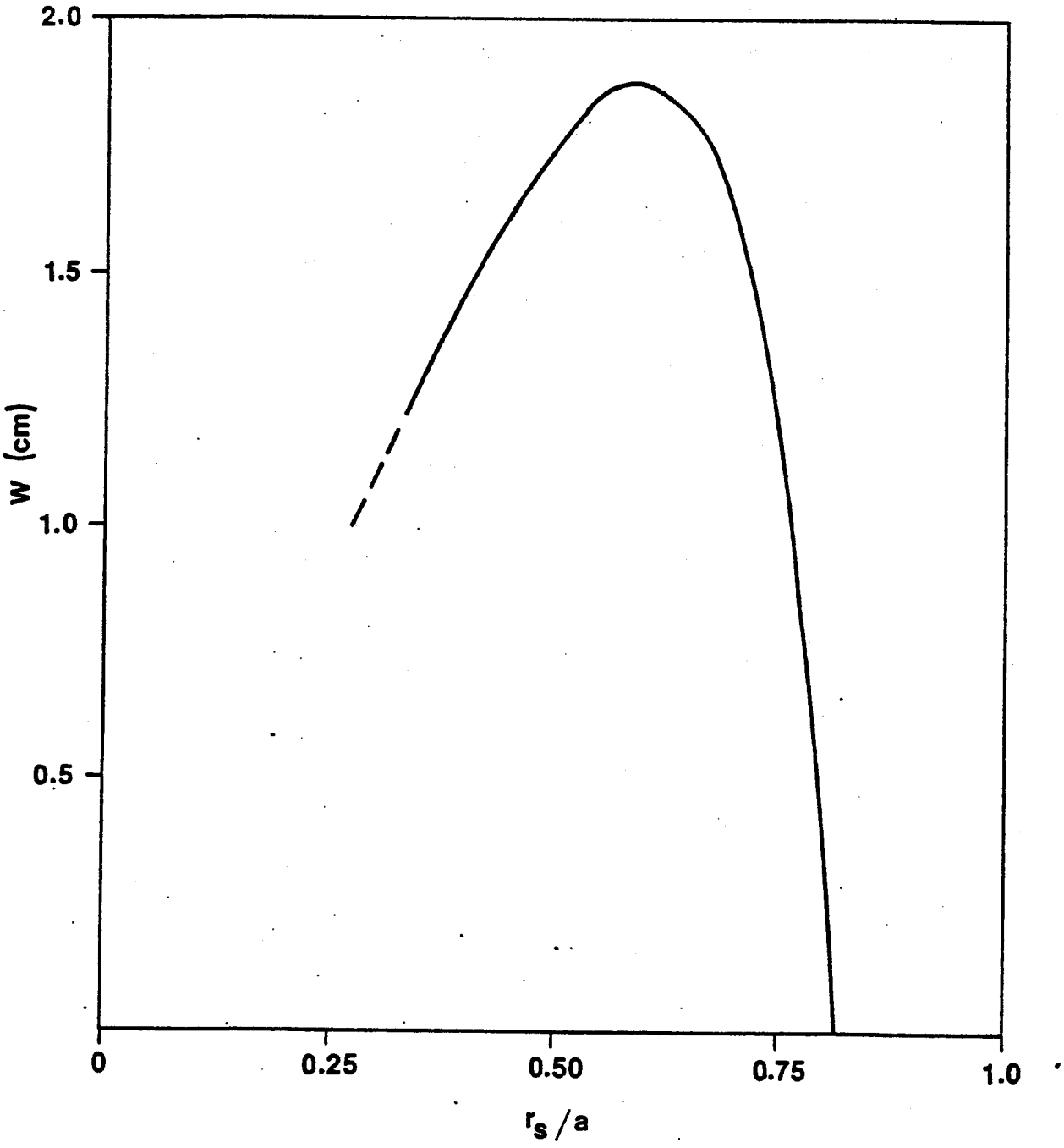


FIG. 9 — Saturated magnetic island size versus magnetic island radial position for the $m = 2/n = 1$ mode.

grow and then shrink in accordance with Fig. 9 and eventually disappear. In addition, the elementary physics of the instability does not have an explicit dependence on the electron density, although there can be an indirect effect through coupling to the plasma current profile. In the next section several corrections and modifications to the elementary theory will be discussed. In Alcator C these extra effects may stabilize the tearing mode.

II.5 Other non-ideal effects

So far we have only looked at elementary resistive MHD tearing theory, i.e. the only non-ideal term that has been included is resistivity (in equation 10). The effects of other non-ideal physics on these modes has been studied by various theorists and some of this work will be summarized here. For MHD theory to be applicable, the plasma must be collisional enough to be described by fluid equations. But this condition is not satisfied in many present-day tokamak experiments because the tearing layer width, $\epsilon$, is much less than the ion gyroradius, $\rho_i$, at the resonant surface. Obviously single-particle orbits and kinetic effects are very important in such devices and this problem has been worked out in great detail by Drake and Lee[38,39]. They define three separate regimes: collisionless, semi-collisional, and collisional (MHD valid); and calculate the growth rate and tearing layer width in each. In Alcator C, using the typical parameters mentioned in equation (40), we find that:

$$\rho_i \simeq 0.28 \text{ mm}$$
$$\text{thus} \quad \frac{\epsilon}{\rho_i} \approx O(1) \tag{59}$$

Therefore in our experiment the plasma is on the borderline between the collisional and semi-collisional regimes. At the transition, however, the growth rate is continuous across this region so it shouldn't make too much difference which growth rate formula is used. This is born out in an actual calculation of $\gamma$ using the formula derived by Drake and Lee for the semi-collisional regime—$\gamma$ turns out to be 4.1 kHz, which is not significantly different from the value of 4.5 kHz derived from elementary resistive MHD theory. So for our purposes, we may safely ignore these kinetic corrections.

Another class of non-ideal effects involve density and temperature gradients which give rise to diamagnetic drifts. This problem has been examined by many people[10,11] and there is general agreement on the principal results. The diamagnetic frequencies are usually defined as follows:

$$\omega_{*e} = \frac{T_{eo}}{eB_t a^2}$$

$$\omega_{*i} = \frac{T_{io}}{eB_t a^2} \tag{60}$$

$$\text{and} \qquad \omega_* = \omega_{*e} + \omega_{*i}$$

(In these definitions the pressure gradient has been approximated as $n_o T_o/a$.) The linear dispersion relation for modes growing as $e^{-i\omega t}$ when diamagnetic effects are included becomes:[42]

$$\omega(\omega - \omega_{*i})(\omega - \omega_*)^3 = (i\gamma_T)^5 \tag{61}$$

where $\gamma_T$ = elementary resistive tearing mode growth rate. Clearly if the diamagnetic terms are ignored, we recover the original result, $\omega = i\gamma_T$. For finite gradients, the frequency gains a real component of $O(\omega_*)$ and therefore the islands should be seen to rotate at about the diamagnetic frequency. This instability is called the drift tearing mode and such behavior is indeed observed in tokamaks. In fact, without this oscillation, the modes are not discernible experimentally. (There is disagreement over whether the island rotation is simply mode rotation or actual plasma fluid flow.) The effect of diamagnetic drifts on the imaginary part of the frequency (i.e. the growth rate) depends on the relative size of $\omega_*$ to $\gamma_T$ and also on the size of the island. In general, the qualitative result is that the growth rate is somewhat reduced (although definitely not stabilized) in the linear regime when the island width is smaller than the tearing layer. But once the width surpasses $\epsilon$, the diamagnetic effects are quenched and the tearing mode's non-linear growth and saturation is essentially unaffected, except for the real rotation which continues even after the magnetic island reaches a steady state. In Alcator C, $\omega_* \approx \gamma_T$ and under these conditions, the growth and saturation of magnetic islands has been followed by Monticello and White[42] using a

computer code which integrates the drift tearing mode equations. Their results are shown in Fig. 10 and verify the analytic assertion that diamagnetic terms don't effect the stability or the non-linear behavior of the tearing mode.

Effects of toroidicity may become very important once the islands have grown to macroscopic widths. For finite aspect ratio, the equilibrium magnetic field is stronger on the inside of the torus than the outside. To first order in $a/R$, the toroidal field can be approximated as:

$$B_{zo}(r) \simeq B_{zo}(0)\left[1 - \frac{r}{R}\cos\theta\right] \tag{62}$$

and since

$$\cos\theta = \frac{e^{i\theta} + e^{-i\theta}}{2}$$

the effect of bending the cylindrical plasma into a torus introduces $(m, n) = (\pm 1, 0)$ perturbations which may then couple with helical instabilities of mode $(m, n)$ to give additional modes of the form $(m \pm 1, n)$. The size of these additional islands may be of the same order as the original driving mode[43].

With magnetic islands of different helicity existing at different radii, a catastrophic result is possible. If the widths of the modes continue to grow, several islands starting from different radii may touch or overlap. Carreras et al[44,45,46] have shown by analytical and numerical methods that this leads to strong non-linear destabilization and results in rapid growth of many modes (on the pure MHD time scale). This in turn leads to destruction of closed magnetic flux surfaces, stochastic magnetic field lines, rapid conversion of magnetic energy to kinetic energy, and the ensuing loss of particle and energy confinement over much of the plasma cross-section. Such a scenario is currently hypothesized as the cause of the major disruption in tokamaks, and it seems to explain the anomalously fast destruction of the current profile.

The effects just mentioned yield modifications of the initial linear growth rate, but do not change the stability criteria for the pure tearing mode: $\Delta' > 0$. On the other hand, two

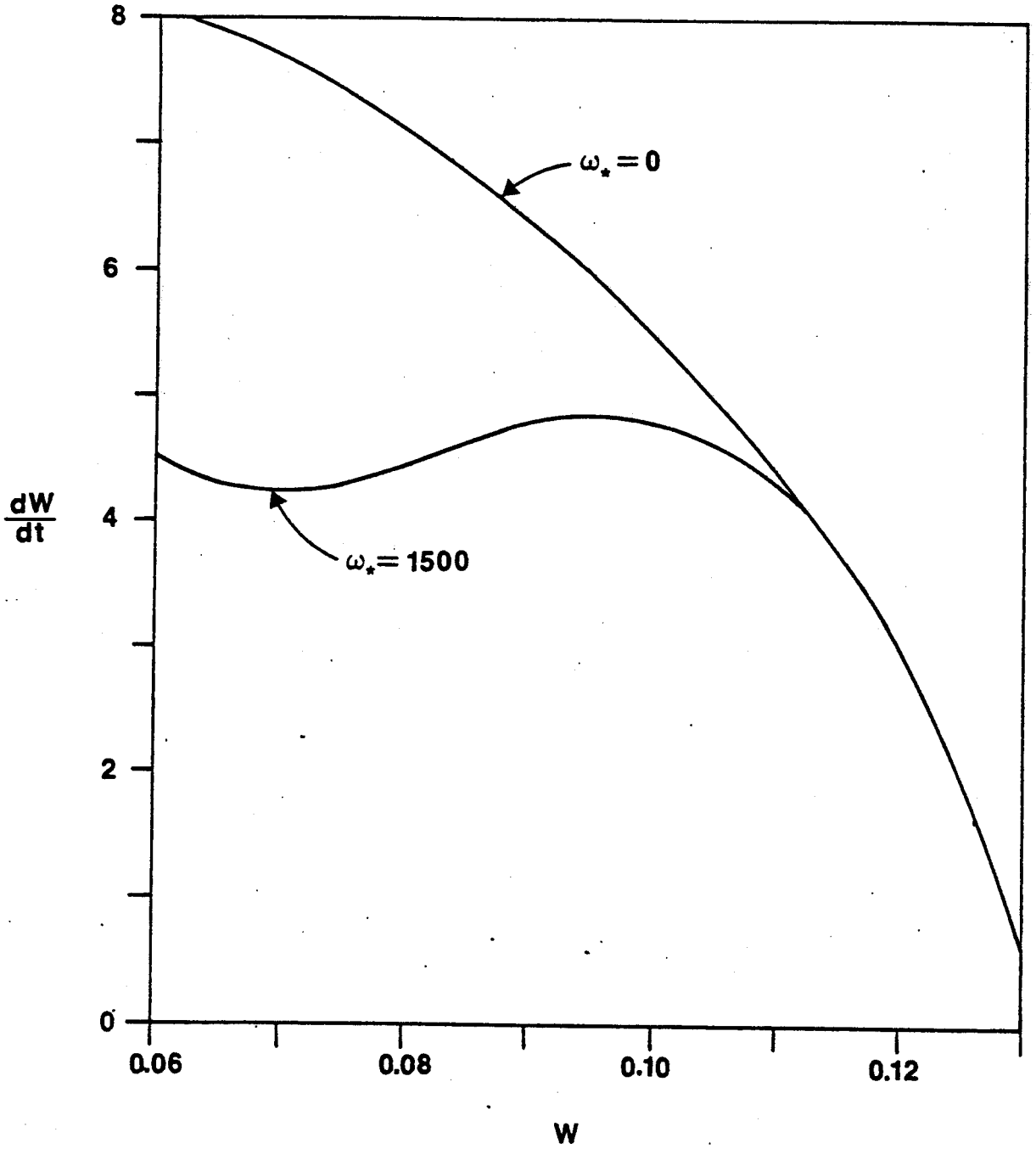


FIG. 10 — Effect of diamagnetic terms on non-linear tearing mode growth rate for the case where $\omega_* \approx \gamma_T$. Time is normalized to the resistive time, $\tau_R$, and width is scaled to the minor radius, $a$. (Reprinted from ref. [42].)

more corrections to be discussed, radial diffusive flow and finite beta, can definitely alter the stability criterion. The effect of a diffusive velocity on tearing modes has been investigated by Taylor et al[47]. For plasmas having finite resistivity, such diffusion will occur on the slow resistive time scale and, mistakenly, might be considered negligible on the tearing mode time scale. According to Dobrott[48], this is incorrect, since the length scale which is relevant to the problem is the tearing layer width, $\epsilon$, and not the plasma radius, $a$. The net effect of a radial diffusive flow is to alter the stability criterion in a way which helps to stabilize the tearing mode. The corrected criterion for instability becomes:

$$\Delta' > 1.021 \left| \frac{F''}{F'} \right|_{r_s} \tag{63}$$

where $F \equiv \boldsymbol{k} \cdot \boldsymbol{B}_o$. For the Gaussian current profile used in Fig. 6 of section II.4, equation (63) evaluates to:

$$\Delta' > 0.10 \quad \text{cm}^{-1}$$

for the $m = 2/n = 1$ mode. From Fig. 8 it is seen that:

$$\Delta' = 0.09 \quad \text{cm}^{-1}$$

and therefore the radial diffusive flow could actually predict enhanced stability of the $m = 2$ mode in Alcator C. This correction is seen to be independent of density and magnetic field (and only weakly dependent on current).

Corrections due to finite beta could also modify the stability criterion of the tearing modes in the operating regime of Alcator C. Glasser, Greene, and Johnson[49] have analyzed the general toroidal case with compressibility and find that the instability criterion for low $m$-number is actually:

$$\Delta > \Delta_c \tag{64}$$

where $\Delta \equiv r_s \Delta'$ is dimensionless. (The high $m$-number modes are stabilized by shear for any reasonably peaked current profile.) In the large aspect ratio limit, the parameter $\Delta_c$ is

given by[50]:

$$\Delta_c = A|D_R|^{5/6} \tag{65}$$

where

$$A = 1.54\frac{r}{a}\left[S\frac{a^2 m}{R}\frac{dq/dr}{q^2}\Big/(1+2q^2)^{1/2}\right]^{1/3}$$

and

$$D_R = -\frac{2\mu_o}{B_t^2}\frac{q^2(-dp/dr)}{r(dq/dr)^2}$$
$$\times\left\{q^2 - 1 + \frac{q^3 dq/dr}{r^3}\int_0^r\left[\frac{r^3}{q^2} + \frac{2\mu_o R_o^2 r^2}{B_t^2}\left(-\frac{dp}{dr}\right)\right]dr\right\}$$

All quantities which are functions of radius are evaluated at the resonant surface, $r_s$, where $q(r_s) = m/n$. Several important points are evident; first, for peaked $J(r)$, the shear parameter, $dq/dr$, is positive and therefore the coefficient "$A$" is real and positive. Thus

$$\Delta_c > 0$$

and this means that the instability criterion, equation (64), implies the equilibrium is more stable to tearing modes than the simple results of section II.2 (equation 29) would indicate. The $\beta$ dependence of $\Delta_c$ is contained in $D_R$. If the pressure profile is also assumed to be peaked (a good assumption during steady state in Alcator C) then the integral contains a term which goes like:

$$\frac{2\mu_o}{B_t^2}\left(-\frac{dp}{dr}\right) \sim -\beta' \sim \frac{\beta}{a}$$

This expression also multiplies the entire bracketed quantity. Since both terms of the integrand are positive definite, as well as the coefficient, and since $q^2 - 1 > 0$ everywhere outside the $q = 1$ surface, the magnitude of $D_R$ increases at least linearly with $\beta$. In fact if the integral dominates the other terms in brackets, $|D_R|$ could almost go like $\beta^2$. The

net result is that finite beta is therefore a stabilizing influence; higher $\beta$'s should lead to greater stability of the tearing mode. In order to estimate the importance of this effect, Hastie, Sykes, Turner and Wesson[51] carried out calculations using realistic current profiles, and their theoretical work has shown that, in general, for a peaked current profile the finite $\beta$ effect should become significant in the large aspect ratio expansion when:[52]

$$\beta_p \geq \left(\frac{R}{a}\right)^{12/5} S^{-2/5}$$

For the Alcator C tokamak, where $R/a \simeq 4$ and $S \simeq 10^7$, this condition translates to:

$$\beta_p \geq 0.03$$

and this is certainly well satisfied during the steady state portion of the discharge, even for the volume average, $\langle\beta_p\rangle$. A detailed numerical calculation is therefore warranted.

According to equation (64), the finite $\beta$ correction should stabilize the low-$m$ modes when $\Delta_c(\beta) > r_s\Delta'$, where $\Delta_c(\beta)$ is given by the expressions in equation (65). In this calculation Alcator C profiles are used for the temperature, current (both Gaussian), and density (parabolic to the one-half power). For the typical $q = 3.4$ plasma at 60 kG with $\overline{n} = 2 \times 10^{14}$ cm$^{-3}$ and $T_e(0) = T_i(0) = 1100$ eV, one finds:

$$\Delta_c = 3.98$$

$$r_s\Delta' = 11.8 \text{ cm } \times 0.09 \text{ cm}^{-1} = 1.06 \text{ for the 2/1 mode}$$

and therefore the finite $\beta$ correction should, in theory, stabilize the $m = 2$ tearing mode in Alcator. This correction should become even more important as $\overline{n}/B^2$ (and thus $\beta$) is raised. In summary, although elementary resistive MHD theory predicts $m = 2/n = 1$ magnetic islands during the steady state portion of Alcator C discharges, certain modifications, namely finite beta and radial diffusion, theoretically could stabilize all $m \geq 2$ modes. It should be pointed out that the credibility of these corrections is not as well founded as the elementary theory, and to some extent this thesis study could be a test of these hypotheses.

In all of the theory presented in this chapter the plasma has always been assumed to be in a static equilibrium, $v_o = 0$ (or at least no faster than the resistive diffusion speed). No one has yet documented the effects of an equilibrium fluid flow on the tearing mode. A poloidal rotation, for example, will give rise to a centripetal force which could influence the stability criterion. As we shall see, just such a modification may be needed to explain the experimental findings described in the next chapter.

## II.6 Stabilization of tearing modes

*If* this hypothesis is born out by experimental studies of the disruptive instability, then it suggests a means for avoiding the major disruption—namely stabilization of the principal tearing modes existing prior to the disruption. For most tokamaks, the $m = 2$, $n = 1$ and $m = 3$, $n = 2$ modes should be the dominant ones. Three schemes have been suggested[53]: (1) Changing the shape of the current profile near the resonant surface in such a way that the $\Delta'$ parameter is reduced, (2) Use of non-resonant helical windings to decouple $J(r)$ and $q(r)$ profiles, and (3) Feedback of properly phased helical magnetic fields resonant with the tearing mode of interest. It should be pointed out that in any case, it would not be necessary to completely shrink an island down to zero width; it should suffice to simply force the saturated size to remain small enough so that adjacent islands don't come near each other. This would eliminate the non-linear coupling and explosive growth.

The first method is conceptually simpler to understand since it relies only on the physics and techniques already presented in section II.3. However the implementation of this method may be difficult since it would probably involve the use of neutral beam or RF heating with a very selective power deposition profile. There is also the question of time response if such profile modification is done in a feedback loop. The second method has already been tried and has met with some success[54]. The third technique is more complicated theoretically but much more flexible and ideal for use in a feedback mode. The basic concept is to remove the outer boundary constraint of equation (54) which is a consequence of having a conducting wall at the plasma surface. If the outer part of the perturbed flux function in Fig. 6 is pulled down at $r = a$, then the discontinuity in $\tilde{\psi}'$ at the singular surface,

$r_s$, could be reduced or even eliminated. This is therefore a method to control $\Delta'$ directly without having to play around with the current profile or the $q$ profile. Pulling $\tilde{\psi}$ down at the edge of the plasma could be accomplished by turning on a resonant radial magnetic field perturbation with properly designed coils near the surface of the plasma. Therefore the boundary condition is now a free parameter which, in principle, could be controlled with feedback circuitry hooked up to a set of Mirnov loops, for example. The effect of various settings of $\tilde{B}_r(a)$ on the perturbed flux functions is shown in Fig. 11. The current profile is the same Gaussian used in Fig. 6. The change in $\Delta'(W)$ is shown in Fig. 12. The major problems with magnetic feedback stabilization involve the stringent requirements on the phase shift of the applied field. Improper phase delays could destabilize tearing modes[53,55], but this might be overcome by switching the feedback on and off at periodic intervals.

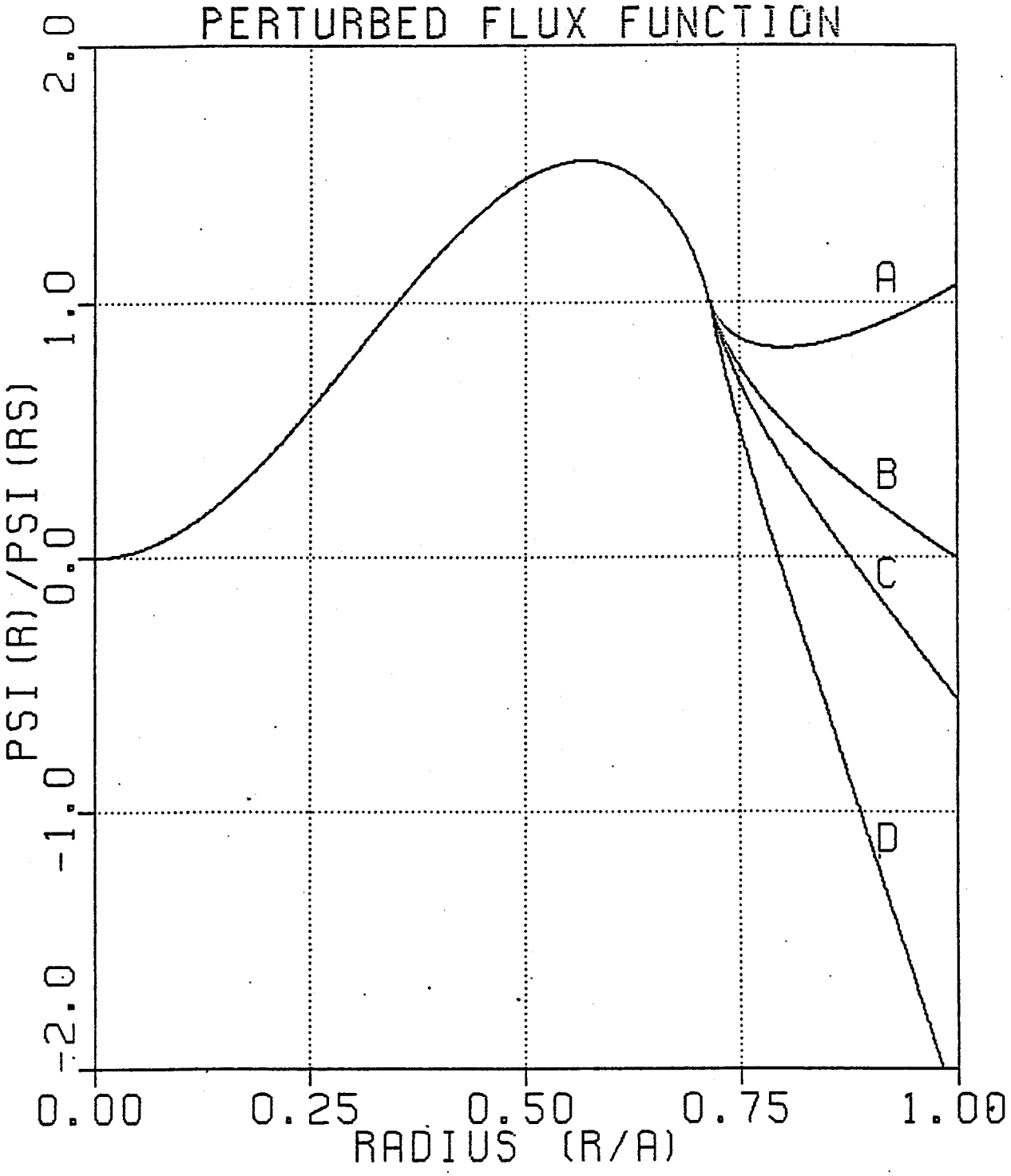


FIG. 11 — Perturbed $m = 2/n = 1$ flux functions for several feedback levels. Curve B is the no-feedback case ($\tilde{\psi}(a) = 0$).

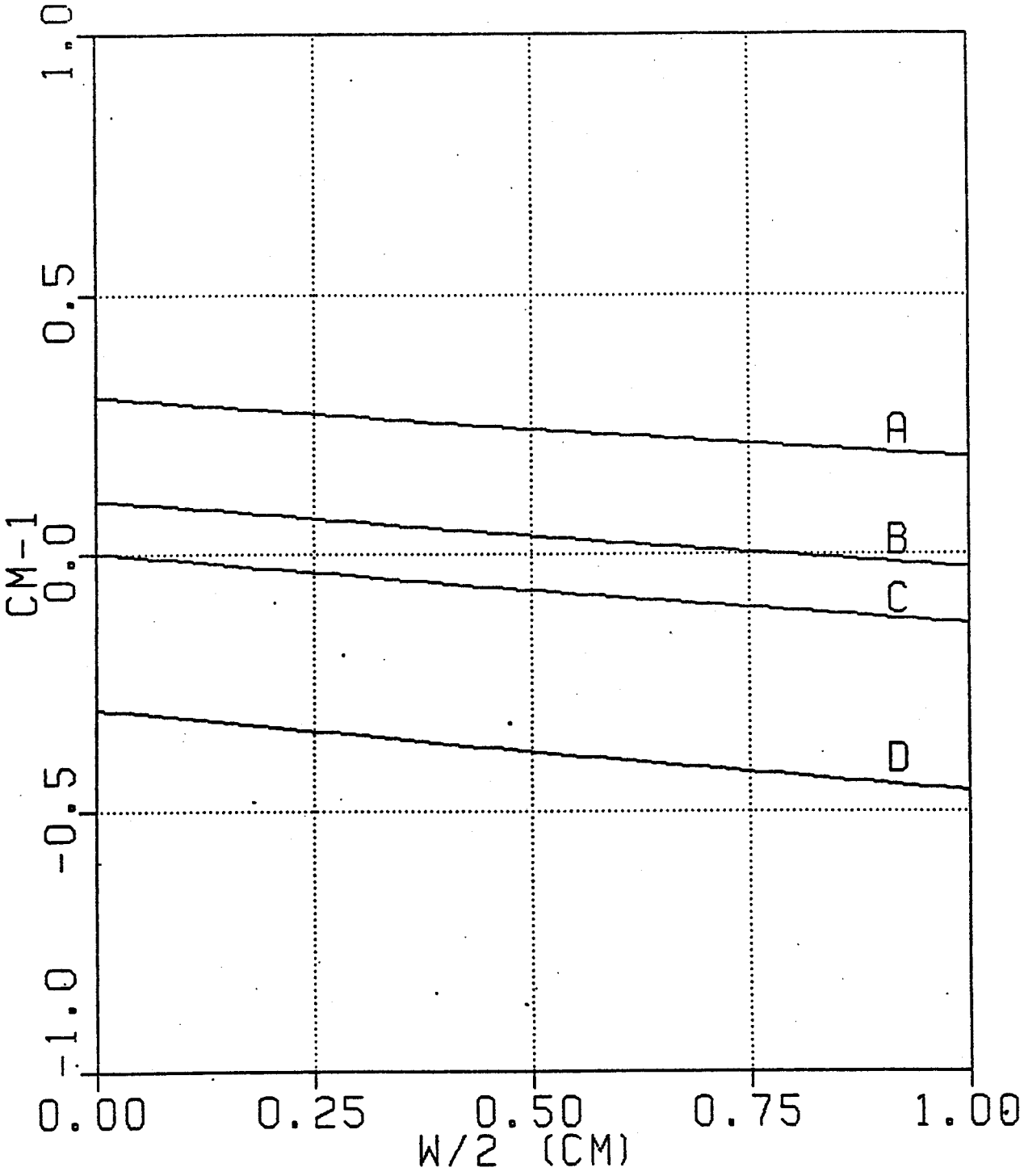


FIG. 12 — Effects of various feedback levels on $\Delta'(W)$. Curve C is the marginally stable case.

# III. THE $m$-SPECTRUM ANALYZER

## III.1 Motivation for the experiment

The importance of resistive MHD tearing modes in tokamak plasmas has been shown theoretically. The major issues of energy confinement and disruptions are involved, as well as the possibility of successful stabilization. For these reasons, this experimental study was undertaken to learn as much as possible about tearing mode activity in Alcator C. Specifically the original goals we had in mind were:

(1) Look for the existence of magnetic islands on Alcator C.

(2) Determine the mode numbers of any activity detected, preferably in real time, if possible.

(3) Measure the amplitudes and frequencies of each mode observed, again in real time.

(4) Determine the relation of MHD activity to plasma current, density, temperature profiles, magnetic field, impurity levels, working gas and any other parameters which can be identified. Compare to theory.

(5) Pay particular attention to determining which modes, if any, play a role in major disruptions. Because of the unpredictable nature of these events, it is almost imperative that we have the capability of studying the entire duration of a plasma shot with relatively fast time response—$O(100\mu\text{sec})$.

(6) Verify the applicability of resistive MHD tearing theory to a real fusion plasma, especially disruptions, and document any discrepancies that are found.

(7) Determine the feasibility of feedback stabilization schemes based upon the successes or failures of the present MHD tearing mode theory.

III.2 Magnetic pickup coils

In the introduction two primary means of measuring tearing mode activity are mentioned, and both rely on the rotation of magnetic islands and the perturbations in equilibrium quantities which result. The easiest way is to detect fluctuations in the poloidal magnetic field with simple pickup coils arranged around a poloidal cross-section (Mirnov loops) as shown in Fig. 13. Because of vacuum compatibility requirements, the coils on Alcator C were situated outside the vacuum vessel liner during the initial construction of the machine. This does not present any problems with loss of sensitivity however, because the stainless steel liner is only a millimeter thick near the coils and attenuates magnetic field by about 30% at a frequency of 25 kHz. (From preliminary investigation the rotation frequencies of magnetic islands on Alcator C were found to be within the range: $5 \leq \nu_m \leq 30$ kHz.) The liner is relatively close to the plasma surface, permitting the pickup coils to be about 4 cm from the edge of the 16 cm-radius plasma. This gives an additional $1/r$ falloff of the field on the order of 50%, depending on the exact radial location of the perturbed currents.

As shown in Fig. 13, there are twelve coils wound around a flexible non-conducting belt—each coil having an angular extent of 30° and consisting of many turns[56]. Also on the machine are a set of loops which were each intended to be orthogonal to all but one $m$-mode. These coils should have been built with a winding density proportional to $\cos(m\theta)$, but instead they were wound with a square wave pattern. This defeated their purpose since for example, the intended $m = 2$ coil would actually be sensitive to all even-$m$ modes. Since there are only twelve individual loops in the $\theta$-direction, the highest mode number which can be accurately detected is $m = 6$. There are actually two identical sets of these coil belts spaced 120° apart in the toroidal direction, in principle enabling one to distinguish between the toroidal mode numbers $n = 1$ and $n = 2$, assuming that the higher $n$-modes are not excited. The Mirnov coils were calibrated in bench tests and found to have a sensitivity of $7 \times 10^{-3}$ volt-sec/Tesla and a frequency response better than 100 kHz. For an oscillation at 10 kHz, each coil would output about 44 millivolts/gauss. Calibration in place on the fully assembled tokamak was also done using the 60 Hz liner current. This test provided a fairly

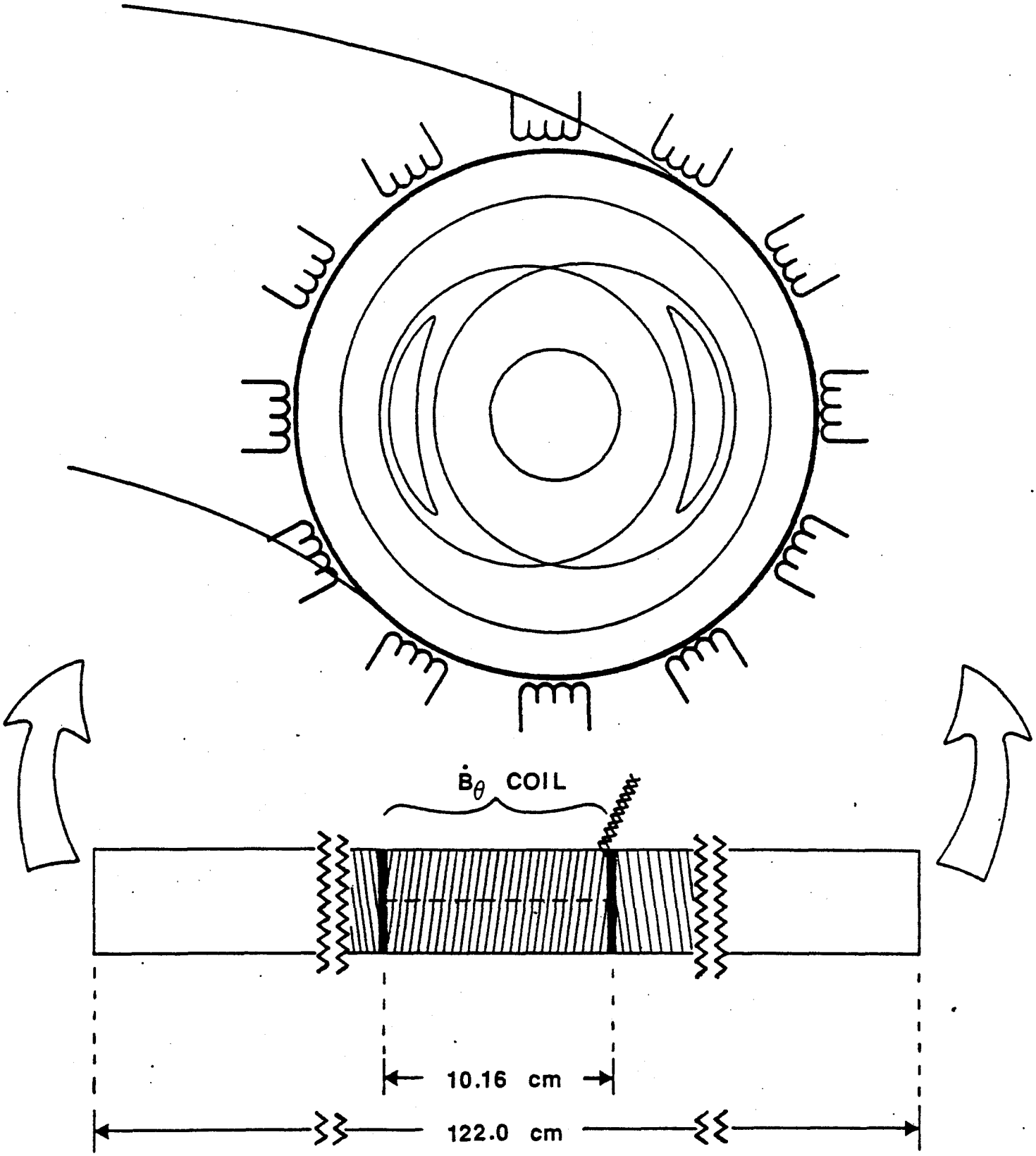


FIG. 13 — Schematic diagram of the $\dot{B}_\theta$ pickup coils used by the $m$-spectrum analyzer on Alcator C. The twelve coils are wound around a flexible belt which, in turn, is wrapped around a poloidal circumference of the vacuum vessel.

quantitative measurement of the toroidal effects on individual loop sensitivities, as seen in Fig. 14. As a consequence of the bellows construction the liner current density should be roughly uniform in $\theta$ and therefore the inner coil should measure a higher poloidal field, and the outer coil should measure a lower field than the average, with the variation having an amplitude on the order of $r_{coil}/R = 30\%$. The calibration data shows the expected $\cos(\theta)$ dependence with an amplitude of 28%. Subtracting out this effect leaves a coil-to-coil variation of less than 5% in sensitivity, which is quite acceptable for our purpose.

Up until now, the technique for measuring $m$-mode numbers consisted of photographing or digitizing the voltage signals from all the pickup loops available and then plotting the fluctuation amplitude on a polar graph, as shown in Fig. 3. However, if we wish to achieve the stated objectives of this thesis, then this simple method becomes impractical because of the tremendous amount of data which must be collected. In order to accurately map out an island rotating at 25 kHz, it would be necessary to digitize each signal at a minimum rate of about 100 kHz. (Photography would be out of the question.) With twelve probes and a nominal discharge duration of 500 milliseconds, this would result in more than a half-megaword of data for a single shot. This is about twice the total collected for all other experiments on Alcator C and would strain our present data archiving systems far beyond their capacities. And that would only be the beginning of the logistical problems. Processing such huge volumes of information to detect the $m$-mode structures would be impossible between shots, and would even be difficult between runs.

This raises another interesting problem concerning the actual methods used to label the $m$-number of the measured perturbations. If only one pure mode exists, then it is possible to identify its poloidal mode number from visual inspection of the polar graphs. But if two or more modes are present at the same time, then the polar graph will be distorted and may not be clearly identifiable as any one mode. Careful examination of Fig. 3 bears this out. Other modes probably exist even for the $m = 2, 3$, and 4 graphs. Obviously the proper procedure for determining $m$-numbers is to take the Fourier transform of $\dot{B}_\theta(\theta)$ from $\theta = 0$ to $2\pi$. In principle this would give the amplitude of each mode present (up to $m = 6$) and the

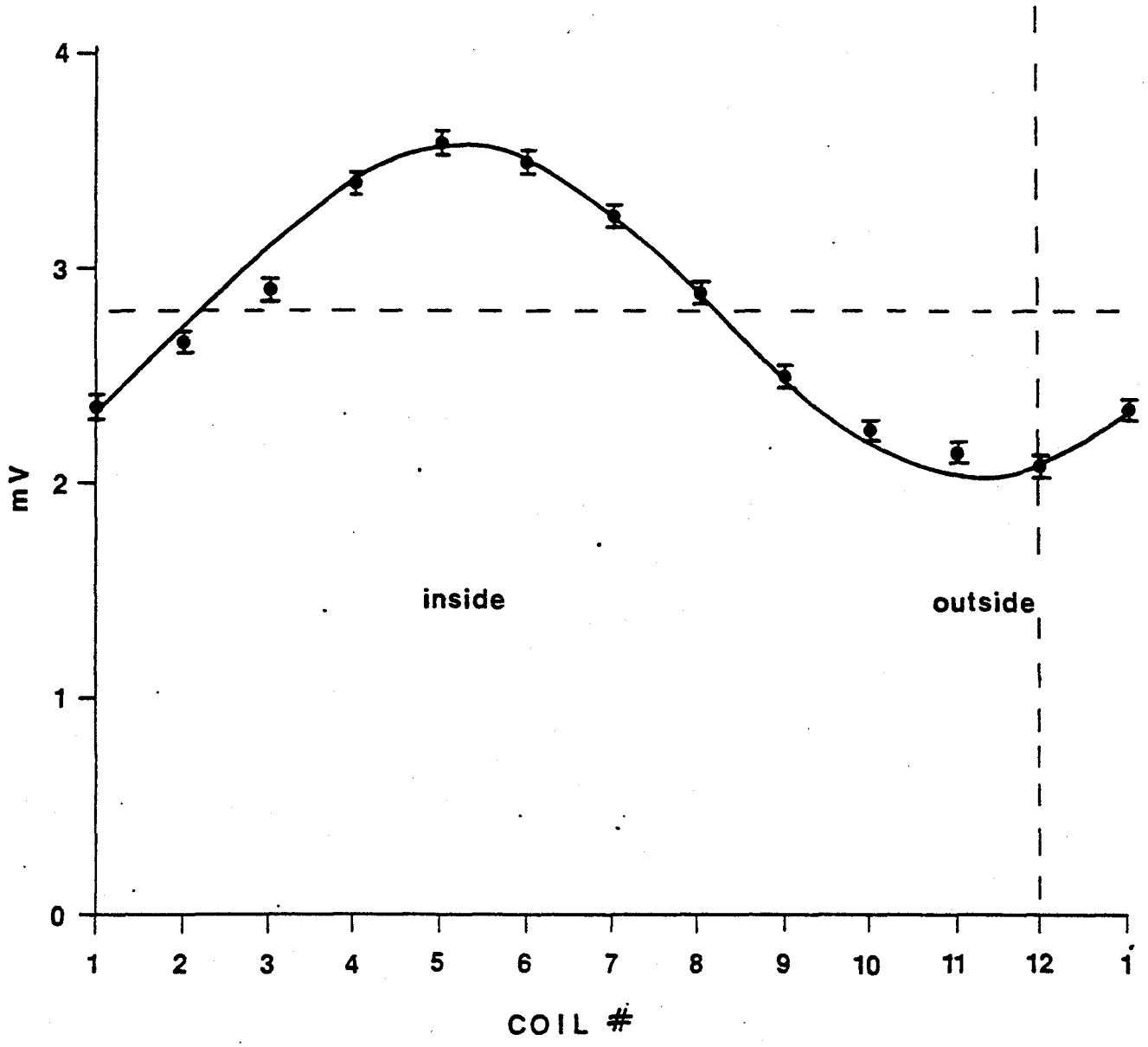


FIG. 14 — Calibration of coil sensitivity. The sinusoidal variation is due to the toroidal geometry.

rotation phase between modes, although for this study, only the magnitude of the Fourier transform is needed to satisfy our objectives. Further difficulty arises in sorting out the individual rotation frequency of each mode from loops which superpose the oscillations from all modes present. A scheme which also makes use of the Fourier transform was developed and will be explained shortly.

### III.3 The multiplexing concept

For all of the above reasons a new instrument, now called the "$m$-spectrum analyzer", was envisioned which would monitor the twelve individual pickup coils and output the amplitudes and rotation frequencies for each of the $m = 1, 2, 3, 4$, and 5 modes *in real time* and for the entire duration of the discharge[57]. This would virtually eliminate the digital data processing requirements and reduce the data acquisition requirements by more than an order of magnitude, since the ten channels of refined output need only be digitized at 10 kHz for 0.5 seconds, yielding only 50K words.

The basic idea is to use analog circuitry to get a readout of $\dot{B}_\theta(\theta)$ on a very short "framing" time compared to island rotation and to repeat these "frames" of $\dot{B}_\theta(\theta)$ at very fast rates. The series of frames must then be Fourier analyzed by more analog logic to get the amplitude of each $e^{im\theta}$ term in the series. These frames are taken by the technique of multiplexing. A digitally controlled solid state switcher samples and outputs each probe voltage for 500 nanoseconds before switching to the next probe signal. The multiplexer samples all the way around poloidally, outputting the twelve loop signals sequentially in 6 $\mu$sec, thus yielding a single frame of $\dot{B}_\theta(\theta)$. This process is repeated continuously so that the framing rate is about 167 kHz. There is a reason for such rapid multiplexing—it is desirable to have a snapshot of $\dot{B}_\theta(\theta)$ which is not significantly blurred by mode rotation. The frame rate of 167 kHz is about an order of magnitude faster than the typical oscillation frequency of 10 or 20 kHz, and therefore satisfies our criteria. Even faster multiplexing may be desirable, but 500 nanosecond switching time was state-of-the-art for commercially available monolithic, multi-input chips at the time the $m$-spectrum analyzer was designed.

Before any of the twelve loop signals enter the multiplexer, they must be filtered to get rid of the quasi d.c. level due to the large, slowly changing bulk plasma current. In addition, the Alcator C power supplies have relatively large noise levels arising from the rectification of the 360 Hz primary power lines. Appreciable noise exists even at higher harmonics of 360 Hz and at the 60 Hz sub-harmonics, so the pickup signals are first passed through single-pole highpass RC filters with a 3 dB frequency of 3 kHz. Since the filter transform falls off only as $1/\omega$, islands rotating at rates as slow as 1 or 2 kHz should still be seen even though their measured amplitudes will be somewhat attenuated. At the high frequency end, lowpass RC filters are used to get rid of noise above 50 kHz which may be due to such things as RF pickup, thermal fluctuations, etc. and then the signals are amplified by a factor of 10. Ultimately the baseline noise level which limits signal sensitivity is due to the 360 Hz power supply noise on the vertical field and ohmic heating windings, which the pickup coils are particularly sensitive to. The nominal measured noise level during actual plasma discharges corresponds to a sensitivity of about 6 gauss-kHz. Thus for a 10 kHz oscillation, the $m$-spectrum analyzer can detect perturbation levels as low as $\sim\frac{1}{2}$ gauss.

If a pure, solitary $m = 1$ mode was present and rotating at a negligible rate (compared to the multiplexing frequency) then the output from an ideal multiplexer would look like the waveform shown in the upper half of Fig. 15. (The phase is arbitrary.) As the multiplexer samples around in $\theta$, it would detect a single sinusoidal variation in $\dot{B}_\theta$. The sharp jumps which occur where the ideal multiplexer switches between sampled signals gives rise to an artificial $m = 12$ component plus its higher harmonics, so this does not interfere with the modes of interest to us. Of course for the actual non-ideal multiplexer used in the $m$-spectrum analyzer, the settling time is 100 to 200 nanoseconds, so the real output trace for a pure, solitary $m = 1$ perturbation is somewhat smoother than that pictured. Since the multiplexer continues cycling around $\theta$, the exhibited waveform for such a hypothetical mode would repeat its sinusoidal shape over and over again. The result is a 167 kHz sine wave with smaller 2 MHz and higher harmonics superposed. If a pure, solitary $m = 2$ set of magnetic islands was present and rotating at a negligible rate (rotation can not be

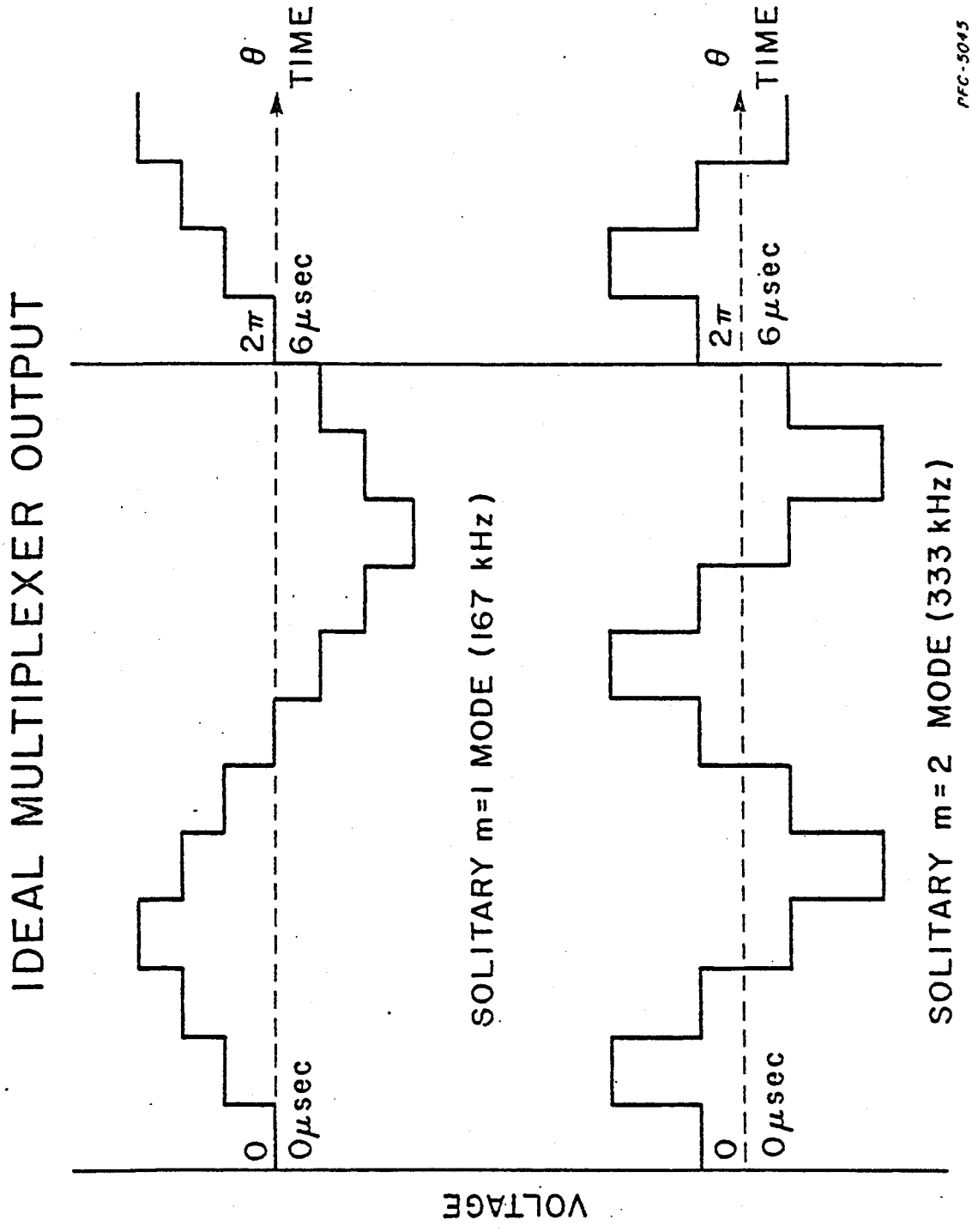


FIG. 15 — Signal output from an ideal multiplexer for an $m = 1$ and an $m = 2$ mode.

completely ignored since then the pickup coils would not see any fluctuations), the output of the ideal multiplexer would be the signal shown in the lower half of Fig. 15, since two islands exist around the poloidal cross-section. Because the multiplexer samples around continuously, the resulting waveform for this hypothetical case would be a sine wave at twice the basic multiplexing frequency, or 333 kHz, plus the 2 MHz and higher harmonics from the switching noise superposed on top. Similarly for any pure, solitary tearing instability of mode number "$m$", up to $m = 6$, the multiplexer output is a sinusoidal waveform with frequency:

$$\nu_m = \frac{m}{6} \text{ MHz} \tag{66}$$

plus 2 MHz and higher frequency noise superposed on top.

The analog circuitry of the $m$-spectrum analyzer as described so far is linear in $B_\theta$. If the constraint of having a solitary $m$-mode in the plasma is removed and several different modes now exist simultaneously, the output of the multiplexer is a more complicated waveform. But since it is a linear device, the net signal is a superposition of two or more arbitrarily phased waves characterized by equation (66) plus the higher multi-megahertz switching noise. The Fourier transform from d.c. to 1 MHz of the multiplexer output signal would consist of a series of $\delta$-function-like spikes at the $\nu_m$'s present in the plasma. The amplitude of each $\nu_m$ peak would be proportional to the amplitude of $\dot{B}_\theta$ for that $m$-mode. It makes no difference whether or not magnetic islands of different helicities have different rotation frequencies. The only hypothetical assumption which has been entailed is that the mode frequencies are negligible compared to the basic multiplexing rate.

For testing purposes, the inputs to the $m$-spectrum analyzer circuitry were artificially set up with various patterns to check the output of the multiplexer. Figure 16 shows the frequency spectrum for one such test pattern. In this case, eleven coil inputs were grounded and the remaining input was held at a constant positive voltage. The output of the multiplexer is a pulse train and the Fourier transform should be a series of spikes consisting of the fundamental at 167 kHz corresponding to $m = 1$, and all of the higher $m$ harmonics

slowly decreasing in amplitude. Figure 16 also gives an idea of how narrow the peaks are. In this spectrum the widths were limited by the resolution setting on the analyzing instrument and is essentially due to the length of time the pulse train is monitored. If the sweep rate of the analyzer were increased (decreased), the spikes would become broader (narrower). It is possible to take the Tektronix spectrum analyzer used for these tests and adapt it for use with the multiplexer in measuring $m$-mode amplitudes during plasma discharges. But a serious problem arises with time response. In order to reasonably resolve the individual frequency (or $m$) peaks over the range shown in Fig. 16, the sweep rate must be set at 50 msec per scan. This is not a fault of the instrument; it is a fundamental limit which can be derived from statistical arguments involving standard deviations and the number of cycles which must be counted to get the necessary resolution. A scan time of 50 msec is too slow however, since this would mean that only about 10 measurements of each mode amplitude could be made during a typical plasma shot. Another consequence of the slow scan time is that no simultaneous measurement of different $m$-modes can be made due to the time difference of $\sim$10 msec between the scans of adjacent mode peaks.

The problem could be solved by just using brute force—purchase many frequency analyzers and set up each one to scan a small region of frequencies within the 0 — 1 MHz range of interest. Although this scenario is both expensive and wasteful, the basic idea is correct and can be implemented in a much simpler, efficient way. Because of the periodicity in $\theta$, we already know that we are only concerned with narrow bands in frequency space centered around the $\nu_m$'s specified by equation (66). (It is important to keep in mind that these frequencies corresponding to different $m$ numbers are determined predominantly by the digital clock which controls the multiplexer switching speed and not by island rotation as long as it is relatively slow.) Instead of using a frequency analyzer adjusted to scan each harmonic band, it would suffice to use very narrow bandpass filters. In fact, for the $m$-spectrum analyzer we use five very high-Q, custom-made passive bandpass filters centered on the $m = 1, 2, 3, 4$, and 5 modes. Each one has a 3 dB width of $\pm 15\%$ of $\nu_m$ and attenuates the input by 50 dB at $0.73\nu_m$ and $1.31\nu_m$. Even with these tight tolerances, one can see

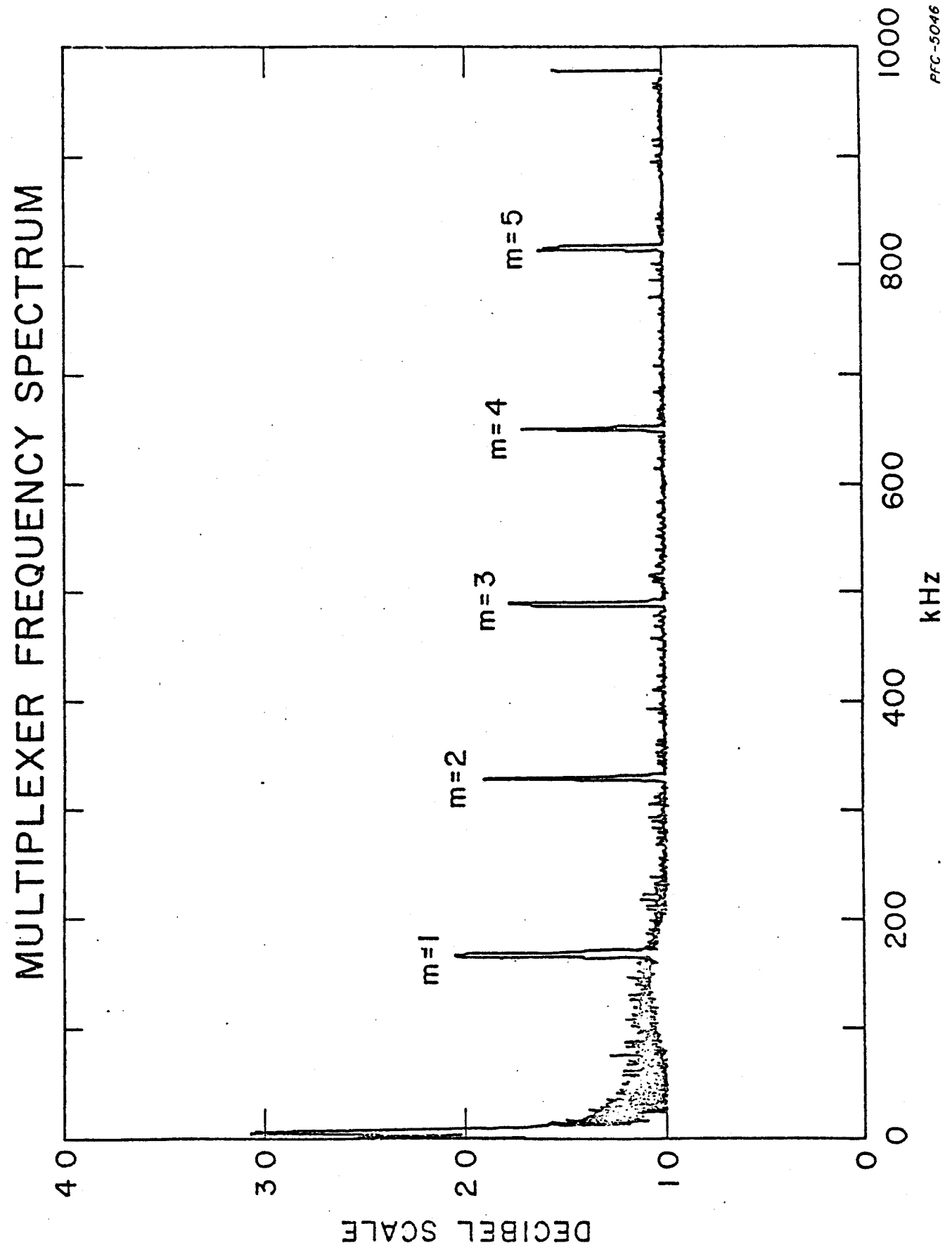


FIG. 16 — Frequency spectrum of multiplexer output.

that the $m = 5$ channel will pickup roughly one or two percent of the $m = 4$ and $m = 6$ signals. The output of each bandpass filter is a sine wave with an amplitude proportional to that of $\dot{B}_0$ for each resistive tearing mode. Simple peak follower circuits will convert the output of the bandpass filters directly into signals which are proportional to the amplitudes of the $\dot{B}_0$'s for each $m$-mode.

In theory the $m$-spectrum analyzer should be able to accurately follow changes in mode amplitude as long as the growth and decay rates are much slower than the multiplexing frequency. In section II.2, the tearing mode growth rates were derived for both the initial linear regime and the more important non-linear regime; and for the parameters relevant to Alcator C, the time scale for macroscopic amplitude changes is on the order of a millisecond, which certainly satisfies the time response criterion. In order to reduce "droop" noise, the peak followers were adjusted to permit the tracking of oscillations up to a frequency of 15 kHz before appreciable distortion sets in. As part of the initial testing program the frequency response and linearity to changes in $\dot{B}_0$ amplitude were measured for the $m = 2$ channel with another artificially inputted test pattern. Eleven coil inputs were again grounded, but this time the twelfth multiplexer input was connected to a signal generator and the voltage was varied with several different waveforms at frequencies from d.c. to 10 kHz. Excellent linearity was observed even with a bipolar triangular oscillation of the amplitude at 10 kHz. The $m$-spectrum analyzer accurately rectified the signals and showed negligible distortion at the crossover points.

### III.4 Measurement of tearing mode rotation frequencies

Figure 17 shows a block diagram of the $m$-spectrum analyzer illustrating the components which have been discussed so far. Also labelled in the diagram is a stage for measuring the rotation frequencies of each mode. Up until now we have neglected any motion of the magnetic islands except to admit that this is what causes the fluctuations picked up by the Mirnov loops. We now allow a finite rotation frequency while continuing to insist that the rate be much less than the basic multiplexing rate. As stated previously, this criterion

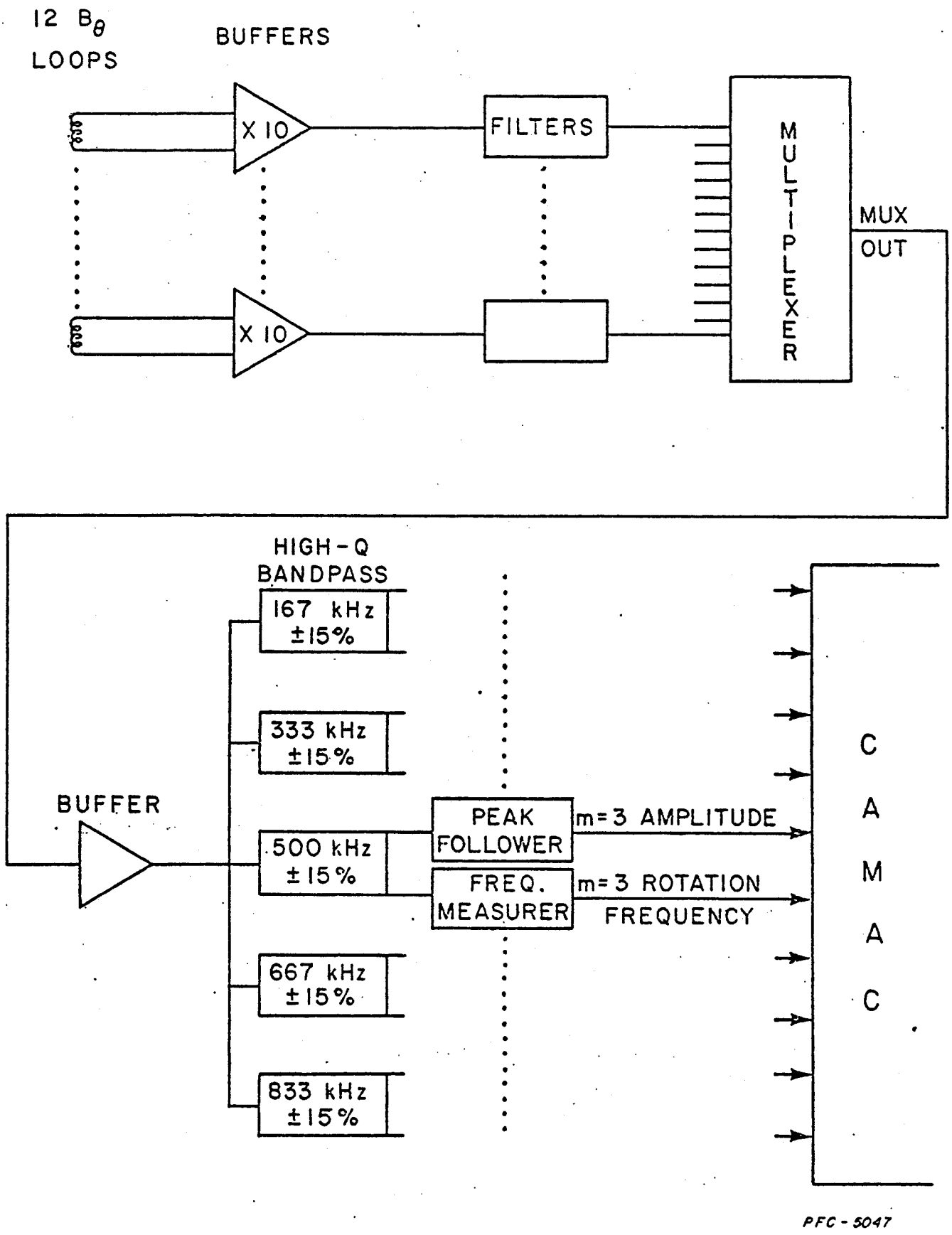


FIG. 17 — Block diagram of the *m*-spectrum analyzer.

is well satisfied in Alcator C, with a maximum measured ratio of $10 - 12\%$. Imagine an $m = 1$ magnetic island rotating with a period of $t$ $\mu$sec in the direction opposite from the multiplexing direction. As it samples from the peak of the island, around the poloidal circumference, the multiplexer will hit the peak again sooner than the $6\,\mu$sec required for a complete revolution. The measured period will be $\sim 6(1 - 6/t)\,\mu$sec, yielding a multiplexer output frequency of:

$$\nu'_m = \nu_m + f_m \tag{67}$$

where $f_m$ is the observed frequency of mode $m$ and $\nu_m$ is given by equation (66). Similarly for a set of islands rotating in the opposite direction, the output frequency for mode $m$ will be reduced by $f_m$. This phenomenon is nothing more than the familiar Doppler shift. Referring to Fig. 16 we see that the effect of finite but slow mode rotation is to shift the spikes slightly left or right from the central frequency. Since the bandpass filters have a 3 dB width of $\pm 15\%$, the rotation speeds found on Alcator C will have no effect on the measured mode amplitudes because the Doppler shifted peaks still fit within the passband. Actually that is what led us to specify a filter width of $\pm 15\%$ in the first place. But the frequency shift can be easily measured with a hybrid frequency-to-voltage (F/V) converter circuit. The output of an F/V converter is an analog signal which is proportional to input frequency plus an offset. Both the constant of proportionality and the offset are adjustable within certain bounds so that the F/V resolution of a frequency shift can be set to be independent of the central frequency. For our experiment the logical transfer function for the bipolar frequency measuring circuit is:

$$+V_{max} \leftrightarrow \nu'_m = 15\% \text{ above } \nu_m$$

$$-V_{max} \leftrightarrow \nu'_m = 15\% \text{ below } \nu_m$$

for each mode $m$. Substituting in equations (66) and (67) and knowing a priori that $V_{max} = 5$ volts, the actual transfer function for the frequency circuits in the $m$-spectrum analyzer should be:

$$V_m(\text{volts}) = 0.2\frac{f_m(\text{kHz})}{m} \tag{68}$$

where $f_m$ is the observed frequency of mode $m$.

Only two frequency measuring boards were actually built and so they were designed to be compatible with any of the $m$-channels of interest. The input to the frequency measuring circuit is the sine wave emerging from one of the bandpass filters. This signal is turned into a square wave of TTL-level amplitude by a comparator which must be properly adjusted to discriminate against pickup generated from the tokamak power supplies. (Even so, the output of the frequency circuits is quite noisy for low level MHD activity.) The square wave is fed next into a digital counter which resets after $m$ counts. The value of $m$ can be set with dip switches on the pc board for any of the $m$-spectrum analyzer channels, and therefore the circuits meet the compatibility specifications. The effect of the counter is to divide the square wave frequency by $m$, resulting in a pulse train with a Doppler shifted frequency near the basic multiplexer rate. This signal is finally fed into the hybrid frequency-to-voltage converter which has its offset adjusted to subtract out the 167 kHz "carrier", leaving an output voltage proportional to just the magnetic island rotation rate. The gain is set to match equation (68).

A calibration of the two frequency boards was done in the completely assembled $m$-spectrum analyzer and the agreement with equation (68) was reasonable. However, Fig. 18 shows that the discrepancies are large enough to require the use of slightly different calibration coefficients for each $m$ mode and each frequency measuring board. These constants were determined by linear regression fits to the calibration data and they are utilized by the computer programs which process the $m$-spectrum analyzer frequency data. Of the five frequency measuring modules planned for the $m$-spectrum analyzer, three were never built because it was found that they were not needed. The reasons for this will be enumerated in section IV.

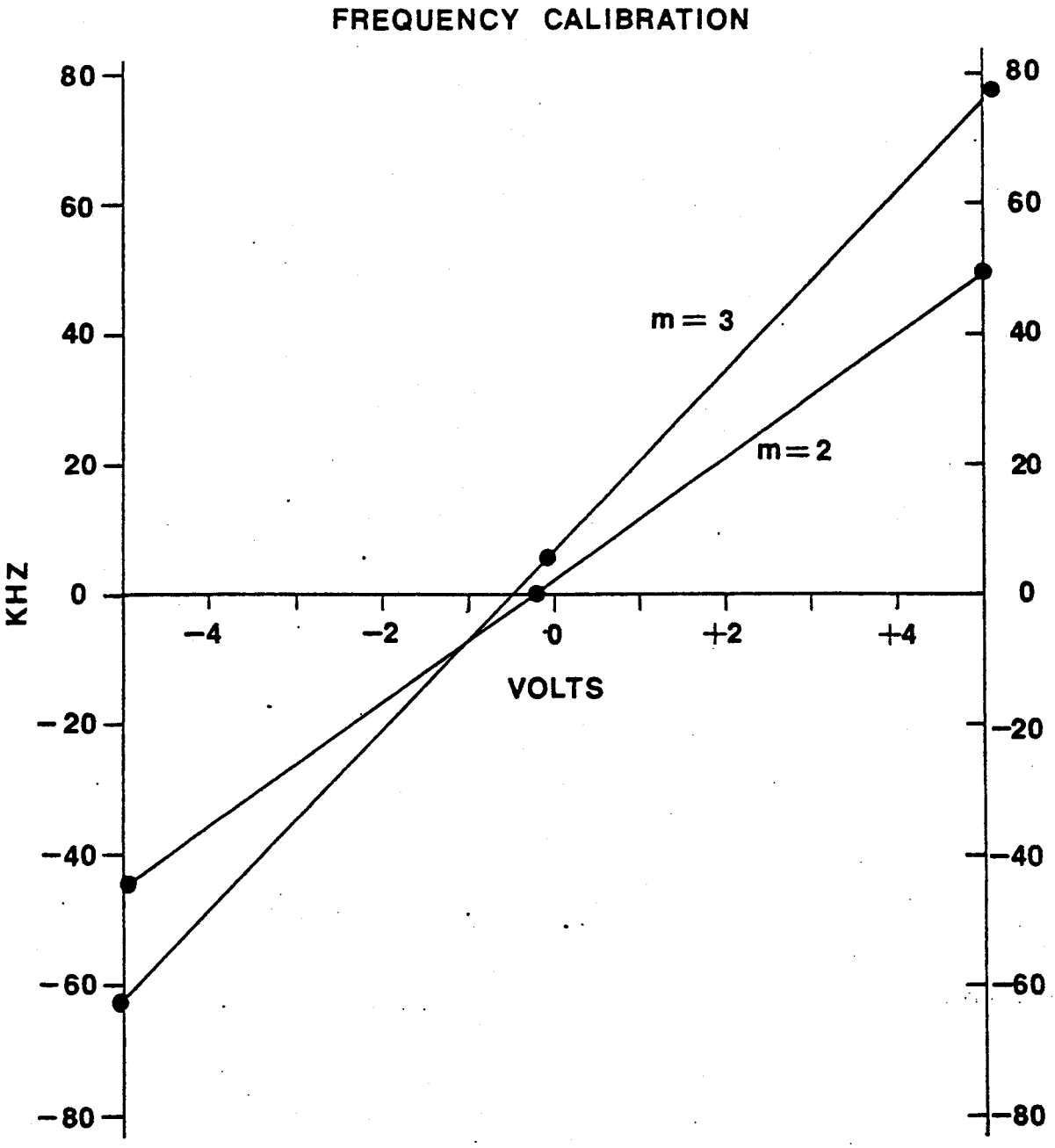


FIG. 18 — Calibration of the $m = 2$ and $m = 3$ frequency-measuring circuits.

III.5 Data acquisition systems

All of the amplitude and frequency data generated by the $m$-spectrum analyzer is digitized during each plasma shot by a 16-channel analog-to-digital converter CAMAC module in real time. Data acquisition starts 30 msec prior to initialization of the plasma current and continues for the entire duration of the discharge at a digitization rate of 10 kHz and with a resolution of 12 bits. (This corresponds to $\sim$2.5 mvolts for the A/D's range of -5 to +5 volts.) The digital data stream is temporarily stored in several CAMAC memory modules. During the five minutes or so between shots the memory is read out via our CAMAC serial highway network which is interfaced to a PDP11/55[58], and eventually winds up in files on magtape. Some of the data is immediately displayed at the experimenter's console for preliminary examination and cataloging purposes.

# IV. EXPERIMENTAL FINDINGS

## IV.1 More calibration and checkout

Although calibration of the individual $\dot{B}_\theta$ pickup loops had been done using the 60 Hz liner current, this technique would not suffice for measurement of the $m$-spectrum analyzer's total throughput sensitivity because the millivolt levels which are produced cannot be resolved from the overall electronic noise arising in the instrument. In addition, the ability of the $m$-spectrum analyzer to Fourier decompose mode numbers had never been tested with fluctuations having the superposed sinusoidal structures expected of actual tearing modes, such as shown in Fig. 15. Only patterns consisting of rectangular pulses could be generated for testing purposes. Both of these problems can be overcome by using the instrument in conjunction with the raw signals from the Mirnov coils during actual plasma discharges. Unfortunately the amount of data one would like to record from the loops is much greater than the resources of Alcator's archiving system permit. Even for this limited calibration check, only four pickup coils (chosen at 90° intervals around the poloidal circumference) could be monitored for just 800 $\mu$sec per shot. It was only possible to record the data on photographs, since there is no capability for digitizing data at the 50 — 100 kHz rates required for these oscillations. Rather large distortions in calculated mode structures can be caused by the inaccuracies inherent in making quantitative measurements from photographs. Under these constraints it is not possible to uniquely determine the poloidal mode numbers from the raw loop data. Nevertheless it is possible to do a consistency check—given the output of the $m$-spectrum analyzer, is it possible to construct magnetic island patterns which duplicate the coil data?

A typical example of this calibration data is shown in Fig. 19. The upper half is an oscillograph of the four $\dot{B}_\theta$ coils monitored and the lower half shows the corresponding mode amplitudes as measured by the $m$-spectrum analyzer for a well-behaved discharge. The $m$-spectrum analyzer output indicates the existence of two modes at 340 msec into the shot, namely $m = 2$ and $m = 3$ with an amplitude ratio of $\sim$0.4. The measured frequencies

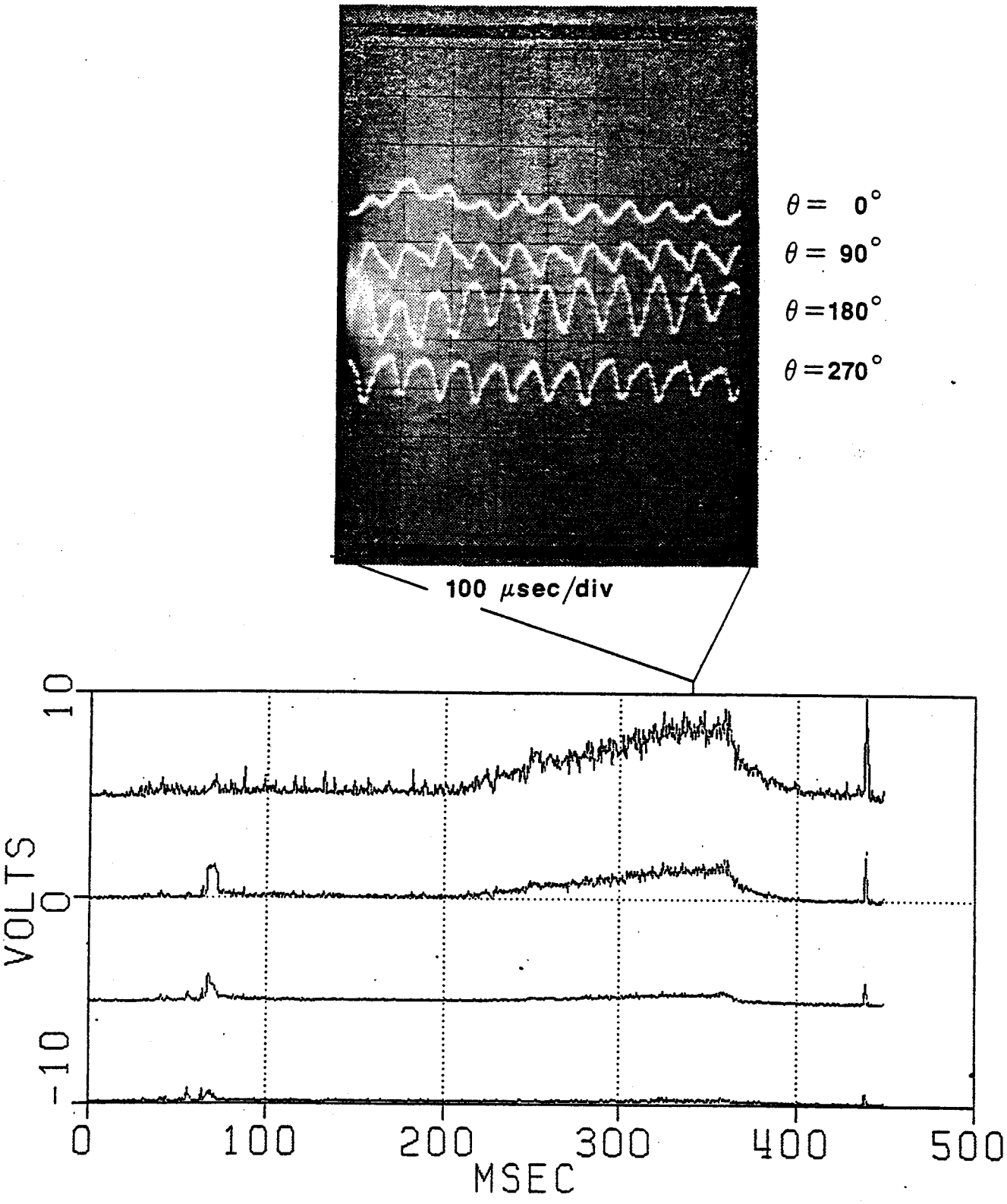


Fig. 19 — Comparison of $m$-spectrum analyzer findings with unprocessed signals from several pickup coils. The four loops are separated by 90° poloidally. The bottom graph shows the amplitude of $B_\theta$ for the $m = 2, 3, 4$ & 5 modes (top to bottom).

are 13.5 and 28 kHz respectively. Looking carefully at the coil signals, it is obvious that more than one mode must be present since the signals are not sinusoidal. By superposing just the measured $m = 2$ and $m = 3$ components with various phase shifts, the four raw coil signals can be matched fairly well. Such a fit was done and is shown in Fig. 20. The raw data from the coils was also used to check the overall gain of the $m$-spectrum analyzer. The calculated sensitivity should be 22.7 volts per kHz per gauss and a measurement of the photographic data gives $\sim$24. These tests indicate that the $m$-spectrum analyzer is working as planned, except for the $m = 1$ channel. That signal exhibits much more noise than the other channels and this might have been expected since the $m = 1$ should be strongly

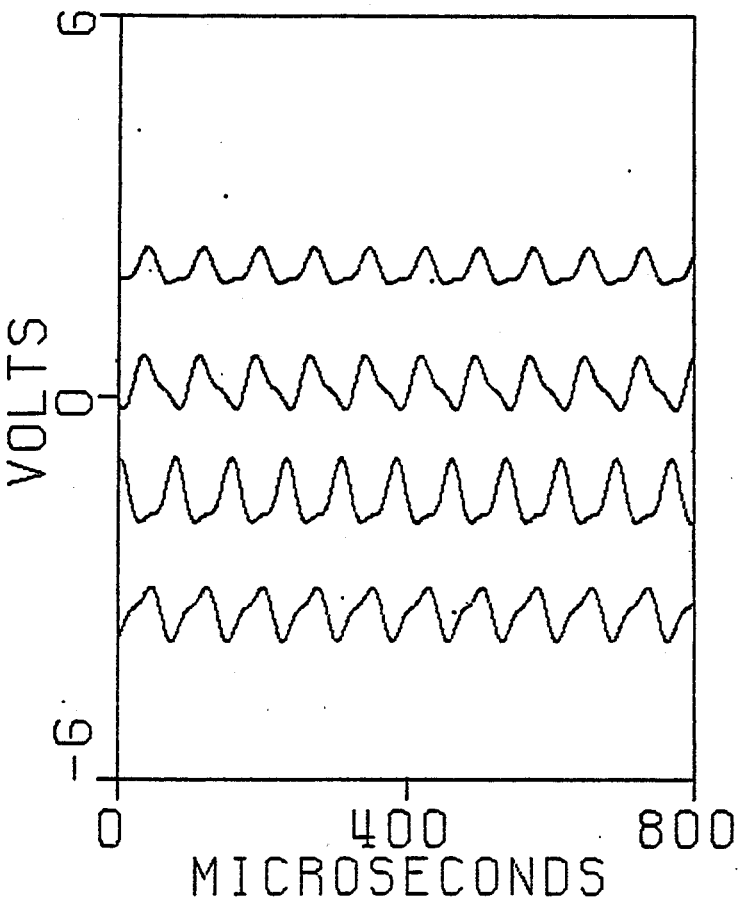


Fig. 20 — Signals generated by the superposition of an $m = 2$ and an $m = 3$ mode with $\nu_2 = 13$ kHz, $\nu_3 = 26$ kHz, $A_3/A_2 = 0.35$, and appropriate phasing. Compare to previous figure.

coupled to the O.H. and vertical field supplies through any 360 Hz in/out plasma motion. For this experiment the problem could not be rectified and so the $m = 1$ channel was not found to be too useful. Fortunately no $m = 1$ islands have been seen outside the $q = 1$ region anyway (with the soft x-ray imaging array) so this is probably not a great loss. A novel method for decoupling the toroidal effects of power supply noise will be discussed in the last section of the thesis.

## IV.2 MHD activity during current rise

The bulk of this thesis study is devoted to the portion of the plasma discharge where the current has reached its flattop level. However, a brief investigation of current rise phenomena has been carried out in order to compare this machine to the detailed findings on other tokamaks. On Alcator A and many other tokamaks a series of tearing modes is detected during the initial part of the discharge when the plasma current is rising to its steady state value. As mentioned in the introduction and pictured in Fig. 3, the series of modes consists of bursts of MHD activity of decreasing $m$-number which proportionately follow the decrease in $q$ at the limiter as the plasma current rises. The changeover from each value of $m$ to the next lower one is usually accompanied by clear signs of a minor disruption such as negative spikes on the loop voltage and/or quick changes in $\frac{dI_p}{dt}$. It is believed that this series of minor disruptions plays an important role in the current profile evolution. The rise time of the plasma current is much faster than the classical resistive or skin time, so the current density profiles should be hollow for a significant fraction of the shot. This is *not* what is usually observed in experiments[59] however, and the minor disruptions during the current rise could account for the anomalously fast current penetration.

In Alcator C, a curious phenomenon is observed. Although many shots exhibit the "typical" MHD behavior during the current rise, there are also large numbers of discharges which have no magnetic fluctuations above the background noise and show no signs of minor disruptions, although these two types of discharges may be quite similar in all other respects. Figs. 21 and 22 show examples of shots with and without tearing mode activity

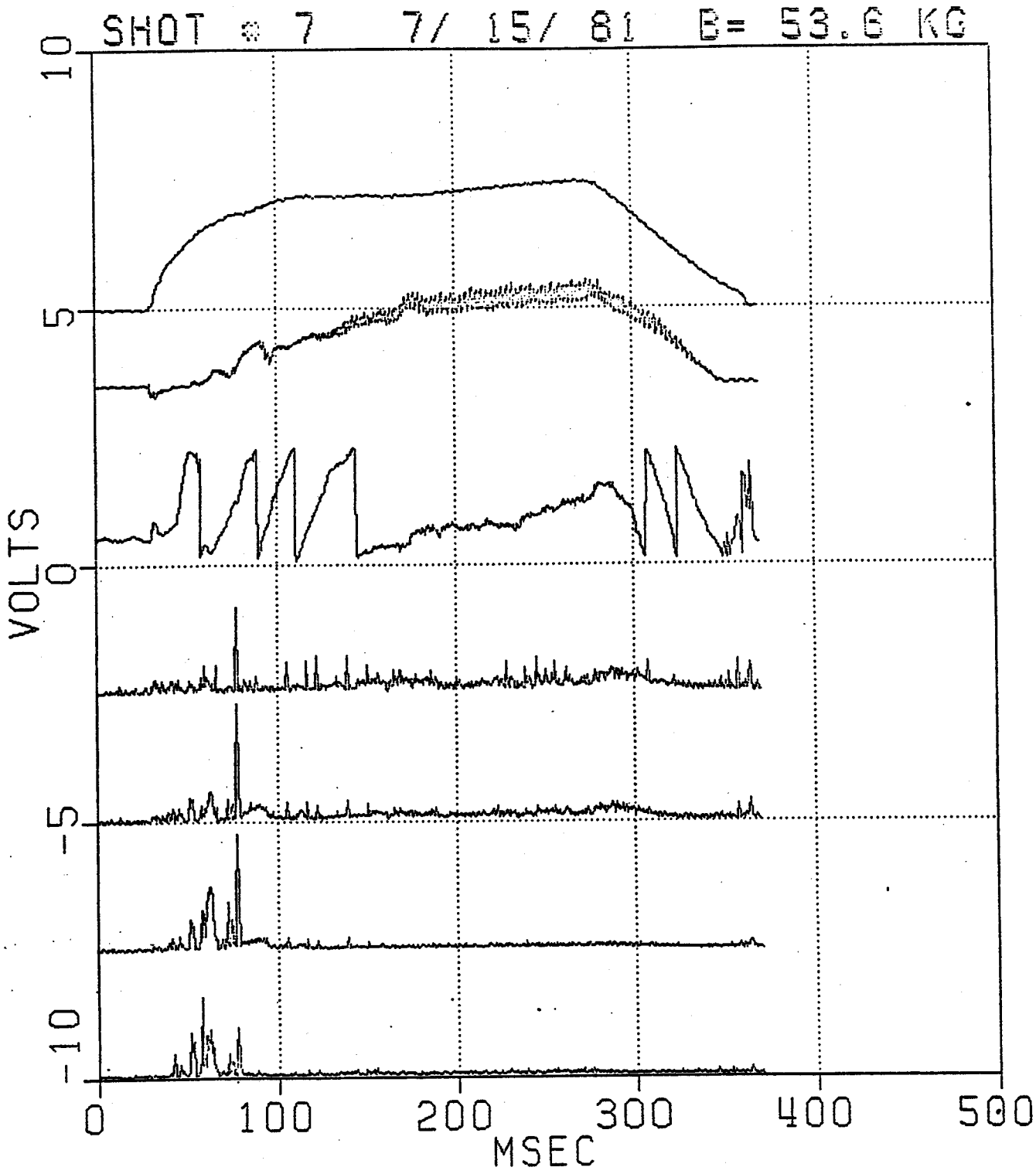


Fig. 21 — Typical discharge at 55 kG showing plasma current (125 ka/V), soft x-ray emission (central chord), line average density ($0.57 \times 10^{14}$ cm$^{-3}$/fringe), and $m = 2, 3, 4$ & 5 amplitudes (46 gauss-kHz/V). Note the bursts of MHD activity during the current rise period of 30-100 msec.

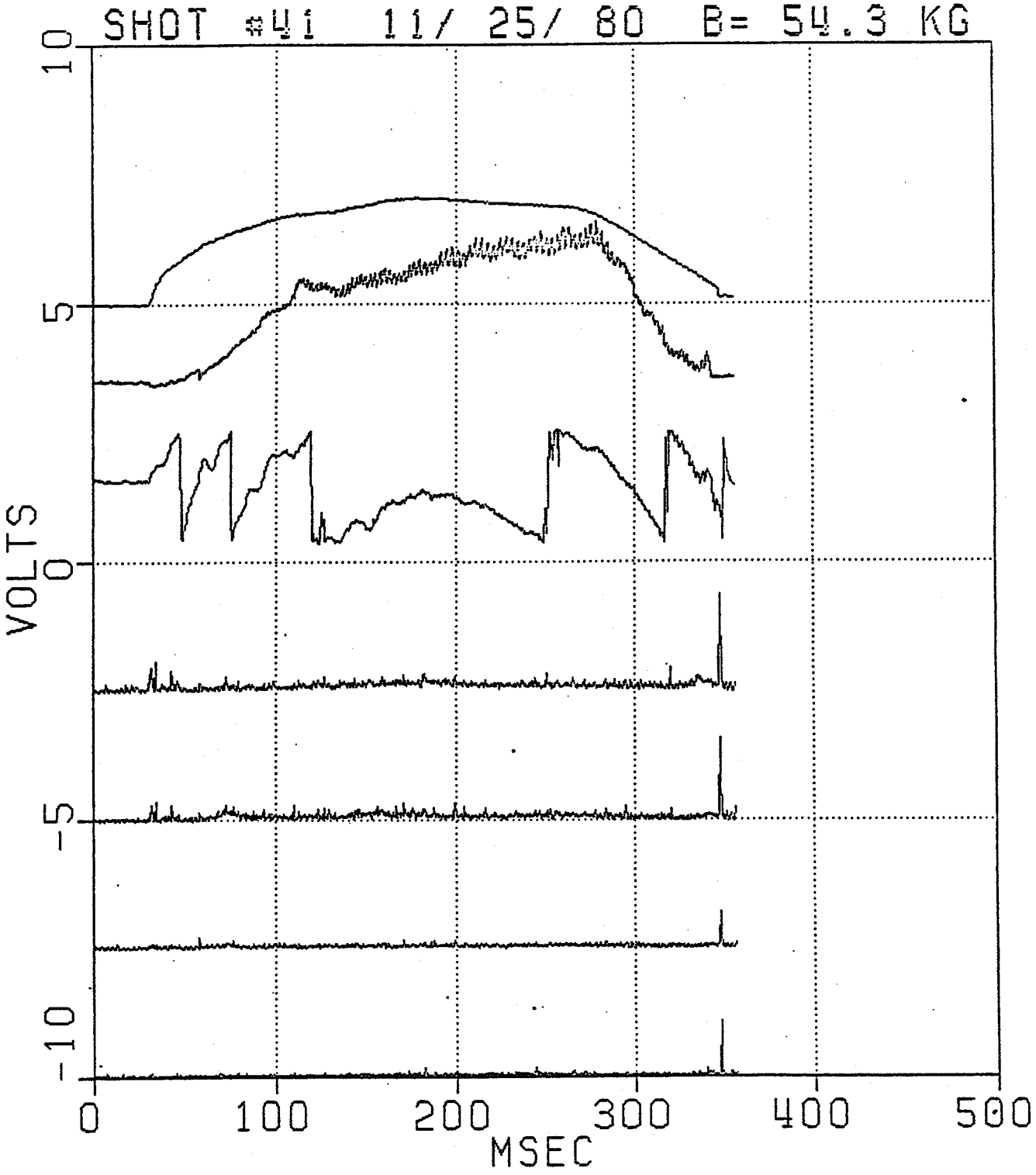


Fig. 22 — Similar discharge showing almost no MHD activity during current rise. All scales are the same as in previous figure.

during current rise under similar conditions. Pictured in both figures are the plasma current, soft x-ray emission (central chord), density, and the $m = 2, 3, 4$, and 5 channels of the $m$-spectrum analyzer. If there is any dependence of MHD activity on the operator's programming of the rate of current rise, it is indeed subtle. After the plasma current profile has reached a quasi-steady state, usually by $\sim$150 msec after commutation, there is no consistently observed difference between shots with current rise activity and shots without it—no enhanced impurity levels, no greater predisposition to disrupt, etc. It appears that MHD activity during current rise is not a requirement for well-formed plasmas in Alcator C.

Even on shots which do have measurable magnetic perturbations during the current rise, the $m$-spectrum analyzer nearly always detects several modes existing simultaneously, as shown in the expanded view in Fig. 23. One mode is sometimes larger than the others and as the current continues to rise, the dominate mode number usually changes, although not always in decreasing order. Even for those discharges in which the dominant mode number decreases monotonically during the current rise, the procession does not follow proportionately the decrease in $q$ at the limiter.

The detection of several simultaneous modes is not surprising in light of the non-ideal effects discussed in section II.5. Because of the toroidal geometry, even a pure $e^{im\theta}$ perturbation would be expected to have sideband modes, $m' = m \pm 1$ with an amplitude of $\sim$30% detected along with it. The $m$-spectrum analyzer measurements alone cannot distinguish unequivocally between the existence of a single mode or of several modes; it should presumably see several $m$-numbers any time MHD activity is detected.

### IV.3 MHD activity during steady state

In Alcator C the current rise phase usually lasts about 150 msec. By that time the soft x-ray emission normally has started sawtoothing, tending to regulate the temperature and current profiles near the central core. The second ohmic current power supply (O.H. 2) turns on at this point and typically does not raise the plasma current by more that

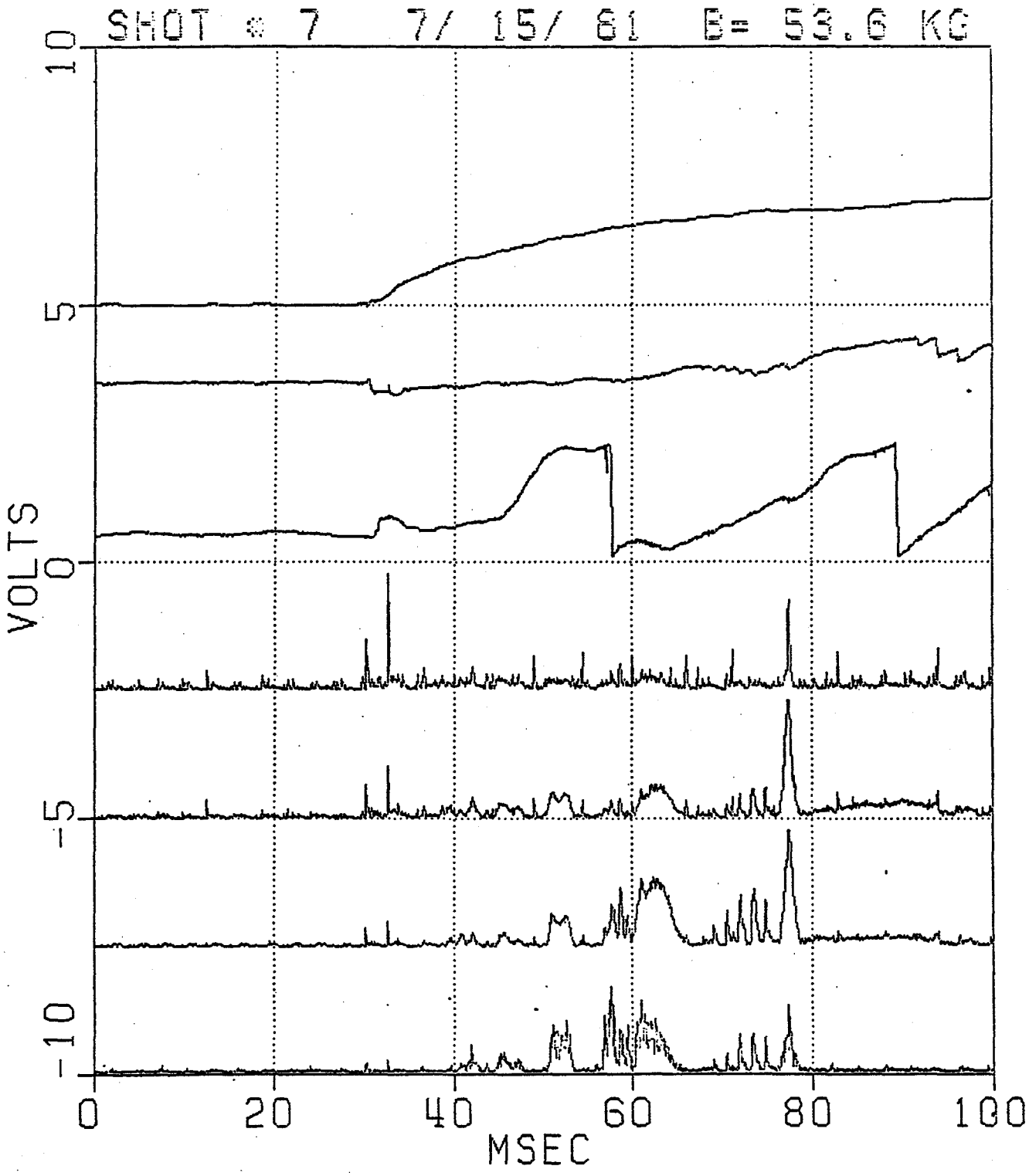


Fig. 23 — Expanded view of MHD activity during current rise. Note the simultaneous occurrence of several mode numbers.

15% during the rest of the discharge. The only macroscopic quantity which is usually programmed for substantial continued growth during the "steady state" is the plasma density. (The maximum density is an operator-programmable parameter and can be readily varied.) So the "steady state" is not really a steady state; I call it that because electron cyclotron measurements show that the electron temperature profiles are nearly constant over this time period, and presumably one can therefore conclude that the current density profile is also constant. As far as resistive tearing modes go, this should constitute a steady state, since the theoretical derivation of the stability parameter, $\Delta'$, depended only on the current profile and the toroidal magnetic field. As detailed in the introduction, on many large tokamak experiments this portion of the discharge is sometimes accompanied by a set of $m = 2/n = 1$ and $m = 3/n = 1$ or $m = 3/n = 2$ magnetic islands of macroscopic size observed with both Mirnov loops and soft x-ray detectors. In Alcator C, however, no activity is expected, at least during the steady state, because of the stabilizing effects of finite beta and/or radial diffusion. Even before the $m$-spectrum analyzer was installed on the machine, a lack of MHD activity (compared to Alcator A) was evident from cursory examination of the Mirnov loop signals. Once the $m$-spectrum analyzer went into operation in November 1980, this admittedly subjective observation was quantitatively verified for the densities which are commonly run. An example of the "average" Alcator C discharge is shown in Fig. 24. The term "average" applies to the characteristics of the MHD activity in this case. By far, most of the discharges have the MHD behavior depicted in this shot. Also, in terms of the parameter space that Alcator C has explored with respect to current, density, and magnetic field, the shot shown in Fig. 24 falls near the middle. The $m$-spectrum analyzer clearly shows that after the current rise phase, there are no measurable magnetic perturbations above the noise level ($\sim$6 gauss-kHz) for the rest of the shot.

Just because the $m$-spectrum analyzer shows no signals above the noise level during the current flattop does not immediately prove that magnetic islands do not exist in the plasma. This situation could also be realized if the islands are assumed to be stationary—i.e. not rotating. As mentioned previously, non-rotating perturbations would give no mag-

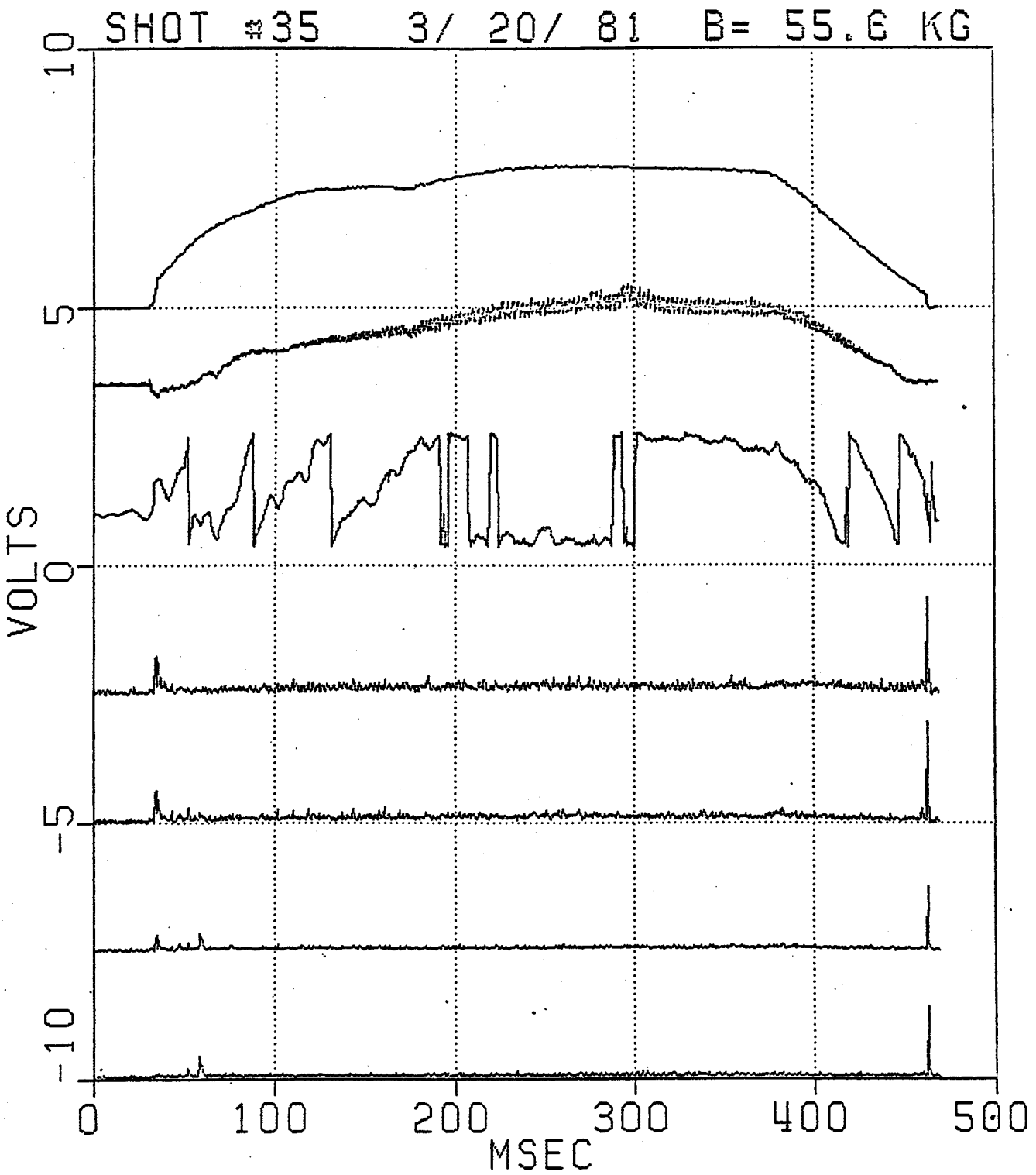


Fig. 24 — Typical Alcator C discharge at 55 kG in hydrogen. The data are presented in the same format as described previously. Note the sawtoothing x-ray emission and the lack of MHD activity after the current rise.

netic oscillations, and therefore no pickup signal on the inputs to the multiplexer. There is previous experimental evidence of such phenomena on other tokamaks. In Alcator A magnetic island oscillations are sometimes seen to slow down and become distorted as their amplitude gets larger[60]. Eventually the oscillations may even grind to a halt, although careful examination of the phase of the perturbation clearly shows that the island amplitude does not shrink during this process. Evidently rotating tearing modes which grow to large widths can "stick", apparently on an external asymmetric structure such as a limiter or magnetic field anomaly. Major disruptions have been observed up to tens of milliseconds after the halt in rotation and are assumed to be caused by continued pure growth of the instability. There is also data suggesting that large magnetic islands can even "unstick" and suddenly begin rotating again[22]. In these cases, phase and amplitude information indicate that the mode starts off from the same position and with about the same amplitude as when it first "stuck". So there is ample proof that non-rotating islands do occur in other tokamaks, but only after a tearing mode has grown to large amplitude. This is not the case in Alcator C, where normally no mode is seen at all during the current plateau. Nevertheless, the hypothesis of finite size non-rotating magnetic islands cannot be dismissed solely on the basis of the information in Fig. 24. There are other hints, however, that such a hypothesis might not be true. Large magnetic islands, even when standing still, would be expected to enhance the transport of energy across the separatrix width, and therefore the confinement time would decrease even in the presence of non-rotating islands. But at the densities shown, the energy confinement time is found to be increasing nearly linearly with density; i.e. it obeys the "Alcator scaling law"[61]. This probably indicates that the plasma transport processes are not being adversely affected by any undetectable magnetic islands.

In order to better understand the physical processes determining energy confinement, several of the operating parameters of the C machine have been varied over a wide range individually in an attempt to find how confinement time scales with density, current, magnetic field, safety factor, etc. During such a program at 55 kG, a surprising and unexpected behavior of MHD activity was discovered with the $m$-spectrum analyzer—a firm density

threshold. It is the most unique finding of this thesis experiment and this effect will be shown later to have an impact on the maximum densities which can be attained, as well as major disruptions.

At 55 kG, substantial numbers of discharges are run in both hydrogen and deuterium which reach densities well above those in "average" shots already displayed. Figure 25 shows a typical hydrogen plasma at this field, for which the line average density reaches a peak value of $3.0 \times 10^{14}$ cm$^{-3}$ (5.3 fringes). During the steady state portion of the discharge, and after the soft x-ray emission begins to sawtooth, measurable amplitudes on the $m = 2$ and $m = 3$ channels begin growing above the noise level. Coincidentally, when the MHD activity starts at $t = 205$ msec, the line average density is $2.4 \times 10^{14}$ cm$^{-3}$ (4.2 fringes). This peculiar feature is not expected from the resistive MHD theory presented in section II. But the behavior of the $m = 2$ and $m = 3$ amplitudes during the rest of the shot brings this theoretical prediction into question. As the density continues to rise above $2.4 \times 10^{14}$ cm$^{-3}$, the amplitude of the magnetic perturbations also increase, roughly linearly proportional to the amount by which the density surpasses 4.2 fringes. Similarly, as the density falls from its peak value, the MHD amplitudes also decline and eventually return to the noise level. By coincidence, the gains on the density trace and the $m$-spectrum analyzer channels are in the correct proportions to suggest a very strong coupling between the two, at least on this shot. The output of the $m = 4$ and $m = 5$ channels of the $m$-spectrum analyzer show much less activity; only the $m = 2$ and 3 modes have appreciable amplitude during the current flat-top. This precludes any notion that the apparent coupling of density to MHD activity is some kind of electronic cross-talk between data channels.

If the behavior in Fig. 25 occurred only on this shot, or only very rarely, then this phenomenon would still be interesting, but certainly would not indicate any serious deficiencies in the theoretical picture of resistive MHD physics. But surprisingly the basic characteristics typified in Fig. 25 are found to repeat over and over again in other 55 kG shots, provided that the central soft x-rays are sawtoothing. (This restriction tends to sort out the class of plasma discharges which are impurity dominated and very disruptive.

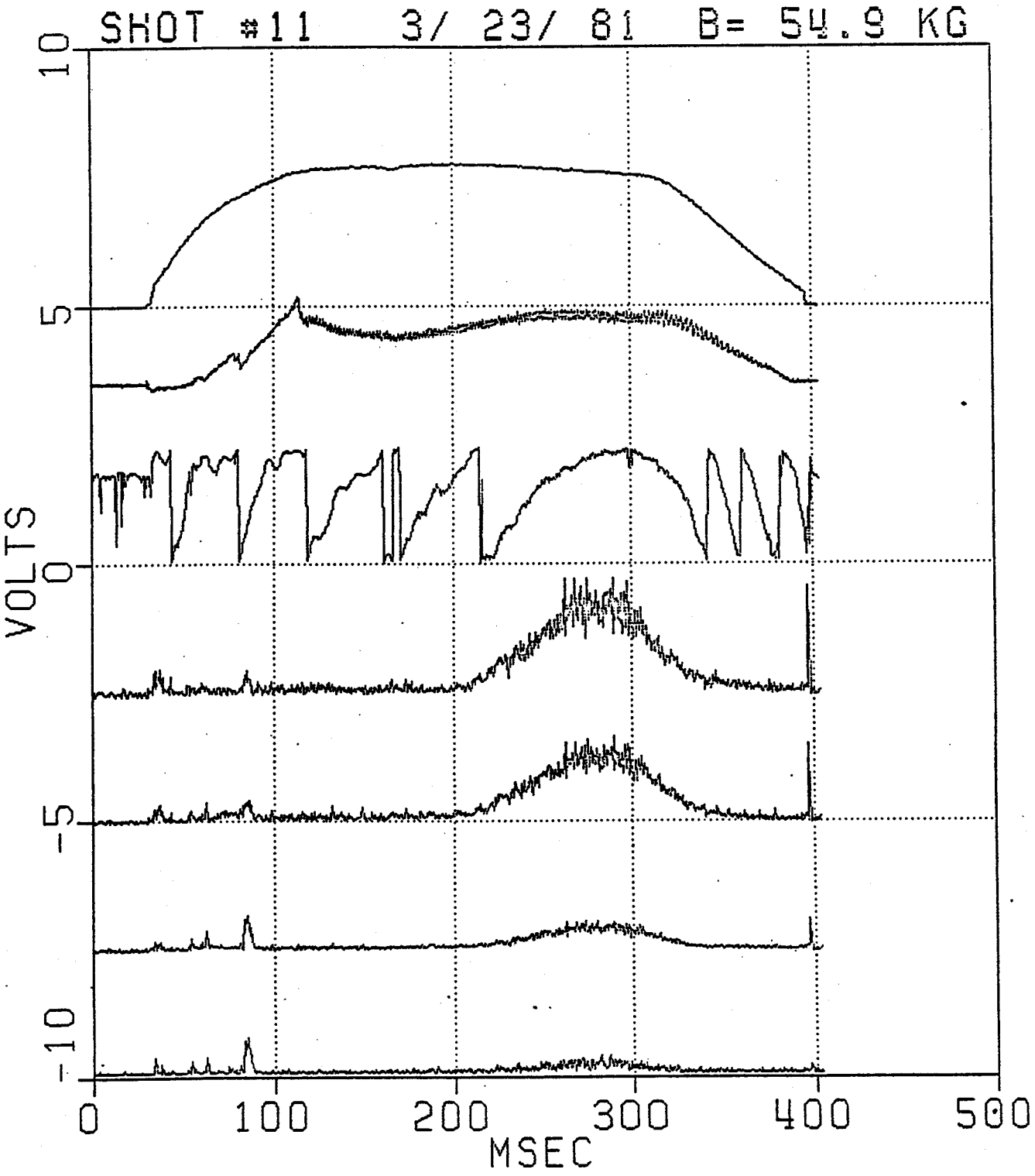


Fig. 25 — Hydrogen discharge at 55 kG which reached a higher density than the previously displayed shots. Note the start of $m = 2$ and 3 instabilities at $\sim$4.2 fringes. The mode amplitude seems to follow the increase and decrease in density above the threshold.

More will be said about these later in the thesis.) In fact, none of these 55 kG shots show measurable MHD activity after the current rise until higher densities are reached later in the discharge. A study of all the 55 kG sawtoothing shots recorded during the time the $m$-spectrum analyzer has been operating shows that whenever MHD activity starts during the steady state, it begins near a density of 4.2 fringes on at least 97% of the shots. Conversely, whenever the line average density goes above that value, measurable fluctuations invariably exist. And as depicted previously, only the $m = 2$ and 3 modes ever show appreciable amplitude after the current rise. This value of density therefore is found to be a threshold for MHD activity during the current plateau. Two additional examples of the threshold phenomenon are displayed in Figs. 26 and 27.

Table 1 lists the line average density at the start of MHD activity for a representative sample of hydrogen plasmas at 55 kG. Clearly the value of the threshold density, $\overline{n}_c$, is quite repeatable. A complete survey of all 55 kG data in hydrogen reveals a standard deviation in $\overline{n}_c$ of 0.4 fringes or only 10% (for sawtoothing discharges during the steady state). Table 2 shows sample density threshold data for another set of discharges under similar conditions—the only difference being that the ions are deuterium rather than hydrogen. The mean value of $\overline{n}_c$ is the same for both isotopes, however the variation around the mean is noticeably larger in deuterium, with a standard deviation of approximately 20%. These standard deviations are not due to experimental or instrumental errors since the interferometer trace can be read to $\pm 0.1$ fringes accurately. Of course, there is also a small degree of subjectivity involved in determining the time at which MHD activity "turns on". In all but a handful of shots, this leads to an uncertainty in $\overline{n}_c$ of only $\pm 0.1$ fringes. It is concluded, therefore, that even though the spread in the data is relatively small, it is statistically significant and presumably due to shot-to-shot variation of the plasma properties involved in tearing mode instabilities. Such variation is certainly plausible because of the substantial differences in such macroscopic quantities as the plasma current (and thus the limiter-$q$), which is also listed in Tables 1 and 2. In fact, if one hypothesizes that the MHD threshold effect is sensitive to internal parameters such as profile shapes, then the measured standard deviation of $\overline{n}_c$

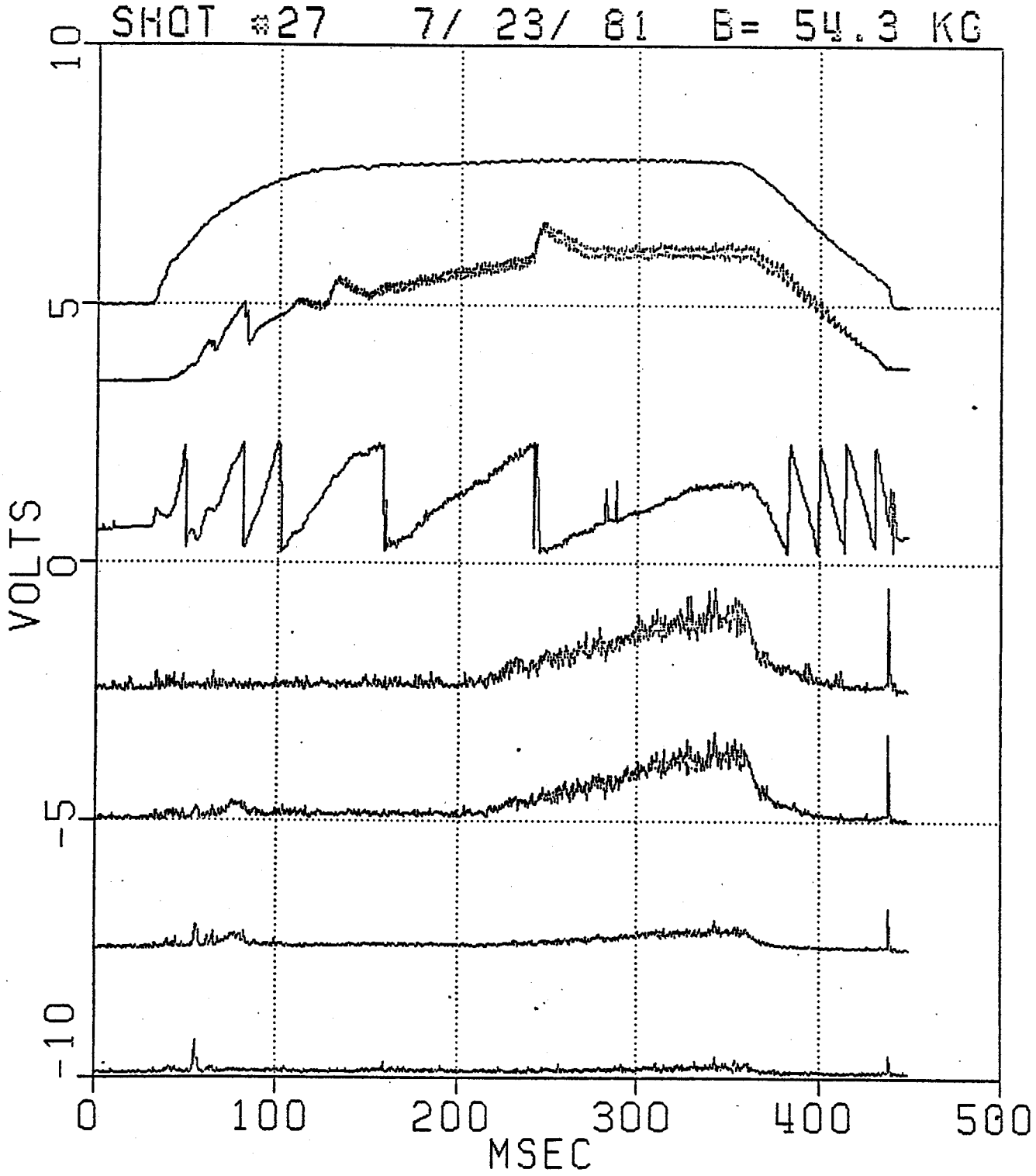


Fig. 26 — Another example of the density threshold effect for MHD activity in Alcator C. The value of $\bar{n}_c$ for this shot is ~4.3 fringes.

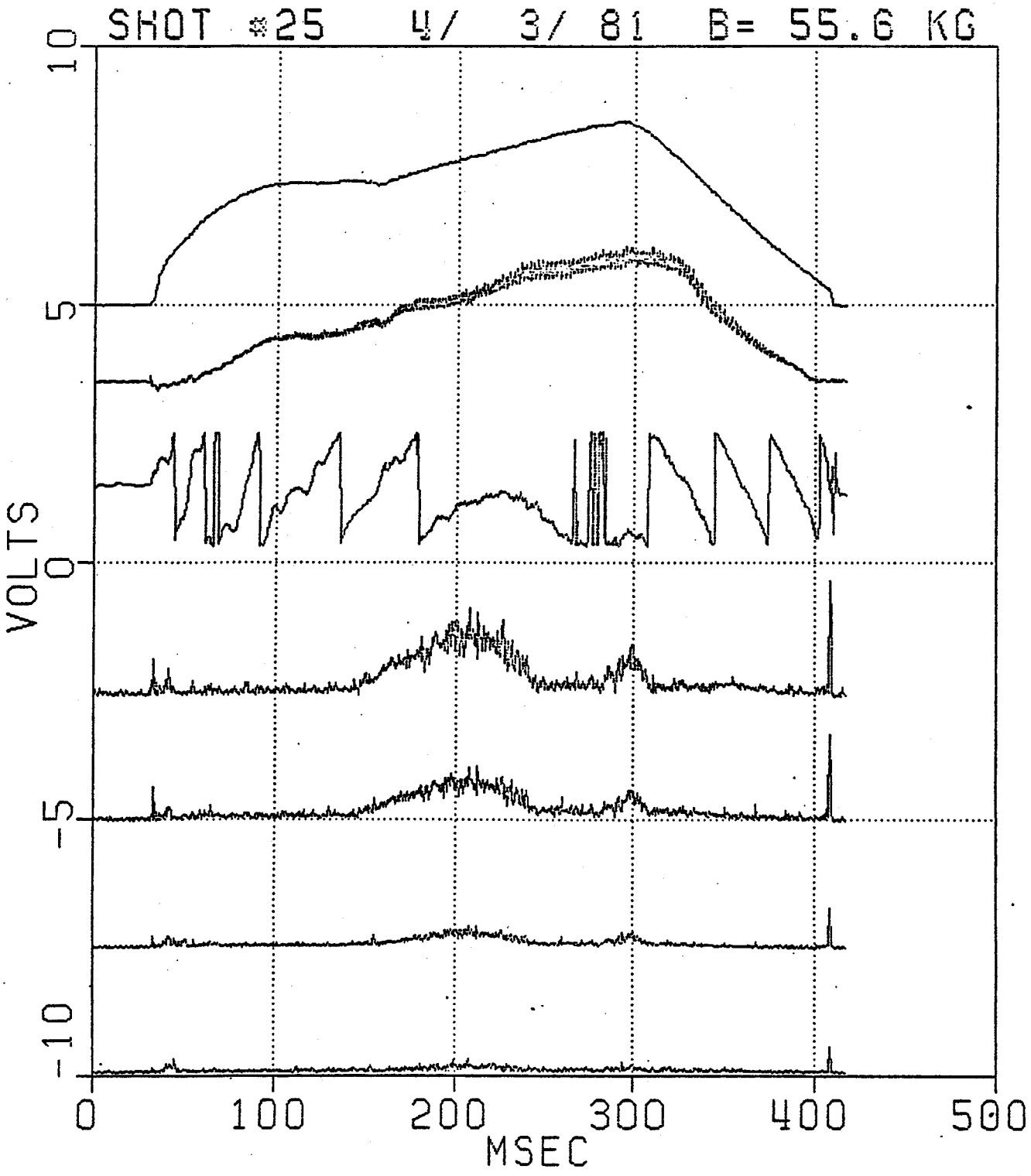


Fig. 27 — One more example of the threshold phenomenon. Note the curious re-occurrence of MHD activity as the density rises slightly for a second time around 300 msec.

is remarkably small. Variables such as the rate of current rise, impurity concentrations, $Z_{eff}$, "marfes" (they will be explained later), peak-to-average density ratio, current profile width, wall loading and recycling, etc. vary much more that 20% from shot-to-shot and/or run-to-run.

In the discussion of the observed density threshold, I have been quite explicit in stating the selection criteria for when this effect applies: after the current rise. Why? What happens to the MHD signals when the plasma current is not constant? Figure 28 is a typical example of the tearing mode history on a shot which had a faster than normal density rise due to the programming of greater pulsed gas inflow during the early part of the discharge. This results in both the usual current rise modes described in section IV.2 and also behavior which looks very much like the steady state $m = 2$ and $m = 3$ perturbations. However in this case these instabilities start at a density somewhat below $2.4 \times 10^{14}$ cm$^{-3}$. If the current profile really plays a key role in tearing mode instabilities, as the theory says it should, then it is not surprising to find a quantitative difference in MHD activity during this time period. Measurements of electron temperature usually show flatter profiles as the current is evolving, relative to the peaked Gaussian shape typical of the steady state. So one would not expect identical MHD behavior—in fact one might even expect there to be a *qualitative* difference because of the different current profile. But the only experimentally observed difference is the slightly lower value of $\overline{n}_c$. Of the shots which display $m = 2$ and 3 magnetic islands, only a small fraction have an initial density rise which is fast enough to reach the levels necessary to produce instabilities during current rise. But in every one of these, the threshold density is always lower than the steady state value of $\overline{n}_c$. (The discharge in Fig. 27 is a marginal example of this.) Similar effects can also be evident during the latter part of a plasma shot when the current is ramped down. This probably accounts for the reason why the steady state MHD activity does not always turn off as the line average density decays back below $\overline{n}_c$ late in the discharge.

The measured rate at which steady state MHD activity grows reveals another important piece of physics. There is no simple relationship between the amplitude of $\dot{B}_\theta$ at the wall

Table 1

Threshold density in hydrogen at 55 kG

| $\overline{n}_c$ ($10^{14}$ cm$^{-3}$) | field (kG) | current (ka) |
|---|---|---|
| 2.45 | 54.9 | 259 |
| 2.53 | 54.9 | 319 |
| 2.54 | 54.9 | 354 |
| 2.42 | 54.9 | 343 |
| 2.29 | 54.9 | 293 |
| 2.26 | 54.9 | 286 |
| 2.37 | 55.6 | 323 |
| 2.48 | 54.9 | 370 |
| 2.53 | 55.6 | 378 |
| 2.76 | 54.9 | 354 |
| 2.21 | 55.7 | 439 |
| 2.58 | 55.6 | 436 |
| 2.48 | 54.9 | 311 |

Table 2

Threshold density in deuterium at 55 kG

| $\overline{n}_c$ ($10^{14}$ cm$^{-3}$) | field (kG) | current (ka) |
|---|---|---|
| 2.47 | 54.3 | 358 |
| 2.47 | 54.3 | 345 |
| 2.57 | 54.3 | 369 |
| 2.20 | 54.3 | 316 |
| 2.14 | 54.3 | 302 |
| 2.20 | 54.3 | 322 |
| 2.31 | 54.3 | 336 |
| 2.44 | 54.9 | 378 |
| 2.32 | 54.9 | 349 |
| 2.57 | 54.9 | 421 |
| 2.76 | 54.9 | 330 |
| 2.92 | 54.9 | 287 |
| 2.49 | 54.9 | 437 |

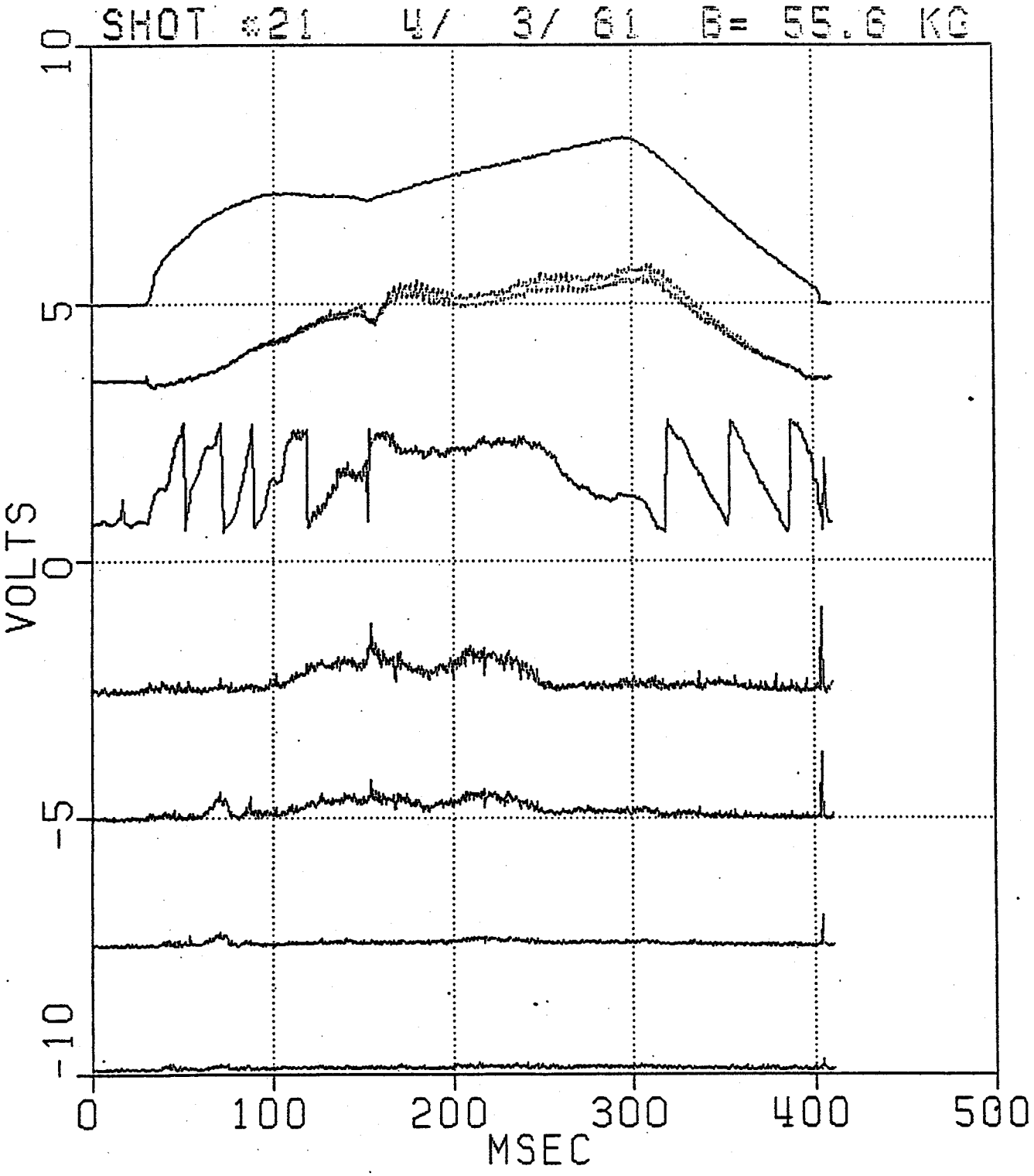


Fig. 28 — Example of "steady state type" MHD activity beginning during the current rise. Note the fast rate of density rise required, and the lower value of $\overline{n}_c$.

and the width of the magnetic island which causes the perturbation, even if the rotation is constant. But rough estimates for a 1-cm wide $m = 2$ island in a $q = 3.4$ plasma with a rotation frequency of 10 kHz give on the order of a volt of signal at the output of the $m$-spectrum analyzer. If a linear dependence is assumed for the moment, then the growth rate in Fig. 25 is:

$$\left(\frac{dW}{dt}\right)_{exp} \sim 1 \text{ cm/50 msec} \sim 0.2 \text{ mm/msec} \ll 1 \text{ mm/msec} \tag{69}$$

Compare this to the theoretical growth rate in the non-linear regime. (The exponential growth rate in equation (39) is only valid in the linear regime, where $W < \epsilon$. But $\epsilon$ is so small, $O$(1 mm), no magnetic perturbations from an island this size could be detected. Therefore in practice, the initial linear regime is never observed.) From equation (44) and Fig. 8:

$$\left(\frac{dW}{dt}\right)_{th} \sim \frac{\eta \Delta'}{\mu_o} \sim 2 \text{ mm/msec} \tag{70}$$

assuming a temperature of 500 eV at the $q = 2$ surface. Thus the theoretical growth rate of the mode is much faster (perhaps an order of magnitude) than the change in amplitude measured by the $m$-spectrum analyzer. Therefore the observed $m = 2$ and 3 tearing modes are apparently always at or near their saturated widths for a given equilibrium. As the equilibrium changes slowly due to the density build up, the island widths adjust nearly instantaneously to satisfy the saturation condition: $\Delta' = 0$ (equation 47).

In the design criteria for the $m$-spectrum analyzer, the ability to continuously monitor MHD activity for the entire duration of the discharge was stressed. This capability played a central role in the discovery of the density threshold and subsequent density dependence of tearing modes in Alcator C. Figure 25 clearly suggests the importance of line average density, yet it shows the data from just a single discharge. Without the $m$-spectrum analyzer, this study would have to be done by inspecting the individual Mirnov loops for an extremely brief moment of each shot, and it is doubtful that such a clear, concise picture of this

fundamental effect would have been realized, especially since no density destabilization was expected from resistive MHD theory. Because of the way in which the tokamak's operating parameters are varied, it is not always easy to sort out the scaling of plasma properties with current, density, magnetic field, impurities, etc. on an individual basis. This problem can become hopelessly complicated when data is selected from short, random samples. The global view of MHD activity afforded by the $m$-spectrum analyzer has plainly revealed unexpected physics after just a handful of shots.

Until now, no mention has been made of the frequency information yielded by the $m$-spectrum analyzer for the MHD activity detected during the current plateau. This data virtually eliminates any remaining doubts concerning the question of whether or not large, invisible, non-rotating islands exist prior to reaching $\overline{n}_c$. Figure 29 shows the $m = 2$ and $m = 3$ frequencies for the shot in Fig. 25, which is a typical discharge exhibiting steady state MHD activity. In order to filter out spurious noise, the frequency-to-voltage converters have discriminator settings which are intended to block out the background due to power supply pickup. Therefore an island must grow slightly above the noise level in order to get an accurate frequency measurement. Nevertheless, it is obvious from the graphs that as soon as the tearing mode reaches the minimum F/V level, its frequency is found to be on the order of 10 kilohertz, and the rotation frequency does not change much as the amplitude of the instability continues to grow and then shrink. This behavior has been determined to exist on the majority of high density shots—large rotation rates in the ion diamagnetic direction are measured *as soon as* MHD activity is detected, regardless of its amplitude. In most plasma shots, no tendency is seen for the magnetic perturbations to gradually speed up from zero or low frequencies ($<$5 kHz) at the start of MHD activity, and the rotation frequency stays fairly constant until the mode disappears into the noise.

Since $\dot{B}_\theta$ rises slowly from noise level to finite amplitude, but the rotation frequency is constant and relatively large, and because:

$$\left|\dot{B}_\theta\right| = \omega\left|\tilde{B}_\theta\right|$$

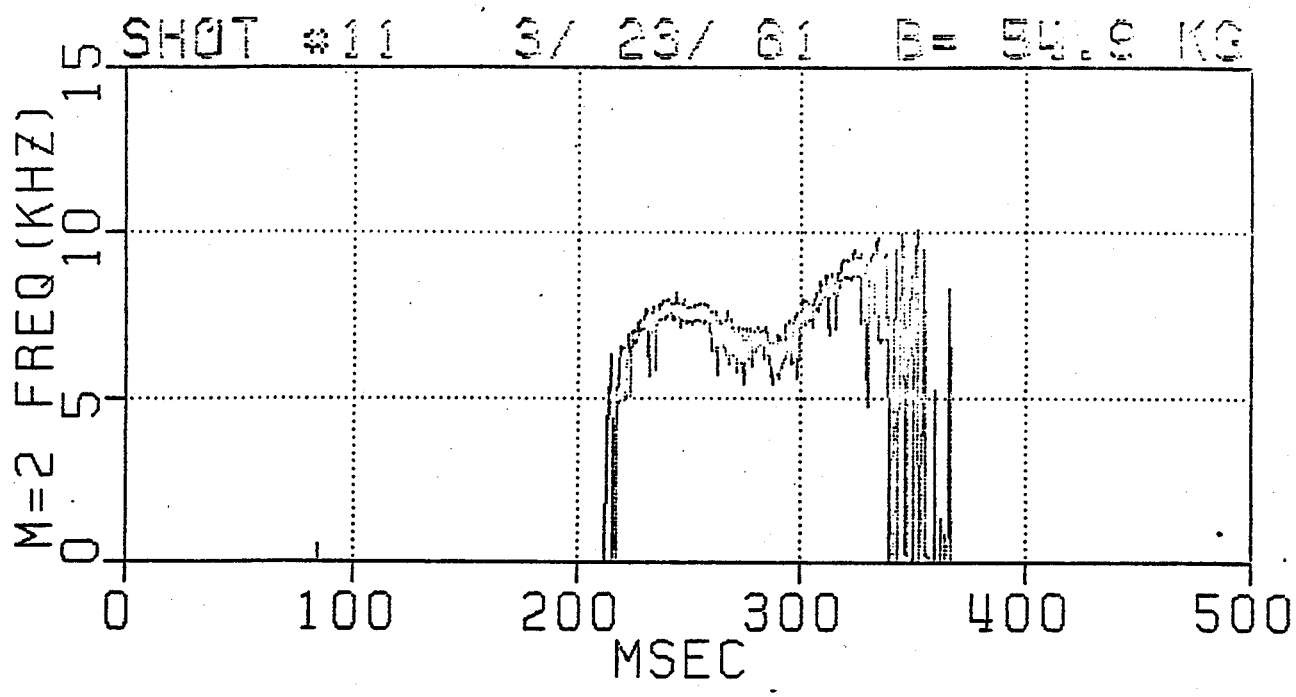


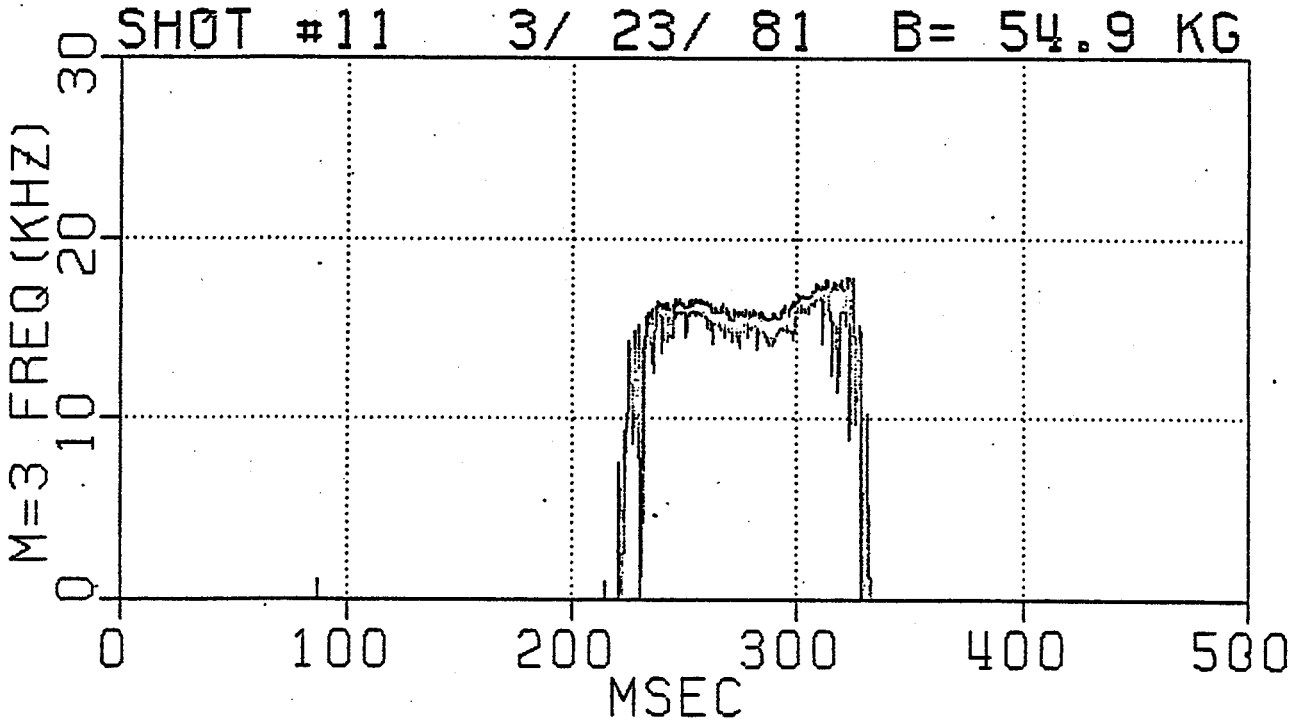


Fig. 29 — Measured frequencies of the $m = 2$ and $m = 3$ modes for the shot displayed in Fig. 25. Large rotation frequencies are observed almost as soon as the perturbations are detected. The signals are relatively constant for the duration of MHD activity.

one is forced to conclude that the mode amplitude, $\tilde{B}_\theta$, must also rise slowly from the noise level to finite size. In other words, as soon as MHD activity is detected during the current plateau, the magnetic island size must be very small. This is in direct contrast with the suggestion of large, non-rotating islands which suddenly start moving. In order to reproduce the observed behavior of $\dot{B}_\theta$, a large island would have to begin rotating very slowly at first and then gradually speed up on a time scale of $\sim$50 msec. And that is definitely not seen on most shots. Of course there is always the far-fetched hypothesis that prior to reaching $\overline{n}_c$, a large stationary island exists, but near $\overline{n}_c$, it suddenly shrinks away and begins rotating at 10 kHz. But why envision such an unlikely evolution if the simple assumption that no mode exists below $\overline{n}_c$ satisfies all the available experimental data? It is the most plausible hypothesis.

A strong density dependence has therefore been discovered for resistive instabilities in Alcator C. Further quantitative measurements have been carried out to better define the effect on perturbation amplitudes after the threshold has been surpassed. In Fig. 30, the amplitude of $\tilde{B}_\theta$ for the $m = 2$ mode at the time the density peaks is plotted against the maximum density reached for many 55 kG shots. The threshold value is easily discernible, as is the general increase in fluctuation level at higher densities. The open circles represent shots which disrupted, and they will be discussed shortly.

An important objective of this thesis is the elucidation of how MHD activity affects global confinement time, which is defined as:

$$\tau_E = \frac{\sum_{e,i} \frac{3}{2}\langle nkT \rangle}{V_R I} \tag{71}$$

where $\langle \cdots \rangle$ indicates a volume integral and $V_R$ is the resistive component of the loop voltage around the torus. This definition is only applicable during the steady state, when all the ohmic heating power going in is exactly balanced by the losses, leaving no net change in plasma energy. Actually if $n, T, V_R$, and $I$ remain relatively constant for longer than approximately one confinement time, equation (71) is still valid. These criteria are reasonably

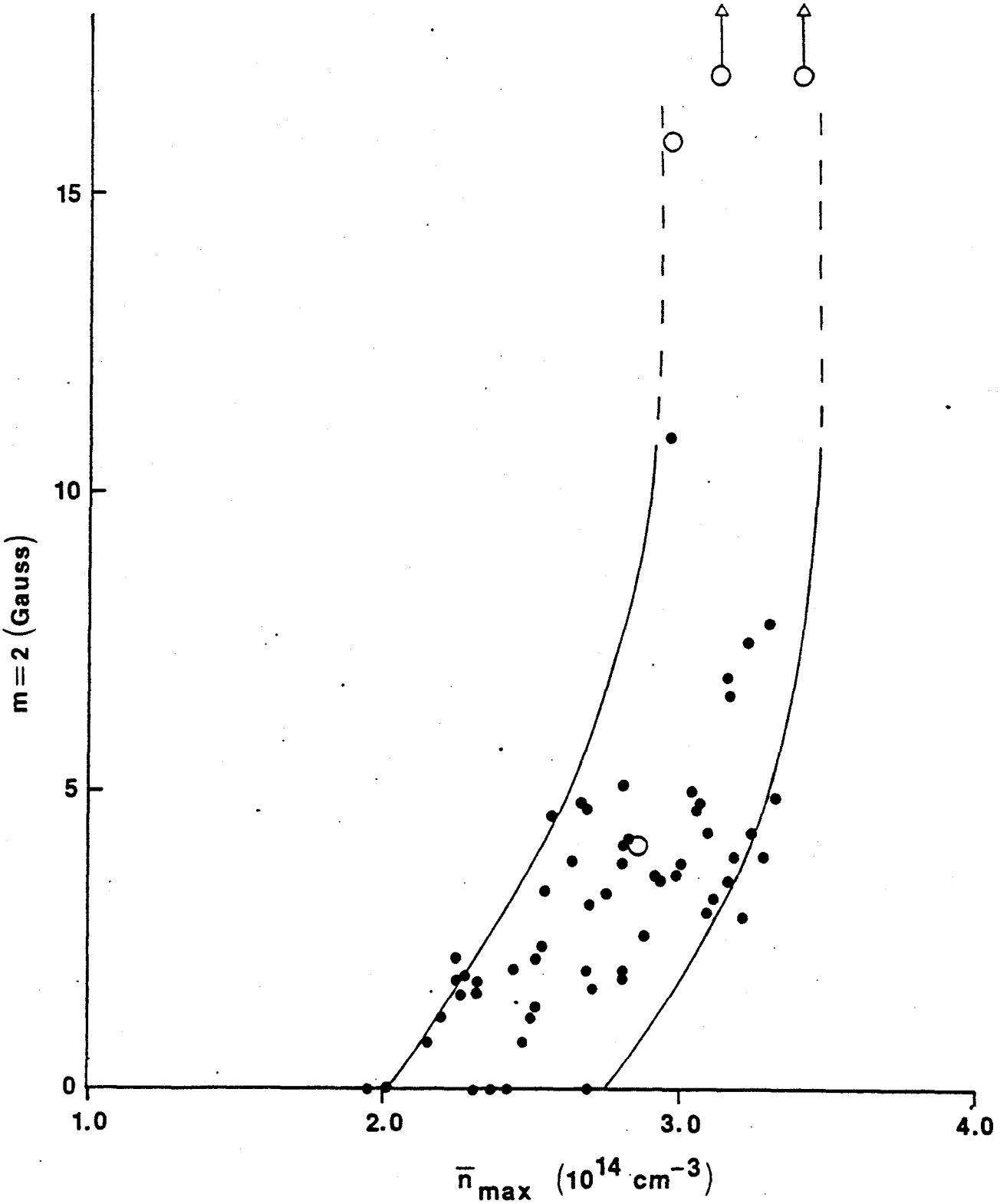


Fig. 30 — Plot of $\tilde{B}_\theta$ amplitude for the $m = 2$ perturbation at the time of maximum density, compiled from many shots at 55 kG. The open circles are discharges which ended in a major disruption. The curved lines indicate the bounds of the trajectories followed by the disruptive shots.

well satisfied at the time the maximum density is reached during the shot. If MHD activity degrades confinement, as one would expect from theory, then a good place to start looking for its effects might be in the graphs of temperature versus density compiled by the confinement measurements group[62,63]. Figure 31 shows central electron and ion temperatures for deuterium discharges at 55 kG. Although the absolute calibration for any of the diagnostic methods employed in making temperature measurements is $\pm 10\%$ or more, the relative calibration is significantly better. This is especially true for the neutron diagnostic, which is extremely sensitive to small temperature changes at this operating regime. (A 50 eV change can alter the neutron flux by $\sim 50\%$.) Measurable MHD amplitudes begin at $\overline{n}_c \simeq 2.4 \times 10^{14}$ cm$^{-3}$, and reach perturbation levels of a few gauss at $3 \times 10^{14}$ cm$^{-3}$. Yet the temperature data shows no corresponding anomalies in this range. The general decrease in $T_e(0)$ and $T_i(0)$ seems to follow the same trend exhibited at densities below $\overline{n}_c$. However, the confinement time depends on volume-averaged temperatures, not just the central ones, so this information might not be sufficient for clarifying confinement issues. Actual measurements of total energy confinement times are plotted in Fig. 32 for many shots over a wide range of operating parameters. The straight line is the "Alcator scaling law" observed on the original $A$ machine. If one insists on fitting the $C$ data with the "$na^{2}$" curve at low densities, then there is an apparent break in $\tau_E$ near $\overline{n}_e = 2 \times 10^{14}$ cm$^{-3}$. A better fit might be a smoothly bending curve which asymptotes to the "$na^{2}$" line at low densities. In either case, there is no change in the trend of $\tau_E$ as the density goes above $\overline{n}_c$, even up to densities where the magnetic perturbations become large. Although the confinement time falls below the Alcator scaling law, it is still rising slowly with $\overline{n}_e$, up to the highest densities attained thus far. So contrary to theory, it does not appear that MHD perturbations affect energy confinement times, even at large amplitudes.

This conclusion was reached by comparing the dependence of both $\tau_E$ and magnetic activity on line average density only. There is also a fairly strong correlation of $\tau_E$ with plasma current, as shown in Fig. 33. In order to illuminate any subtle relationship between confinement and resistive instabilities, it is interesting to look for a similar correlation be-

tween plasma current and MHD activity. The most easily measured variable which characterizes tearing modes in Alcator C is the threshold density. How does $\bar{n}_c$ vary with $I_p$? Because resistive MHD theory does not even predict the threshold phenomenon, there is no theoretical basis for answering this problem. All that is known is that the $\Delta'$ analysis predicts tearing modes should be stabilized by finite beta or radial diffusion effects for the entire range of $q$-values which have been operated at 55 kG. Figure 34 is a plot of $\bar{n}_c$ versus

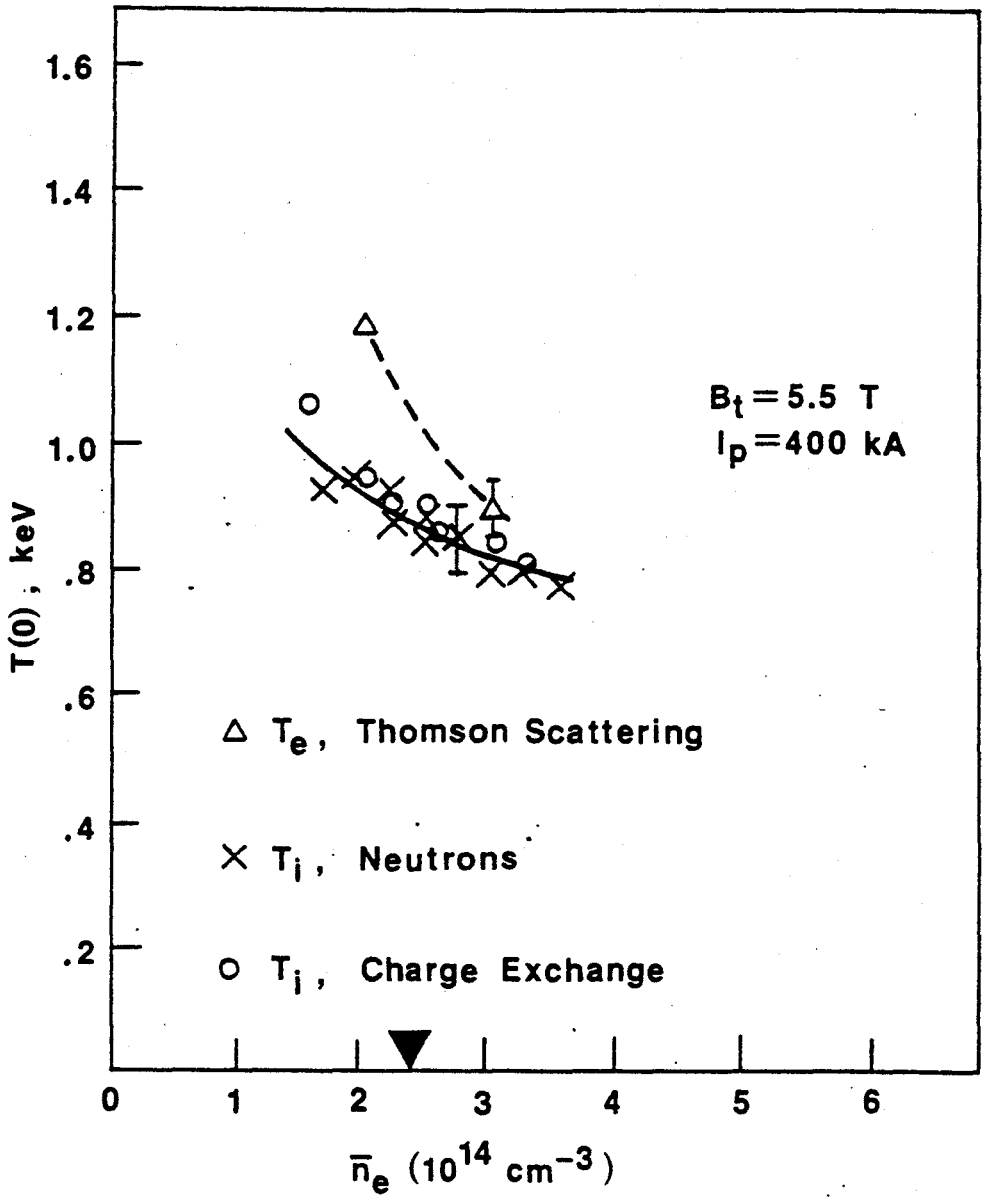


Fig. 31 — Central ion and electron temperatures versus density for well-behaved deuterium discharges at 55 kG (from ref. [62]). The MHD threshold density is indicated by the marker on the horizontal axis.

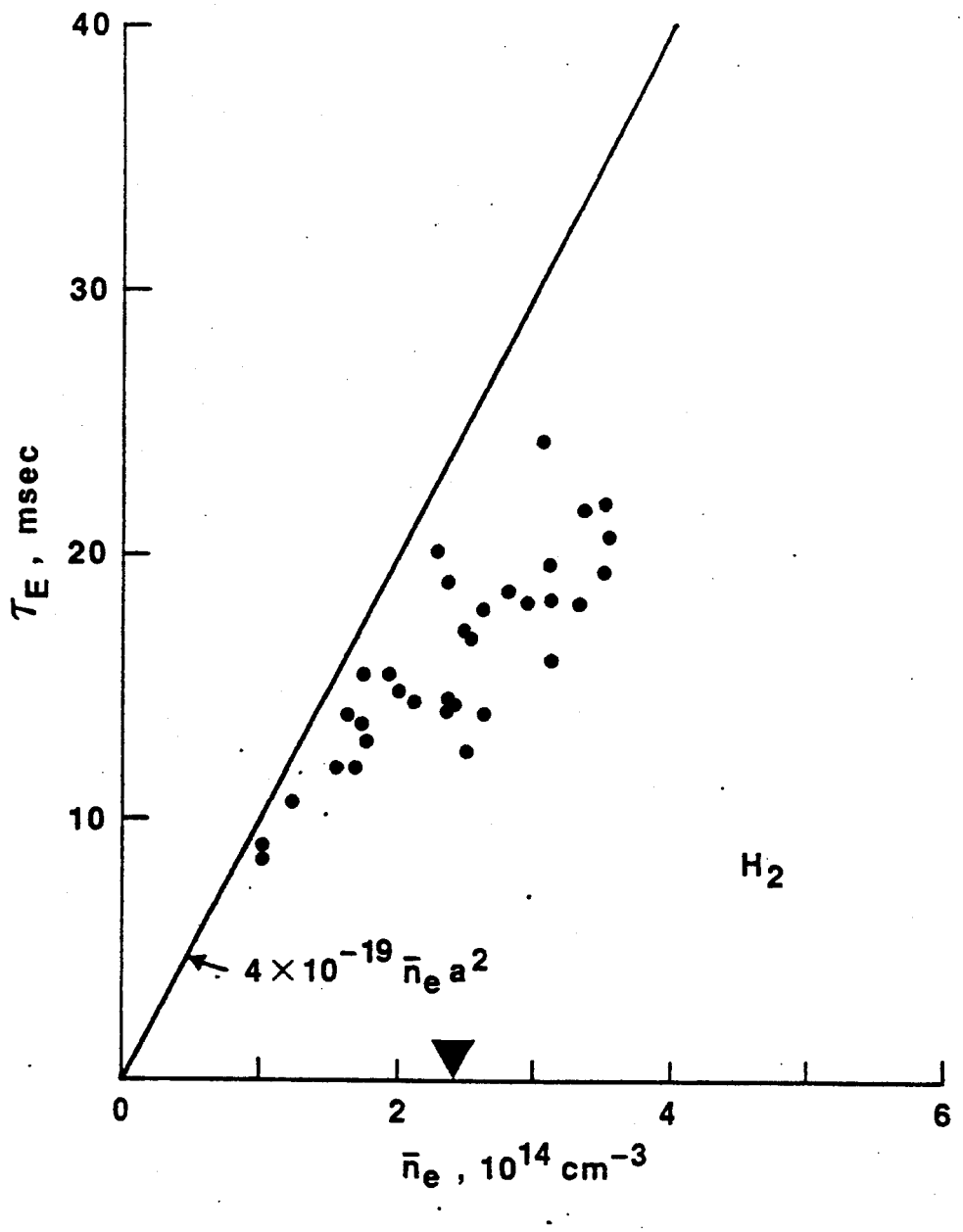


Fig. 32 — Global energy confinement time versus density for hydrogen discharges at 55 kG (from ref. [63]). The straight line is the "Alcator scaling law". The MHD threshold density is indicated by the marker on the horizontal axis.

total plasma current for both isotopes at 55 kG. Given that the standard deviations of $\bar{n}_c$ are 10% in hydrogen and 20% in deuterium, the data on this graph can be fit by a horizontal straight line. In other words, there is no statistically significant dependence of the MHD threshold on $I_p$. Since the energy confinement time definitely does vary with current, this finding gives yet another indication that resistive instabilities do not degrade $\tau_E$ in

Alcator C. Perhaps the simple picture described in the introduction, which predicts thermal conductivity across the island width to be of the order of parallel thermal conductivity must be modified. For example, if radiation is the dominant mechanism for power loss from the plasma, then the increased heat conduction would have only a small effect on $\tau_E$. Extensive measurements of radiated power have been done on Alcator C using an array of bolometric detectors which are sensitive to all wavelengths of interest[6-1]. During sawtoothing discharges the total radiated power is typically only 40% of the ohmic input power, while the majority of the plasma losses presumably ends up on the limiters and at localized spots such as the pulsed gas valves. So for Alcator at least, this does not resolve the paradox of $\tau_E$ independence from tearing modes. Convection and/or anomalously fast ion "ripple losses" could also lessen the expected degradation of energy confinement times due to magnetic islands, but these issues will not be addressed in this thesis. The qualitative calculations and measurements of the possible causes of lack of MHD dependence has only been touched on here and will be left to future researchers.

The $m$-spectrum analyzer on Alcator C has revealed many peculiar properties of MHD instabilities in 55 kG discharges. But so far no important effect has been attributable to these tearing modes. Is there any property of the plasma which is influenced by MHD activity, other that just small magnetic and temperature fluctuations? Yes, there is; magnetic islands seem to have a very detrimental effect on disruptions, which was alluded to in Fig. 30. Note the occurrence of a large number of disruptions around a line average density of 3.0–$3.4\times10^{14}$ cm$^{-3}$. Also from the graph, it is obvious that no data points exist at densities significantly above this value. This is not because such shots have not been attempted; nor have these densities purposely been excluded from Fig. 30. Rather, on every discharge recorded by the $m$-spectrum analyzer where an attempt was made to surpass $\sim$6 fringes at 55 kG, the plasma would invariably disrupt. This suggests a very strong correlation between electron density and disruptions. There is also an indication of an absolute maximum density limit, at least for this toroidal field. Since it has already been shown that MHD activity in Alcator also depends strongly on line average density, perhaps this means there is an

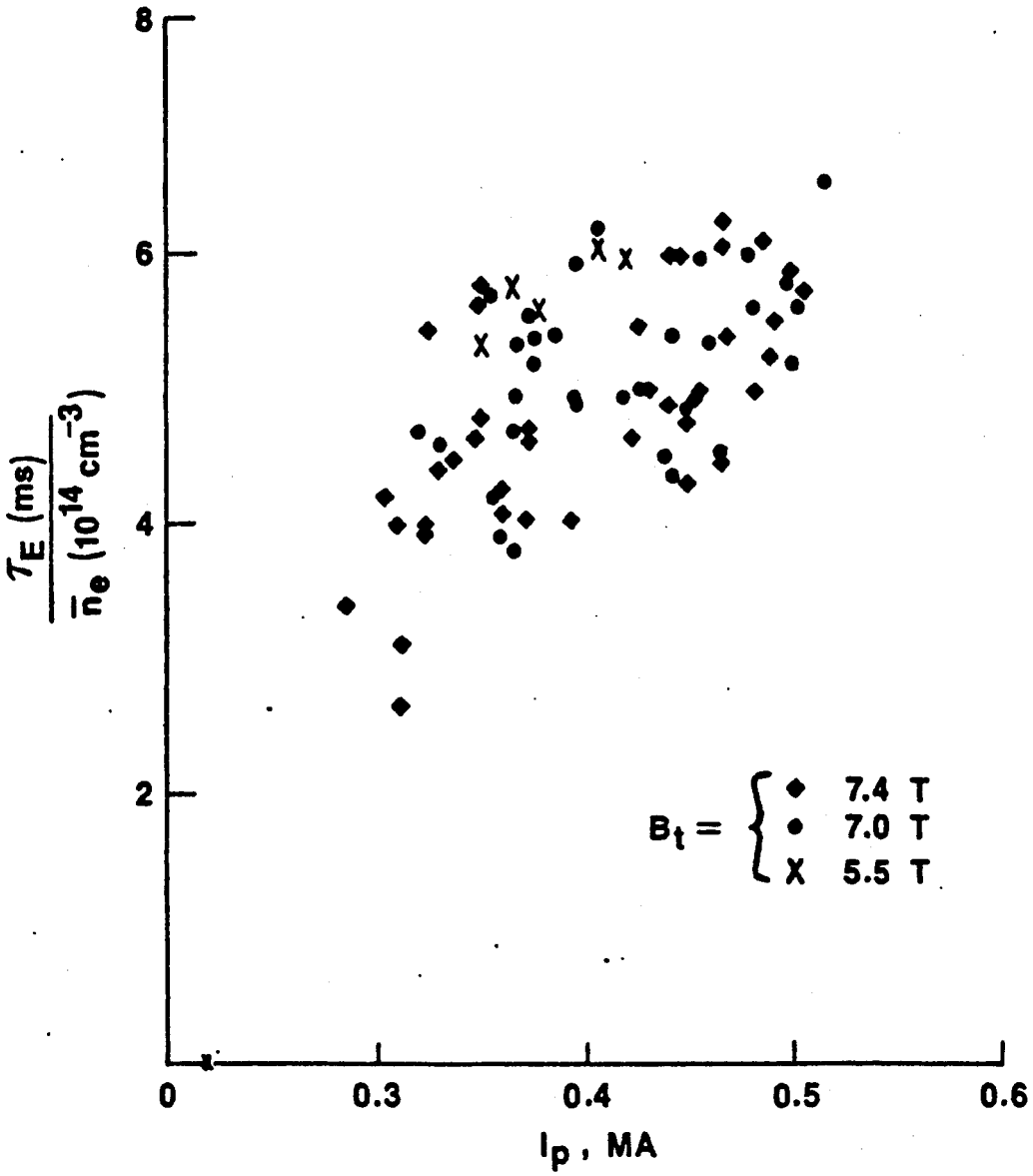


Fig. 33 — Variation of energy confinement time with plasma current. Data from several values of toroidal magnetic field have been included. (From ref. [63]).

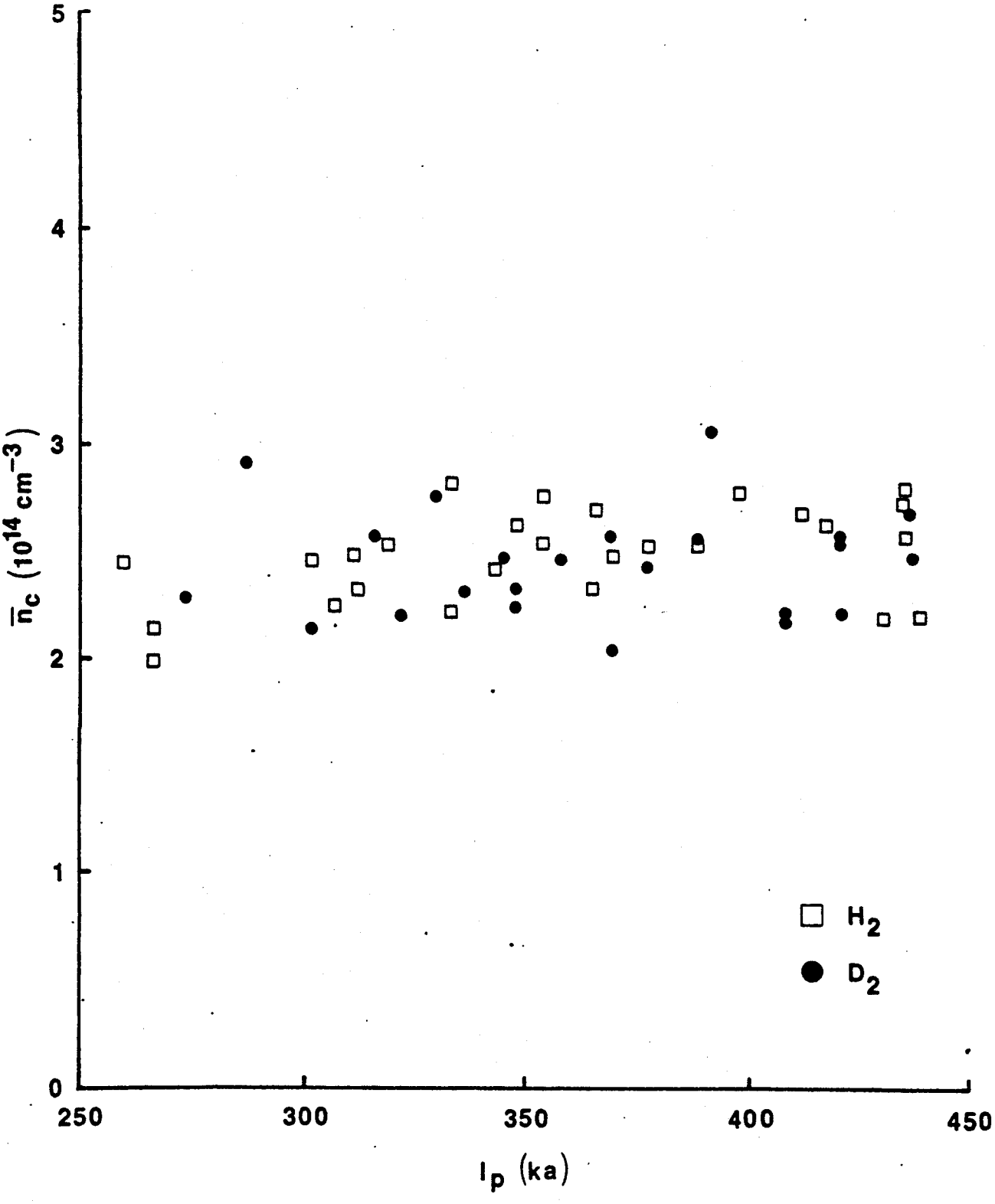


Fig. 34 — Variation of $\bar{n}_c$ with plasma current for 55 kG hydrogen and deuterium plasmas. The data suggests no dependence of the threshold on $I_p$.

experimentally observed connection between magnetic islands and major disruptions. As described previously in section II.5, this dependence is required in the present day theories of the major disruption.

Figure 35 shows a very high density shot which ended in a major disruption. All discharges at 55 kG which reach densities well in excess of $\overline{n}_c$ are quite similar to this. The first thing which should be noted is the now familiar growth of $m = 2$ and 3 modes beginning near the proper value of $\overline{n}_c$ ($\sim$4.7 fringes), which is expected on these sawtoothing shots. Also as the line average density continues to rise, the fluctuation amplitude increases, with the $m = 2$ magnetic perturbations reaching a level of $>$20 gauss. At $\overline{n} = \sim 3.4 \times 10^{14}\,\mathrm{cm}^{-3}$, the soft x-ray emission suddenly drops sharply in just hundreds of microseconds, the density falls so quickly it can't be followed on the interferometer trace, and the plasma current decreases, although on a somewhat slower timescale. At the same time, noisy magnetic perturbations are picked up on all the $m$-channels, but the frequency measuring circuits can not detect any coherent oscillations. Direct observation of the individual Mirnov pickup loops reveals wildly varying signals which swing quickly between the positive and negative supply voltages of the $m$-spectrum analyzer's buffers, indicative of large $dI/dt$. The individual $\dot{B}_\theta$ signals show no sinusoidal oscillations, which explains why the F/V boards don't measure anything. Because all of the lowest Fourier harmonics are detected (at least), but rotation is not measurable, the magnetic fluctuations are ascribed to plasma turbulence resulting from the rapid collapse and inward motion of the current channel during the disruption. The signals do not truly indicate the existence of well-defined tearing modes, or even flux surfaces. The quantitative characteristics of this turbulent plasma cannot be accurately ascertained from Fig. 36, since the $m$-spectrum analyzer has a time response limit of $\sim$70 $\mu$sec, as detailed in section III.3

The processes revealed by the $m$-spectrum analyzer could certainly be in very good qualitative agreement with the hypothetical picture of magnetic island overlap causing explosive growth of instabilities and quickly leading to a disruption. The data from these shots suggests that $m = 2$ and $m = 3$ magnetic islands grow to large widths as the density

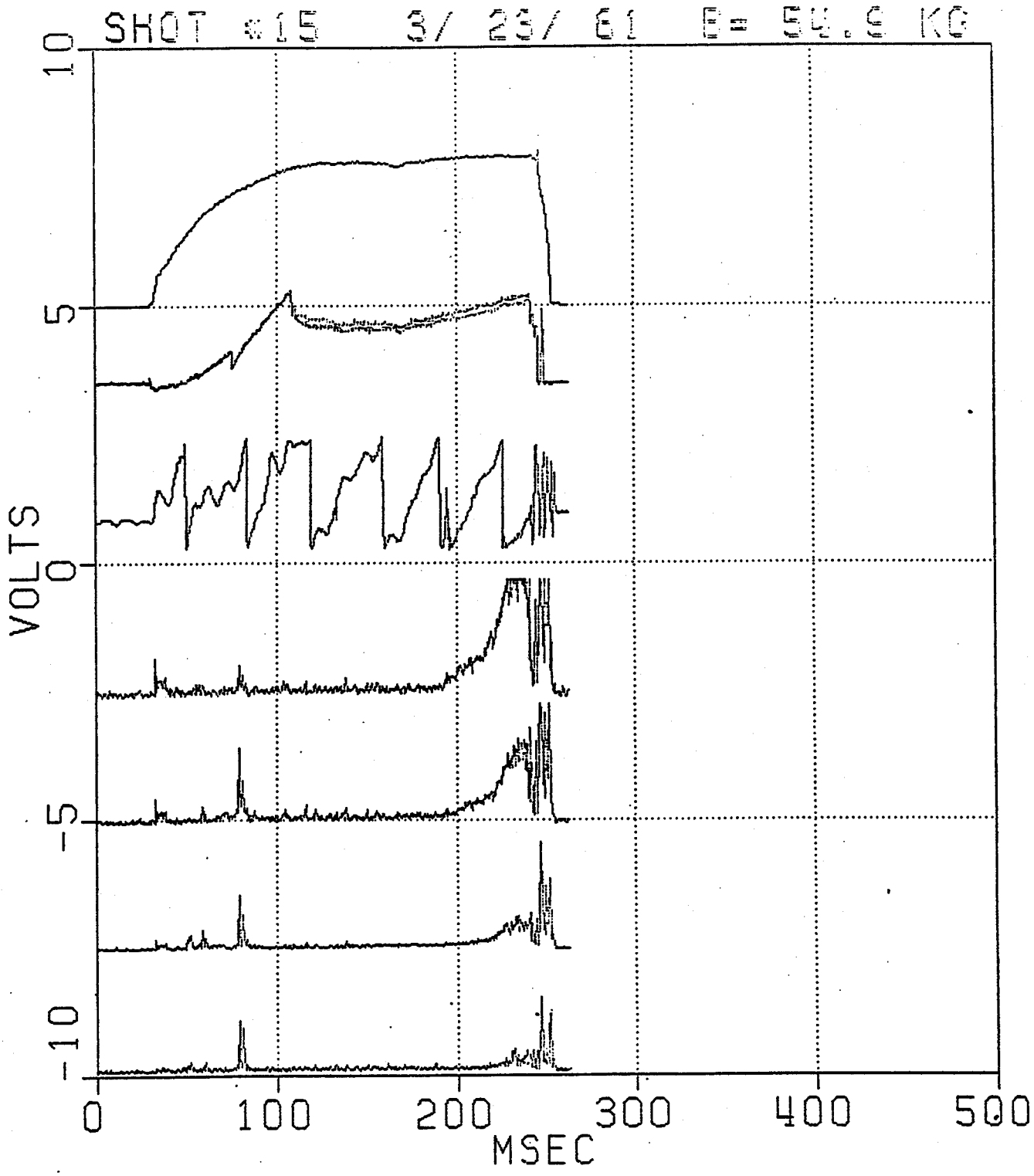


Fig. 35 — Example of a very high density shot which ended in a major disruption. MHD activity is seen to grow to very large amplitude during the 60 msec prior to the current termination.

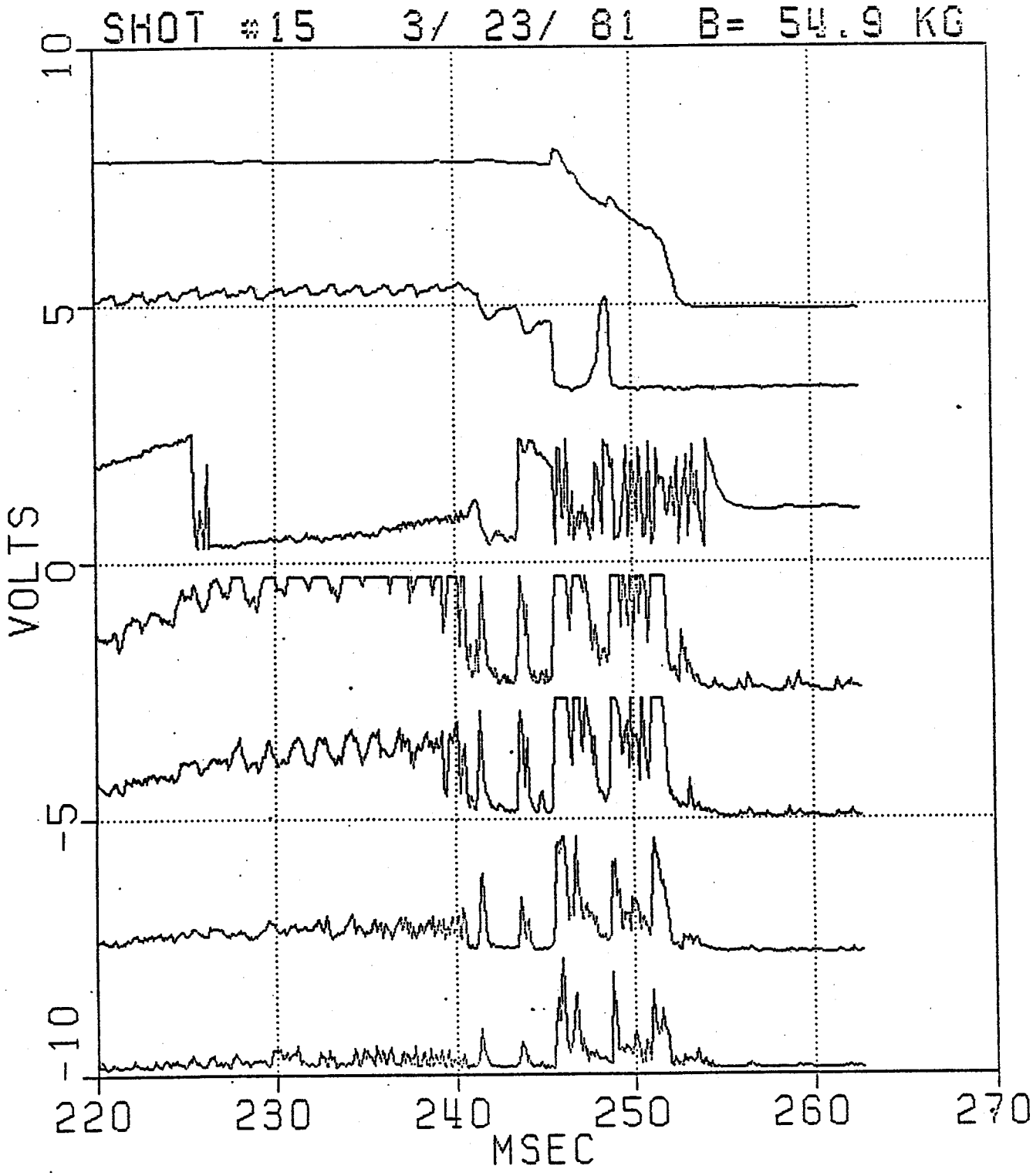


Fig. 36 — Expanded time scale showing more detail of the high density disruption.

rises higher and higher above $\bar{n}_c$ and eventually overlap when $\bar{n}$ reaches $\sim$3.0-3.4$\times 10^{14}$ cm$^{-3}$. Since both the $m = 2$ and $m = 3$ modes always begin at almost the same time, this may be direct experimental evidence of the prediction by several theorists that a 2/1 mode might non-linearly destabilize a 3/2 mode (section II.5). But this scenario cannot be verified with the $m$-spectrum analyzer alone, since it can not distinguish between two distinct sets of helical islands at different radii and one set of modes with distortions due to toroidal coupling. This is because the $\dot{B}_\theta$ pickup loops can only measure fields external to the plasma. The obvious diagnostic to use is the one that can "see" magnetic island perturbations inside the plasma—the soft x-ray diode array. With enough sensitivity and a spatial resolution on the order of a centimeter, such a device could first prove (or disprove) the existence of two different sets of magnetic islands. Assuming 2/1 and 3/2 modes are found, the x-ray imaging experiment might even be able to measure approximate island widths and determine whether or not they overlap prior to a disruption. The present x-ray arrays on Alcator C should be capable of doing this experiment, although no serious effort has been made yet. Such a study will definitely be sought.

Thus the major significance of MHD activity in Alcator C is its relationship to the maximum density attainable at 55 kG and its tentative implication in causing disruptions at high densities. But that is only part of the disruption phenomenon. A careful study of 55 kG shots on Alcator C reveals many disruptions also occurring at low densities. (By low densities I mean below $\bar{n}_c$.) One of these shots is displayed in Fig. 37. Since the line average density never reaches 2.4$\times 10^{14}$ cm$^{-3}$, the character of the MHD activity is far different than in the high density disruptions just described. As expected, no measurable fluctuations are seen after the current rise. When the disruption process starts, noisy saturated signals appear on all $m$-channels, just like in a high density shot. Figure 38 is an expanded graph of this low density discharge illuminating the behavior of macroscopic plasma parameters just prior to the disruption. A careful look at the signals reveals nothing too unusual *before* the actual disruption. There is a hint of an anomaly in the pattern of soft x-ray sawteeth immediately before the disruption. At the same time, however, the $m$-spectrum analyzer

sees only the usual power supply noise—not even the faintest suggestion of MHD activity. Then in just 500 $\mu$sec, the magnetic signals rise from the noise to saturation levels at the disruption. Could this be due to an explosive growth of resistive tearing modes? Probably not, for the following reasons. Since the tearing layer width is so small ($\sim$1 mm), any perturbation of this size is not observable in practice. (Direct proof of island size must await a functioning soft x-ray imaging diagnostic.) Presumably then, the modes which are seen should be in the non-linear regime, and therefore should be growing linearly in time at the Rutherford rate specified in section II.2, equation (44):

$$\frac{dW}{dt} \simeq \frac{\eta \Delta'}{\mu_o} \approx 2 \text{ mm/msec}$$

where a temperature of 500 eV has been assumed at the $q = 2$ surface. But since the measured growth time is only 500 $\mu$sec, the hypothesized island should only grow about a millimeter, nowhere near enough to account for the observations. It is therefore concluded that the observed rise in MHD signals has no direct connection with tearing modes. It is probably due to the inductive effects involved in the collapse of the current channel and resulting turbulence.

All the available evidence gathered from these low density disruptions implies a very disturbing premise: it doesn't appear that resistive tearing instabilities cause, or contribute to, or are even involved in major disruptions occurring at densities below $\overline{n}_c$. This is a very important finding, since all the stabilization schemes which were described in section II, presupposed that disruptions were caused by the overlap of magnetic islands. As explained in section II.6, all stabilization methods presupposed magnetic islands to be the cause of these events, and they will probably fail to work if MHD activity is not involved. At the present time, we have no plausible explanation for the cause of low density disruptions. Impurity radiation may be involved, but calculations of $Z_{eff}$ obtained from measurements of visible bremsstrahlung show no increase until the disruption starts[65].

### IV.4 Variation with toroidal magnetic field

In the previous chapter on MHD activity during the current plateau, all of the data

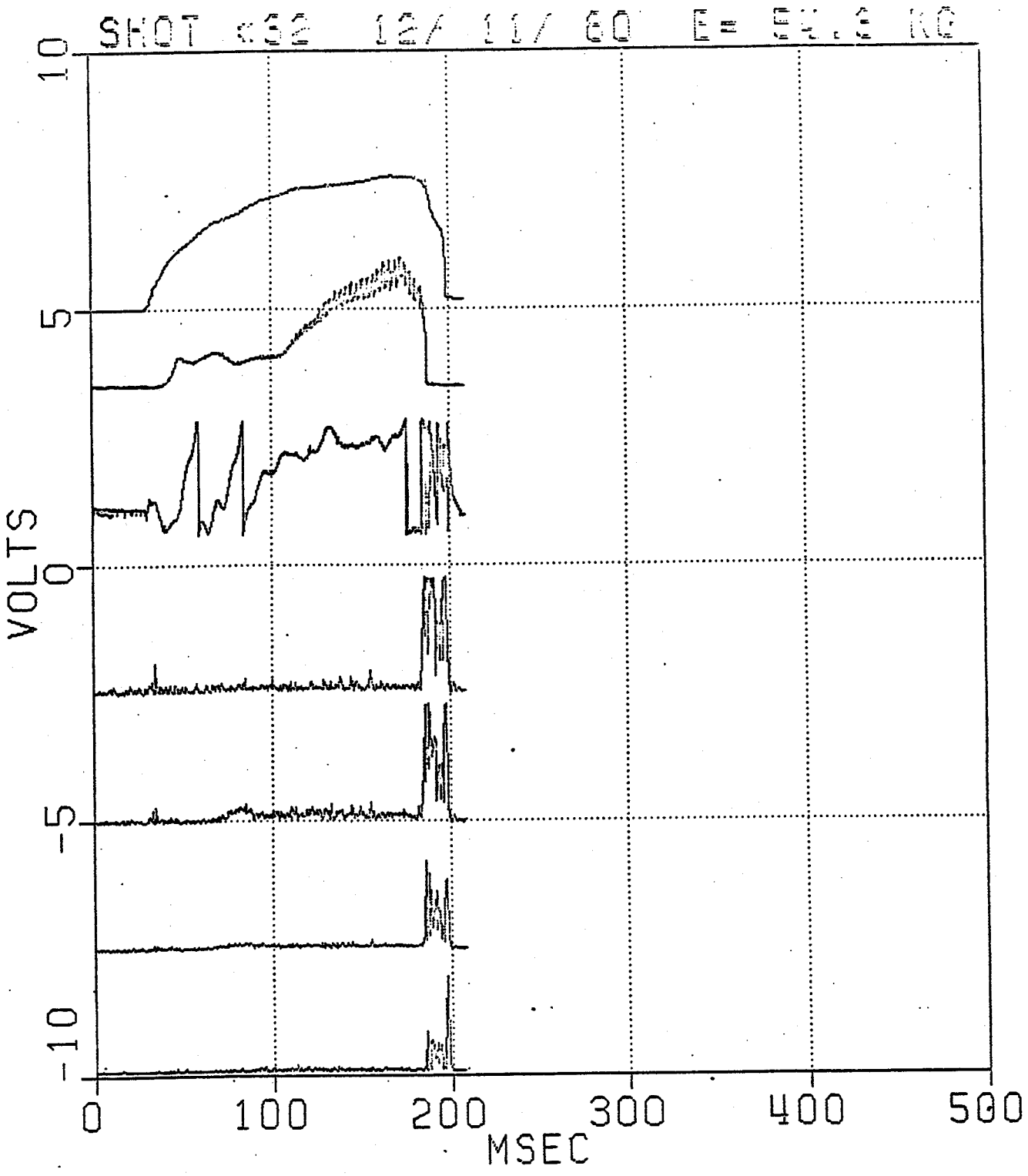


Fig. 37 — A major disruption at a density well below $\bar{n}_c$. No MHD is expected at these low densities and none is seen prior to the current termination.

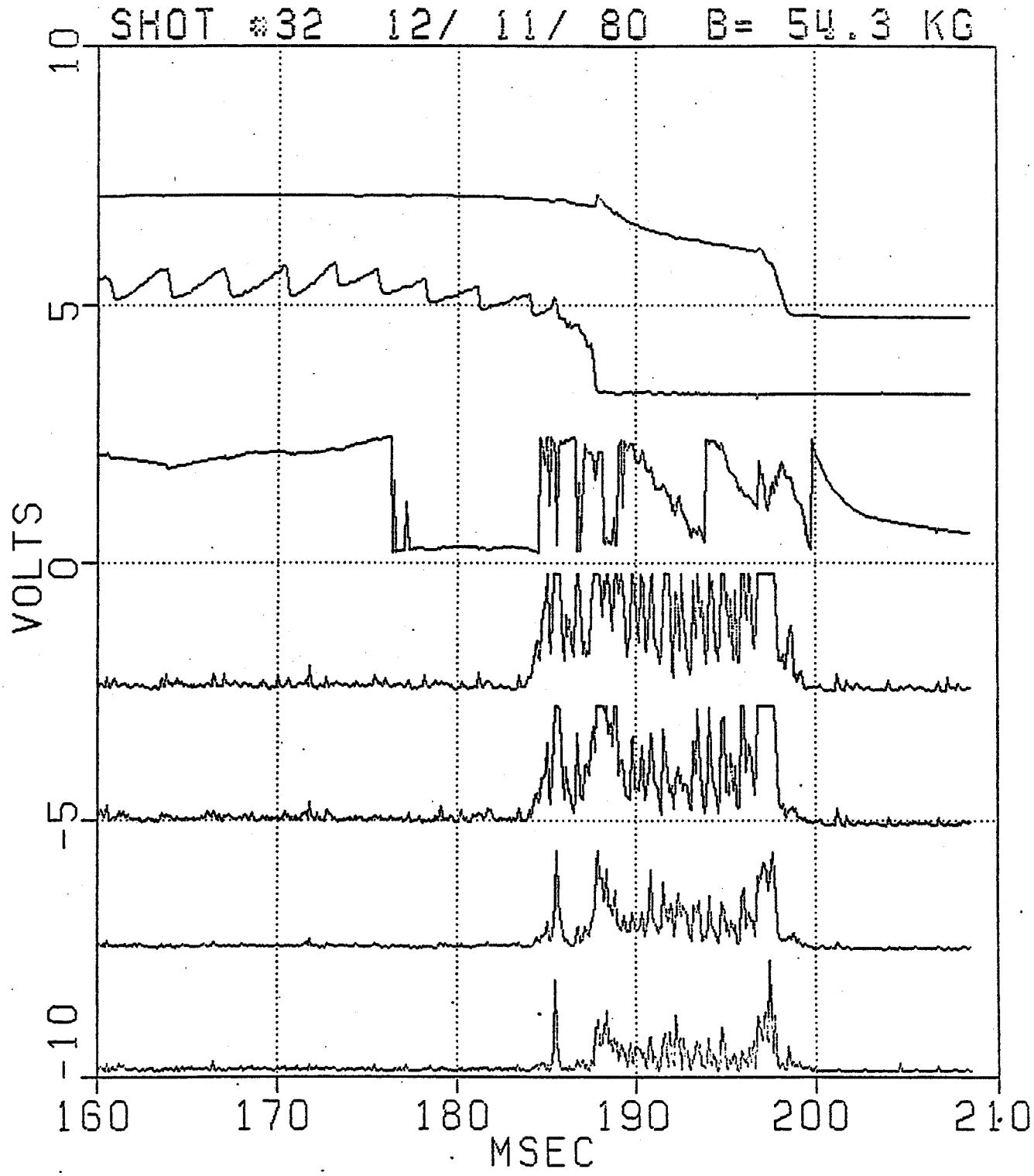


Fig. 38 — Expanded view of the same shot around the time of disruption. Very little indication of an impending disruption exists. The *m*-spectrum analyzer channels saturate in ~500 $\mu$sec.

presented was at a toroidal magnetic field of 55 kG. During the first several months after the $m$-spectrum analyzer was installed, the tokamak was operated predominantly at this field. However a sizable fraction of the discharges were also run at a main field of 78 kG, and here too, the findings were unexpected, even in light of the results already documented.

Figure 39 shows the evolution of the familiar plasma parameters for a typical shot at this higher $B$-field. After the lengthy demonstration of a remarkably repeatable density threshold, $\overline{n}_c \simeq 2.4\times10^{14}$ cm$^{-3}$ at 55 kG, it might be surprising to see no measurable MHD activity on this shot, even though the line average density goes well above this value. Could the value of $\overline{n}_c$ at 78 kG be different from that at 55 kG? If there is really a basic physical mechanism behind the MHD threshold effect, one would not expect it to totally disappear simply because of a 42% increase in the toroidal magnetic field. This should be especially true in Alcator since the density profile does not change systematically with $B_t$. And for the same value of $q(a)$ the temperature profile is also independent of field. Both of these statements are, of course, not absolute. Subtle changes in profiles which might occur may not be detectable with the diagnostic instruments available now, and as has been mentioned previously, tearing mode stability may be strongly influenced by such subtle effects near the resonant surface because of the exaggerated sensitivity of equation (51) to $\partial J_z/\partial r$ there. In any case, it was hypothesized that the density threshold still existed at the higher field, but apparently at a much higher value of $\overline{n}_c$.

Because high densities are not routine operation on Alcator, it took many runs of null results before MHD activity was found during the steady state at 78 kG. A density threshold effect was indeed observed, as evident in Fig. 40. In this example the value of $\overline{n}_c$ is $\sim4.8\times10^{14}$ cm$^{-3}$, or 8.4 fringes. Table 3 lists most of the 78 kG plasma shots which reached densities high enough to trigger MHD activity. The standard deviation in $\overline{n}_c$ at this field is comparable to $\sigma$ at 55 kG. The measurement of the threshold has only been carried out in deuterium because difficulties arise when trying to run hydrogen plasmas at these high densities. (Because energy confinement times are worse in hydrogen, the loop voltage is higher and more ohmic power is required. The reasons for this difference are unknown.)

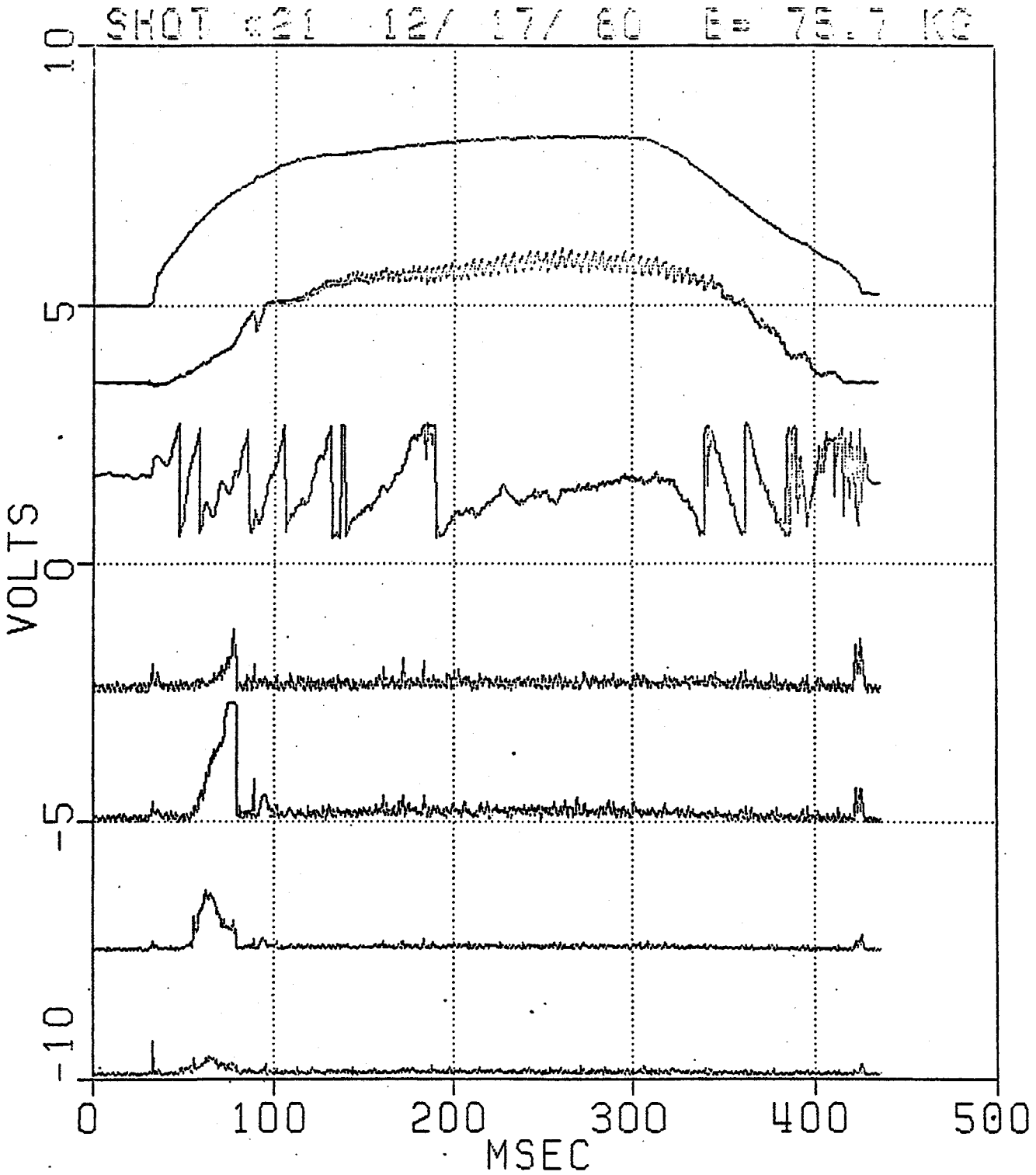


Fig. 39 — Typical discharge at a higher toroidal magnetic field. The scales remain unchanged. Note the lack of MHD activity during the steady state at densities above the value of $\bar{n}_c$ for 55 kG shots.

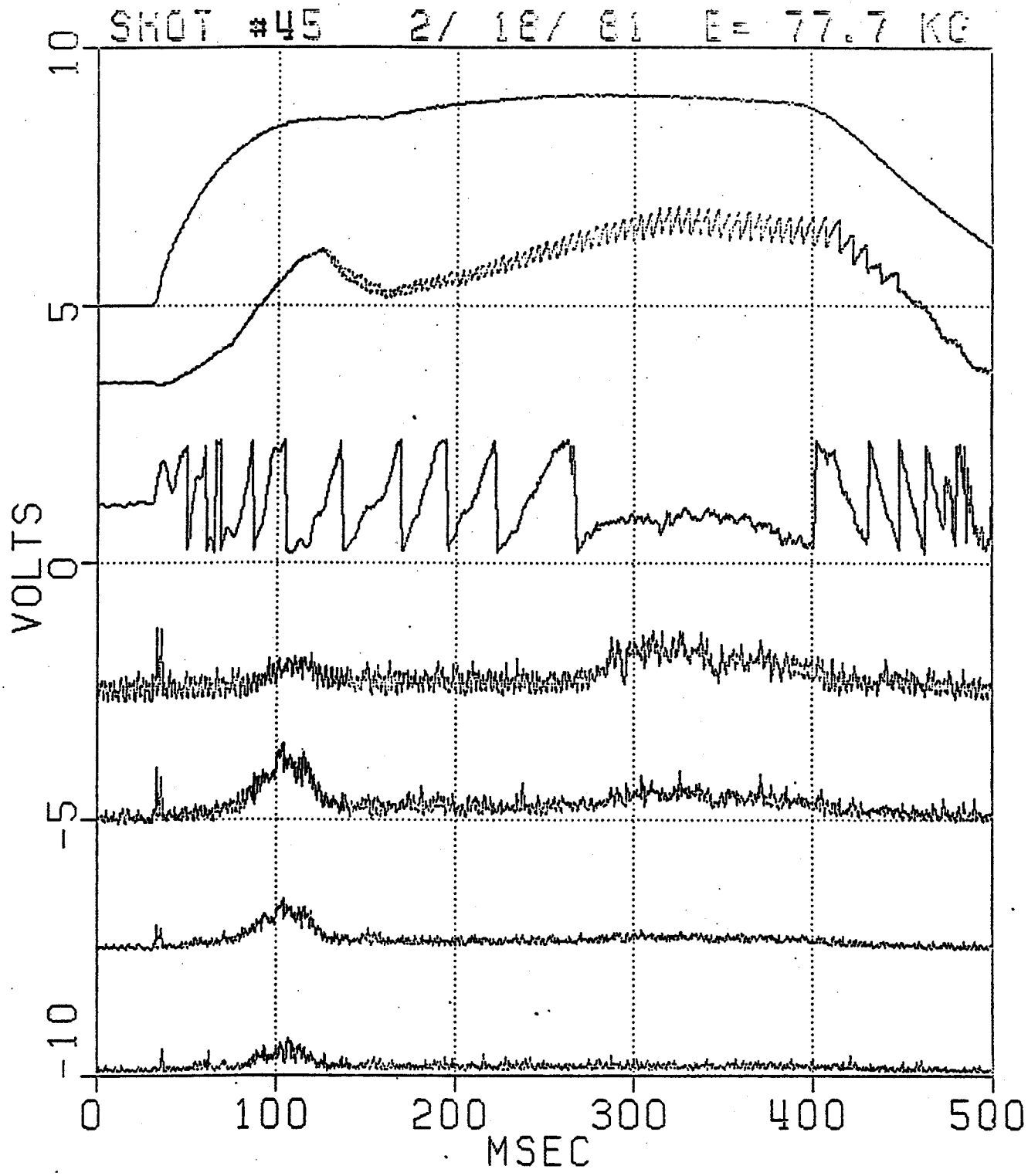


Fig. 40 — Density threshold effect displayed in a 78 kG discharge. Much higher values of density are required to initiate MHD activity after the current rise.

Table 3

Threshold density in deuterium at 78 kG

| $\overline{n}_c$ ($10^{14}$ cm$^{-3}$) | field (kG) | current (ka) |
|---|---|---|
| 4.67 | 77.1 | 332 |
| 5.11 | 77.7 | 491 |
| 4.85 | 77.7 | 504 |
| 4.95 | 77.7 | 522 |
| 3.92 | 76.4 | 459 |
| 4.64 | 76.4 | 495 |

The confirmation of this threshold effect at the higher field suggests the usefulness of determining a scaling law which could give the MHD threshold density at any toroidal field. *If* the empirical function is found to be particularly simple, it might help to elucidate the physical mechanism(s) behind this phenomenon. Two very general possibilities are: (1) a linear fit, and (2) a fit with the functional form, $B^{\alpha}$. Since there were only two sets of data points compiled during the initial period of this thesis study, the straight line fit is trivial:

$$\overline{n}_c\,(10^{14}\,\mathrm{cm}^{-3}) = 0.104\,B(\mathrm{kG}) - 3.33 \tag{72}$$

The most noticeable difference between this linear fit and a form of type (2) is that the curve intercepts the horizontal axis at a finite $B$-field of 32 kG rather than the origin. This means that at very low fields, MHD activity should be evident during the steady state at any density, no matter how low. In principle this conjecture should be easy to prove or disprove experimentally.

The second type of fit is also easy to determine by noting that:

$$\frac{\overline{n}_c|_{78}}{\overline{n}_c|_{55}} = 2.00$$

$$\text{and} \quad \frac{78\ \mathrm{kG}}{55\ \mathrm{kG}} = 1.42 \simeq \sqrt{2.00}$$

Therefore a scaling law having a quadratic dependence:

$$\overline{n}_c = \mathrm{const} \times B^2 \tag{73}$$

gives a nearly perfect fit to the limited data discussed so far, with:

$$\text{constant of proportionality} = 7.9 \times 10^{4}\ \text{cm}^{-3}\text{gauss}^{-2} \tag{74}$$

In more practical terms, equations (73) and (74) can be expressed as:

$$\bar{n}_c\,(10^{14}\text{cm}^{-3}) = 7.9 \times 10^{-4} B^2(\text{kG}^2) \tag{75}$$

The standard deviation of the constant of proportionality for all the data at 55 and 78 kG is 14%. With these two simple laws in mind (eqs. 72 and 75), a long term program was initiated to push for high densities and both high and low extremes in toroidal magnetic field, while measuring the threshold density over the entire parameter space covered by tokamak operations. Much of this work was done in "piggyback" with other experimental programs which also happened to require one or more of these particular extremes.

Initially the specific goal of this undertaking was to acquire data up at ~100 kG and down at 40 kG, and also at any intermediate fields that happened to be encountered in the process. The actual maximum $B$-field achieved, until very recently, was ~95 kG. At this field, extrapolation of the linear fit specified in equation (72) gives:

$$\bar{n}_c(\text{linear}) = 6.6 \times 10^{14}\,\text{cm}^{-3},$$

while the quadratic fit (equation 75) gives:

$$\bar{n}_c(\text{quadratic}) = 7.1 \times 10^{14}\,\text{cm}^{-3}$$

Because of the real variation in the threshold measured at 55 and 78 kG, these two predictions are well within the standard deviation expected at 95 kG, and therefore the two scaling laws cannot be distinguished in the actual experiment. However it is still worthwhile to make this measurement at these highest fields because just the observation of a threshold behavior on MHD activity would be important. Since we have no theoretical understanding

of this phenomenon yet, the prediction of an $\overline{n}_c$ by any empirical law might be considered wild speculation. It could turn out the MHD activity is observed at all densities in 95 kG discharges, and that the density threshold effect might be just an interesting, but irrelevant quirk seen only at intermediate toroidal fields.

The extrapolated predictions for $\overline{n}_c$ at 95 kG are extremely high. They are close to the maximum densities which Alcator C had been designed to achieve. In fact, these densities are among the highest ever run in any tokamak in the world to date. After many days of fine tuning the machine, the record high densities were reached on a handful of shots, and indeed, the MHD threshold effect was confirmed. Figure 41 is the standard depiction of the principle plasma parameters for one of the highest density discharge realized so far. In this case the interferometer trace reaches 11.7 fringes, or $6.7\times10^{14}$ cm$^{-3}$ line average. The familiar $m = 2$ and $m = 3$ amplitudes show measurable activity starting at a density of $6.3\times10^{14}$ cm$^{-3}$ (11 fringes). Table 4 lists the three shots which surpassed this density and exhibited resistive MHD instabilities, and also several shots which apparently were just below the threshold, and demonstrate the finite standard deviation in $\overline{n}_c$. Again, only deuterium plasmas were produced. The measured value of $\overline{n}_c$ is slightly below that predicted by either the linear or quadratic scaling law, but well within one expected standard deviation of both. Although this "error" may be insignificant, there was a qualitative difference noted in the density profile at these high levels. Even though it is normally characterized as broad and flat at all densities, the profile became noticeably flatter near 11 fringes and above. At the same time, the period of the sawteeth oscillations began to decrease with density, as evident from the graph in Fig. 42. It is not known whether these two anomalies are correlated, and there is no suggestion that the onset of MHD caused the profile changes. But it is noted that the net result is to increase the local density at the $q = 2$ surface for a given line average density. If the MHD threshold physics depends directly on density at the resonant surface, then the observed onset would occur at a lower line average density than expected from extrapolation of lower field, lower density results. The set of all the $\overline{n}_c$ data discussed so far, as well as a few points at non-standard fields, is plotted against $B_t$

Table 4

Threshold density in deuterium at 95 kG

| $\overline{n}_c$ ($10^{14}$ cm$^{-3}$) | field (kG) | current (ka) |
|---|---|---|
| 6.44 | 95.8 | 552 |
| 6.37 | 95.8 | 549 |
| 6.32 | 95.8 | 550 |
| 6.61 (no MHD) | 95.8 | 520 |
| 6.44 (no MHD) | 95.8 | 528 |

in Fig. 43, along with the two specified best-fit curves. At this stage both curves fit the data successfully; perhaps the straight line looks slightly more accurate. Obviously in order to distinguish which is the actual scaling law, plasmas must be run at both higher (>110 kG) and lower (25-50 kG) magnetic fields. Unfortunately, problems with Alcator's toroidal current rectifying power supplies have prevented operation of the tokamak above 100 kG to date. Eventually plans do call for confinement experiments at 120 kG, and concerted efforts will, of course, be made to measure the MHD threshold effect. However the densities predicted by either extrapolation method are well beyond the capabilities of any other tokamak in the world. Because of the finite limits of the two ohmic heating power supplies, even Alcator C may not be able to run long enough discharges to enable the buildup of density which might be required. But, if the unexpected flattening of the density profile which appeared near $6\times10^{14}$ cm$^{-3}$ remains at even higher densities, then there is a chance MHD activity might still be seen at 120 kG.

In contrast, operation of Alcator within a range around 40 kG has been achieved in hydrogen without too much trouble. The threshold effect is clearly seen, and the data accumulated on $\overline{n}_c$ seems to favor the $B^2$ curve rather than the straight line. But the relative scatter in the measured values still could leave room for doubt, so the decision was made to undertake a run at 30 kG. This field was chosen because it is less than the intercept of the linear fit, so that formula would predict MHD activity at all densities during the steady state, whereas the quadratic scaling gives a finite threshold density $0.7\times10^{14}$ cm$^{-3}$ (more than 1 fringe). However 30 kG was also less than the machine was initially capable of achieving;

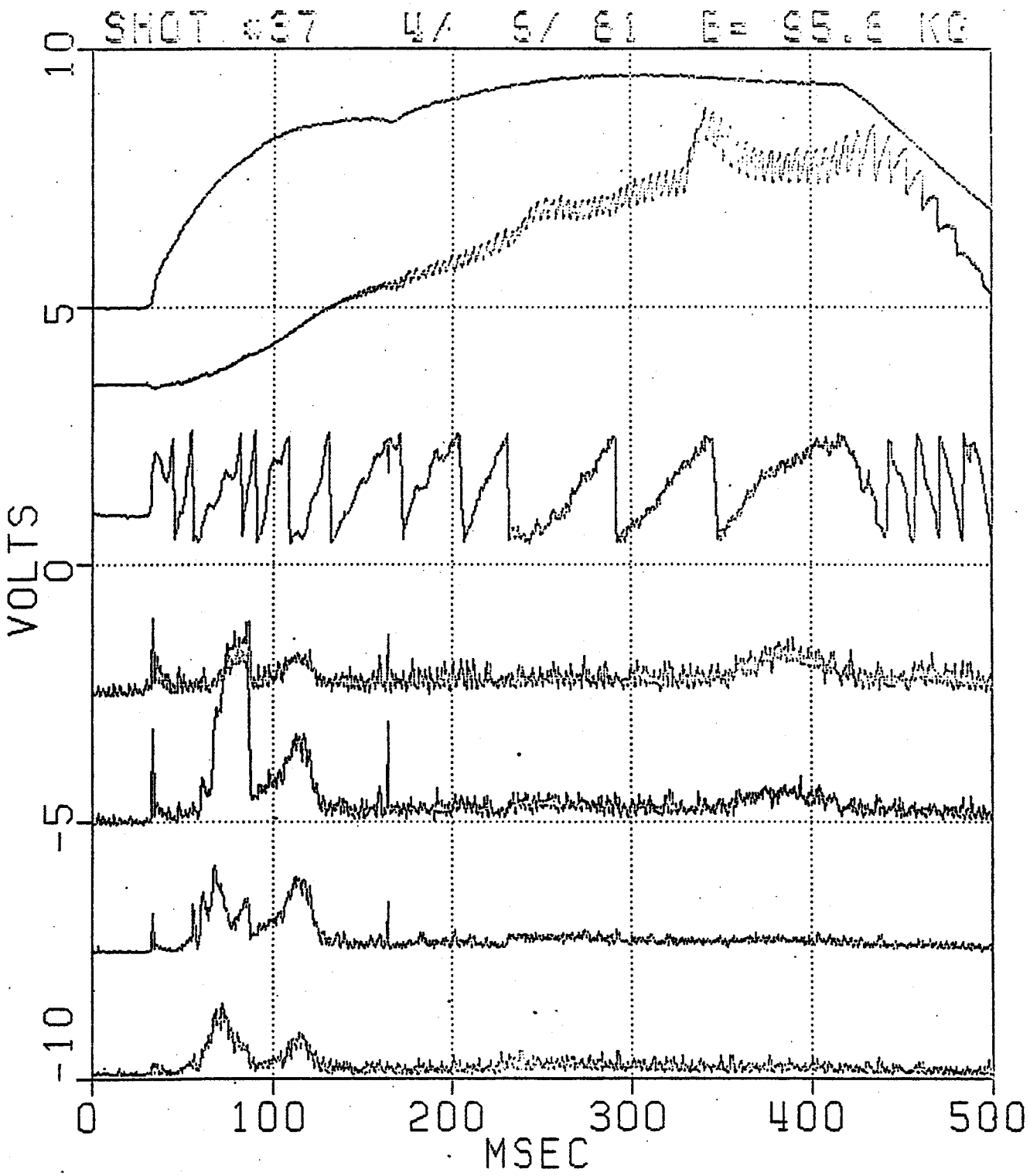


Fig. 41 — Confirmation of the MHD threshold effect at 96 kG. The peak density is one of the highest values achieved so far in any tokamak. MHD perturbations are detected at ~11 fringes ($6.3 \times 10^{14}$ cm$^{-3}$).

specifically the horizontal field supply could not be programmed to properly center the plasma vertically. Modifications were effected which enabled successful operation of several hydrogen discharges at 30 kG. No deuterium plasmas could be sustained because of a well-documented[66] increase in molybdenum impurity levels at very low densities, resulting in a substantial enhancement of radiation and apparently causing hollow temperature profiles and repetitive disruptions. It should also be pointed out that even in hydrogen, sawteeth oscillations could not be resolved on the soft x-ray emission at these low densities. However they are probably present since the hydrogen shots were not dominated by high-$Z$ impurities. The inability to resolve the sawteeth is assumed to be due to the greatly decreased intensity levels (temperatures at 30 kG were lower), as well as the very short sawteeth period (<1

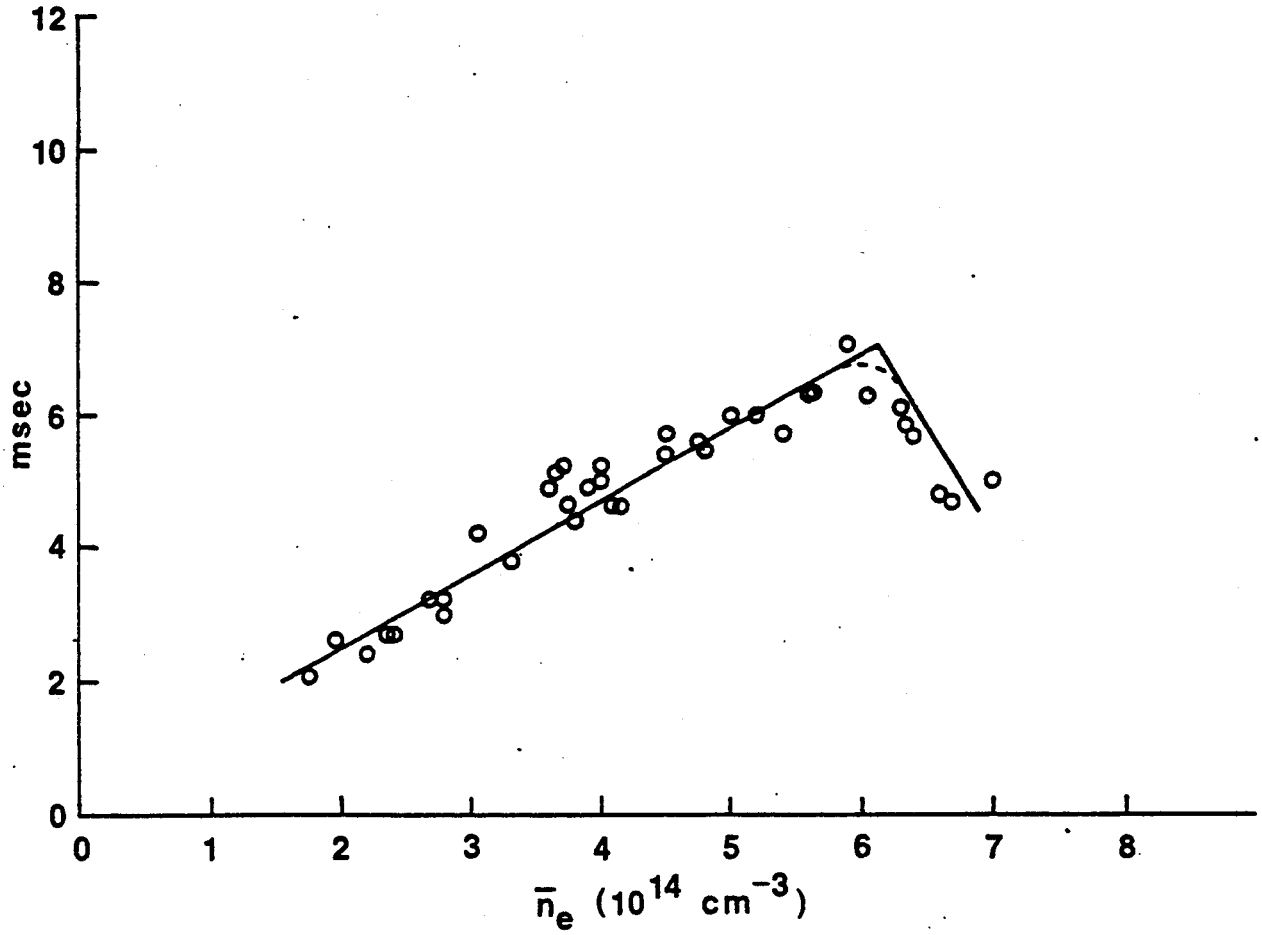


Fig. 42 — Sawtooth period versus density at 95 kG. The turnover at $6.1 \times 10^{14}$ cm$^{-3}$ may be related to a simultaneous flattening of the density profile. Courtesy of Dr. D. Overskei.

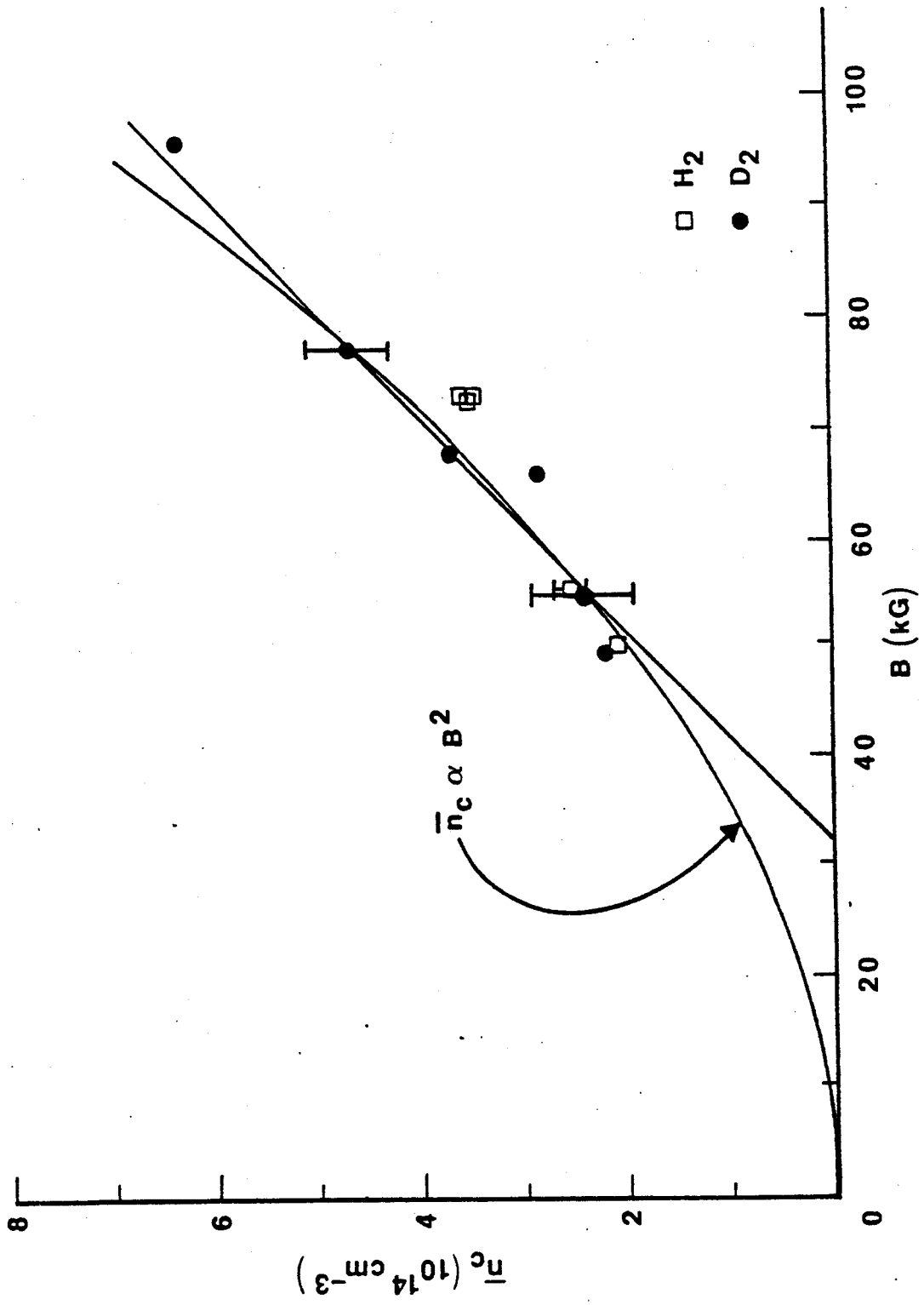


Fig. 43 — Plot of $\overline{n}_c$ versus $B_t$ for the medium and high field regimes discussed so far in the text. Data at low $B$-fields are obviously needed to distinguish between the linear and quadratic fits.

msec) in the one-fringe regime. The macroscopic features of the 30 kG plasmas showed large variations from shot-to-shot, which is to be expected for a first attempt in this new region. Nevertheless, the density threshold effect was definitely operating, in direct contrast with the linear fit predictions. The low field values of $\overline{n}_c$ are plotted with the rest of the data in Fig. 44. The quadratic scaling law specified by equation (75) is an excellent fit to the points over a range spanning more than a factor of 3 variation in toroidal field and an entire order of magnitude in density. This simple dependence of $\overline{n}_c$ on $B^2$ is suggestive of a straightforward physical mechanism which is responsible for the observed MHD behavior in this tokamak. Several plausible hypotheses on the threshold effect will be advanced in section V.

The scaling of this phenomenon with plasma current has already been detailed at 55 kG. During the toroidal field scan program, data was also collected on the current at the start of MHD activity. Except for the 55 kG data, and to lesser extent the 78 kG data, all discharges were run within a very narrow range of the limiter safety factor around $q(a) \simeq 3.4$. Because of this tendency to run higher currents at higher fields, a direct plot of $\overline{n}_c$ versus plasma current, as in Fig. 34, gives the false impression that there is strong correlation between $\overline{n}_c$ and $I_p$. This misleading notion is refuted by the proper study done at 55 kG, where the plasma current was varied independently of the magnetic field. The correct way to sort out any systematic dependence on current over the range of toroidal field is to first divide out the known parametric dependence on $B^2$ and then plot the resulting values of $\overline{n}_c/B^2$ against $I_p$. Figure 45 displays this information for all the data described here. As one might have expected from the findings at 55 kG, there is apparently no dependence of the MHD threshold on plasma current when it is varied as an independent parameter. Here though, the range of $I_p$ has been extended, and now goes from 167 ka to 550 ka. Given the previously specified standard deviation in $\overline{n}_c$, the data in Fig. 45 can be justifiably fit with a horizontal straight line. The intercept of this line is seen to be the constant of proportionality (equation 74) in the quadratic scaling law, $7.9 \times 10^4$ cm$^{-3}$gauss$^{-2}$.

The magnetic field study also yielded a limited amount of information on disruptions.

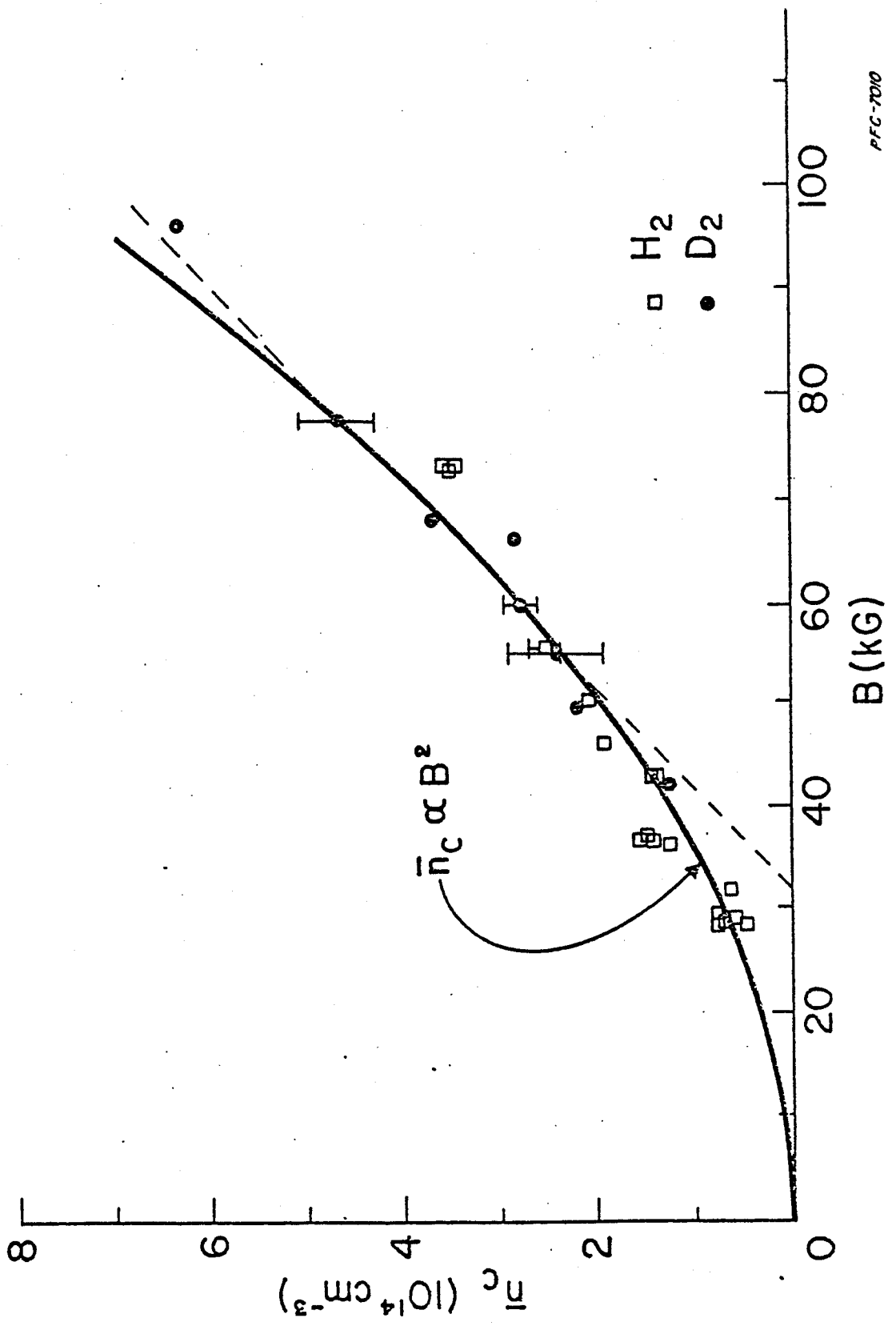


Fig. 44 — Plot of the MHD threshold density versus toroidal magnetic field. The quadratic curve is given by equation 75. The vertical bars are not error bars; they represent the standard deviation at fields for which there are too many points to plot individually.

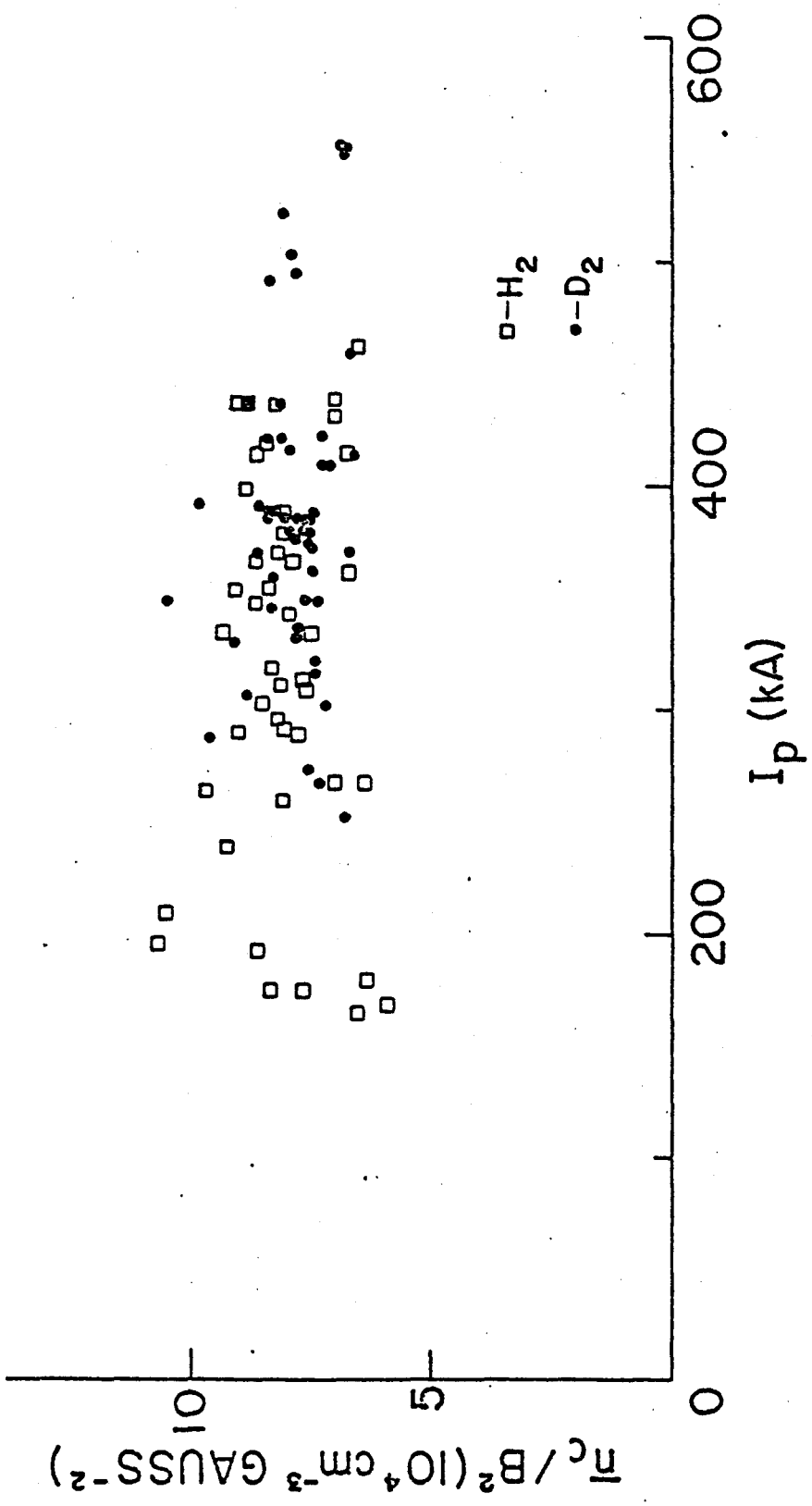


Fig. 45 — Plot of $\bar{n}_c/B^2$ versus $I_p$ for the data displayed in the previous graph. Given the standard deviation of 14%, the threshold seems to be completely independent of plasma current.

Remember that at 55 kG, high density disruptions (i.e. above $\overline{n}_c$) appeared to be caused by growing $m = 2$ and 3 magnetic islands and on the average occurred when the line average density climbed to $\sim$45% above $\overline{n}_c$. After finding that $\overline{n}_c \sim B^2$, one might expect a similar scaling of the disruption limit. But in 1976, Murakami pointed out an empirical linear dependence of the maximum attainable density on the toroidal magnetic field for a dozen prominent tokamak experiments[67]:

$$\overline{n}_{max}(10^{13}\ \mathrm{cm}^{-3}) \simeq K\frac{B_t(\mathrm{tesla})}{R(\mathrm{m})} \tag{76}$$

where

$$K \simeq 1.1$$

and $R$ is the major radius. (For Alcator C, $R = 0.64$ m.) This scaling has some limited theoretical basis—its justification having to do with ohmic power deposition in the plasma core. But in recent years many tokamaks have surpassed the original Murakami limit by a factor of $\sim$4, and in some cases, by 7 or 8. Therefore the Murakami scaling law is no longer considered by many researchers to be relevant.

Because of the extremely high densities required just to initiate MHD activity at 95 kG, the $\dot{B}_\theta$ amplitude has never reached the levels measured during disruptions at lower fields. Presumably this is the reason why no disruptions have occurred yet at 95 kG for densities above $\overline{n}_c$. In fact, even at 80 kG, only a few shots reached the conditions necessary to produce an MHD induced disruption. Fortunately (?), at 40 kG the required densities are relatively easy to achieve, and as a result disruptions are not uncommon at this toroidal field. The available data is graphed in Fig. 46. The curved line is a very suggestive fit which is based on the MHD threshold scaling law of equation (75), but with a coefficient approximately 45% greater than in equation (74):

$$\overline{n}_{max}(10^{14}\ \mathrm{cm}^{-3}) = 11.5 \times 10^{-4} B^2(\mathrm{kG}^2) \tag{77}$$

The series of straight lines indicate Murakami scaling, but with several different enhanced

values for the constant of proportionality. Because of the lack of data at high fields, it would be premature to assume a quadratic relationship between the maximum attainable density and the toroidal field. However, this fit does appear to be qualitatively better than any single Murakami line. Because of the extremely high densities predicted by equation (77) above 95 kG, it might not be possible to get MHD induced disruptions at 100 kG and higher.

Equation (77) gives a very preliminary indication of one factor involved in disruptions and maximum operating conditions. There are most likely other parameters which also influence the density limit. For example, note that there is one point in Fig. 46 which is significantly below the quadratic curve. Of course many disruptions occur at low densities; however, as explained in section IV.3, these events occurring below $\overline{n}_c$ are apparently not caused by MHD activity and are not at all predictable. The graph in Fig. 46 is only for disruptions associated with magnetic oscillations, which are well above $\overline{n}_c$. The anomalous shot was above the threshold and did indeed exhibit large magnetic perturbation amplitudes, so it certainly belongs on the graph. But this discharge also had an unusually fast rate of density rise. Figure 47 shows this shot and the difference in the gas input programming is immediately obvious when compared to the intermediate field data exhibited in previous figures. Obviously the disruption limit is deleteriously effected by high $\frac{d\overline{n}}{dt}$, and this is not reflected in the scaling of equation (77). Another possible factor which has been totally ignored is the plasma current. Conventional wisdom maintains that increased plasma current allows for higher densities. Because of the limited number of disruptions recorded above $\overline{n}_c$, there is virtually no data on any current dependence in this regime. The questions surrounding density limits and disruptions are of critical importance for thermonuclear reactor design, and therefore these first steps toward the answers should be continued and expanded upon in future experimental programs at Alcator. If the quadratic increase with toroidal field is verified (presumably for $\frac{d\overline{n}}{dt}$ not too large) and the confinement time does not decrease at these high densities, then very high magnetic field tokamaks may be more relevant to future machine designs than currently believed. (One must not forget, however,

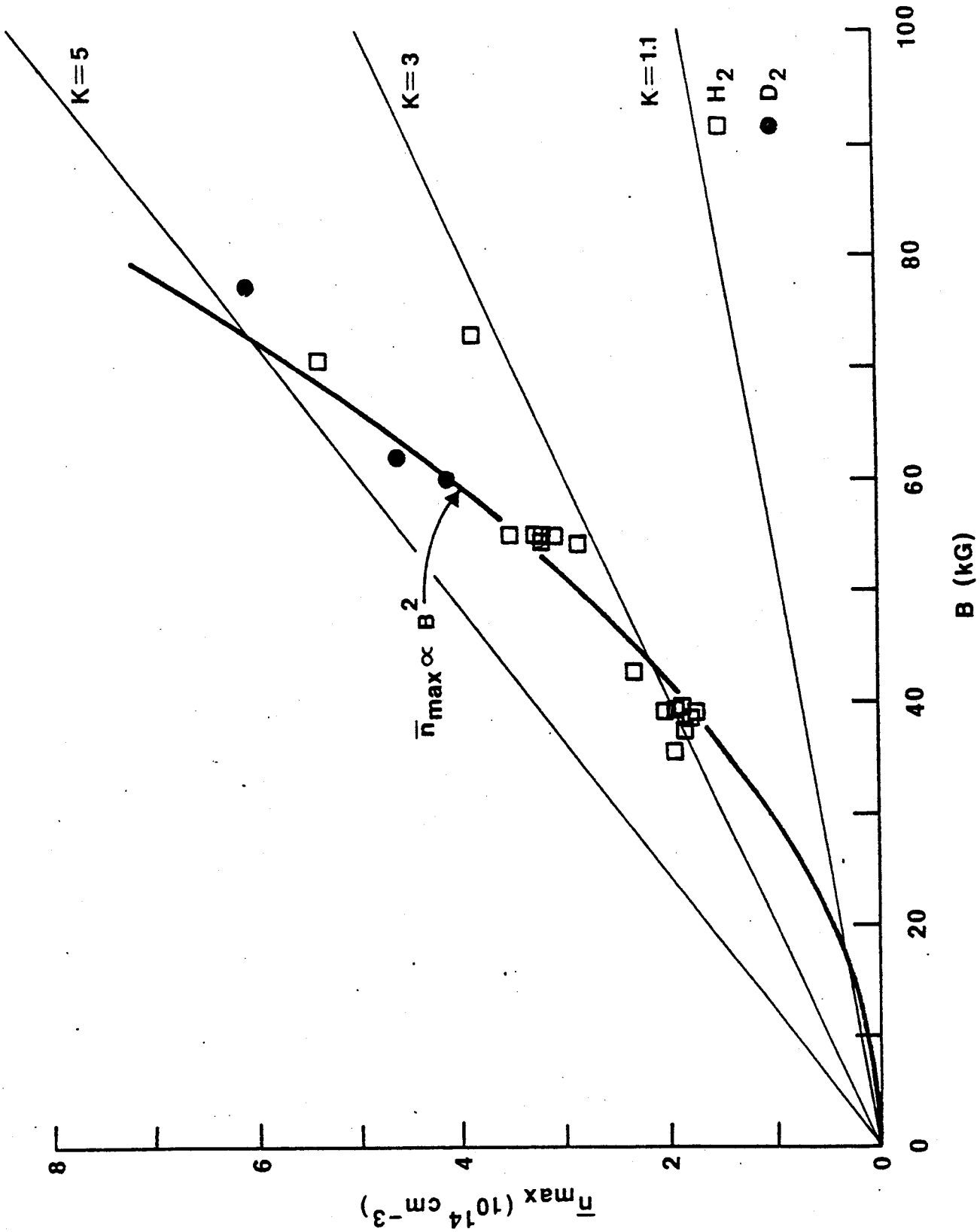


Fig. 46 — Plot of maximum density reached prior to major disruption versus $B_t$. The straight lines represent Murakami scaling with several constants of proportionality. The peak densities achieved in Alcator C are a factor of 3-5 times the original Murakami law ($K = 1.1$).

that most of the disruptions seen in Alcator C occur below $\overline{n}_c$, by processes completely unknown so far).

The classification of the observed disruptions into two distinct groups, one above $\overline{n}_c$ and one below $\overline{n}_c$, does not completely cover the disruption picture in this tokamak. A small subset of plasma shots suddenly terminate right around $\overline{n}_c$, and have a small, but finite MHD amplitude. While this does not fit the characteristics of either low or high density disruptions, I believe that these "transition" shots share the same physical mechanisms as the low density group, as far as the cause of the disruption is concerned. This is because the measured MHD amplitude is much less than the perturbation levels detected for the data in Fig. 46, so it is doubtful that large, overlapping magnetic islands caused the disruptions. Rather it is more logical to assume that the low level of MHD activity which occurs near $\overline{n}_c$ has nothing to do with these disruptions—they are actually examples of the unpredictable low density cases which just happened to occur near $\overline{n}_c$.

On the topic of disruptions, it is interesting to note that total termination of the plasma current does not always occur. In fact some Alcator discharges show a remarkable tolerance to minor (i.e. non-terminating) disruptions. Figure 48 shows one of these pathological shots, and an expansion is displayed below in Fig. 49. The plasma undergoes many repetitive minor disruptions, sometimes up to twenty or more. Spectroscopic analysis indicates enhanced line radiation losses, which is probably the result of high-$Z$ molybdenum impurities building up to intolerable concentrations[68]. The $2^{\underline{nd}}$ harmonic cyclotron emission reveals very low central electron temperatures, as well as hollow temperature profiles. In the expanded view, it is seen that no measurable MHD activity is detected until the soft x-ray signal falls. This is also characteristic of the low density class of major disruptions, and it suggests that high-$Z$ impurities are somehow involved in causing both types of phenomena. The remarkable fact is the repetitive nature of these minor disruptions—the plasma is apparently unable to expel the impurities.

MHD modes have been shown to occur when $\overline{n}/B^2$ is greater than a certain constant. Although plasma density by itself is not usually studied in MHD theory, the plasma pres-

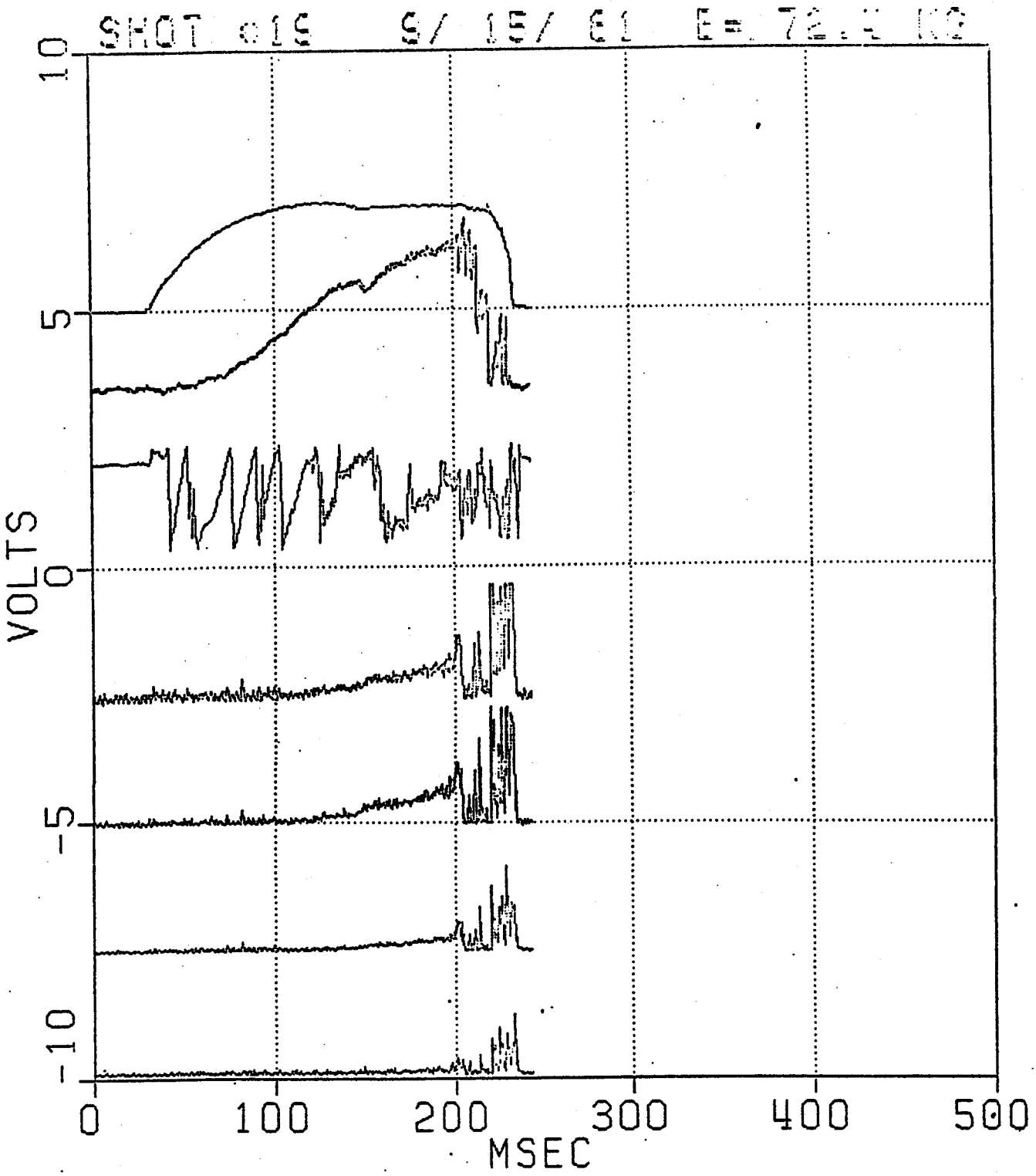


Fig. 47 — High density disruption which is well below the quadratic curve in Fig. 46. Note the abnormally fast rate of density rise, which probably influenced the MHD activity.

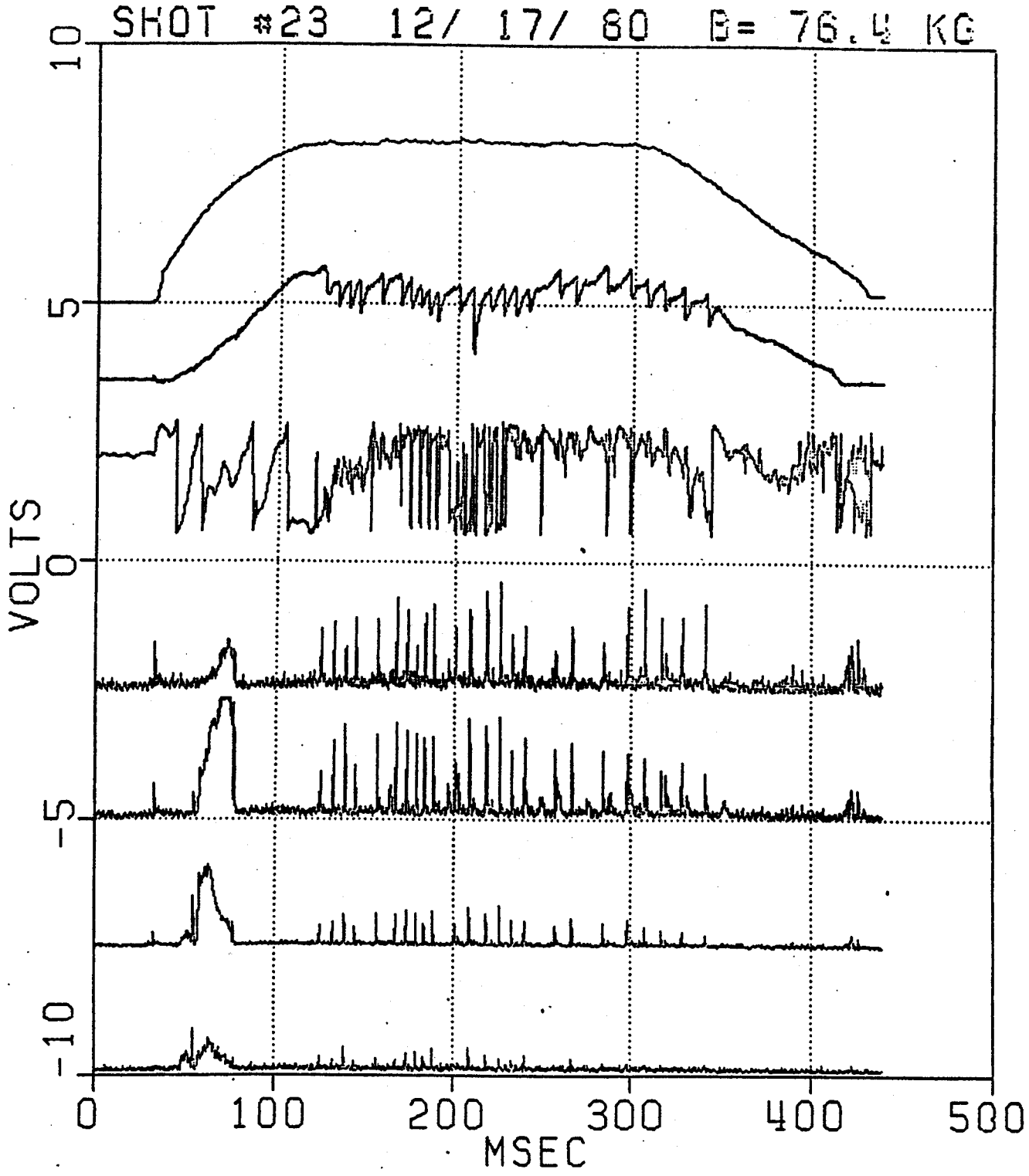


Fig. 48 — Example of a bizarre class of discharges which exhibits many repetitive disruptions. The soft x-rays are not sawtoothing. These shots are characterized by large molybdenum impurity concentrations.

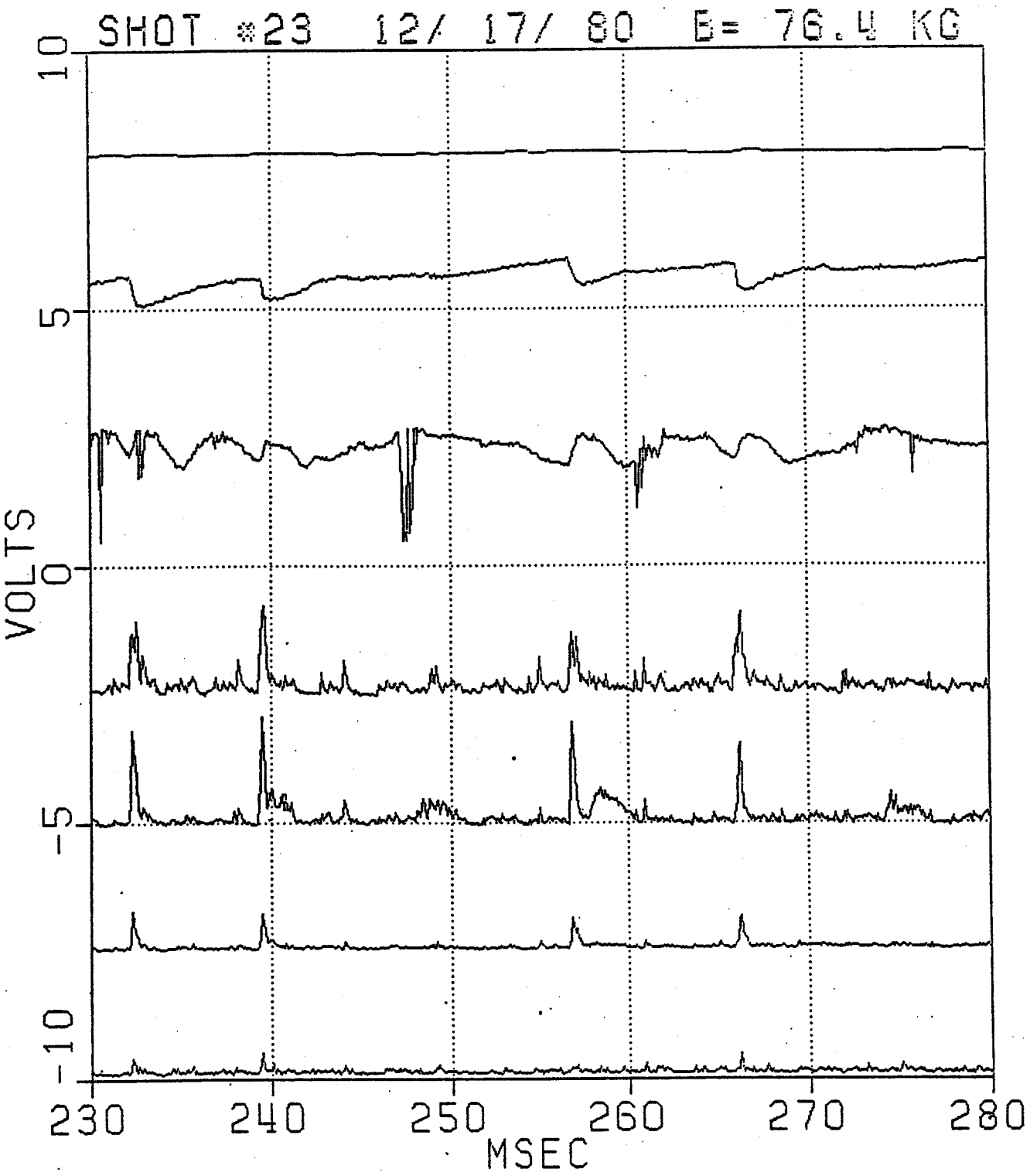


Fig. 49 — Expanded view of the previous figure. Note the lack of MHD activity detected prior to each disruption.

sure, $p = \sum_{e,i} nkT$, is an integral part. In the theory, kinetic pressure often appears as a dimensionless quantity, $\beta$, which is defined to be the ratio of plasma pressure to magnetic field pressure (or $B$-field energy density). Two different $\beta$'s are found to be important in MHD stability analysis (Gaussian units):

$$\beta \equiv \frac{\sum_{e,i} nkT}{B^2/8\pi}$$
$$\text{and} \quad \beta_p \equiv \frac{\sum_{e,i} nkT}{B_p^2/8\pi} \tag{78}$$

where $B_p$ is the poloidal magnetic field, i.e. $B - B_z\hat{z}$. In a straight cylindrical equilibrium this is just $B_\theta$. The total plasma beta in the center of the discharge at the start of MHD activity is therefore:

$$\beta_c(0) = 8\pi\left(\frac{n_o}{\overline{n}_c}\right)\left(\frac{\overline{n}_c}{B^2}\right)(T_{eo} + T_{io}) \tag{79}$$

In Alcator C the shape of the hydrogen or deuterium density profile is invariant throughout the operating parameter range, except for the highest densities (greater than $6.1 \times 10^{14}$ cm$^{-3}$ line average). Therefore the value of $n_o/\overline{n}$ can considered constant with an empirical value of 1.3. At the very high densities achieved in 95 kG discharges, $n_o/\overline{n}$ decreases somewhat to $\sim$1.1 — 1.2. Thus if the peak temperatures *at the start* of MHD activity are found to be approximately the same, then the observed density threshold could also be interpreted as a $\beta$ threshold. This would be advantageous from a theoretical standpoint, since finite $\beta$ is predicted to cause several different types of pressure driven MIID instabilities, however, usually at values of 5-10%. The ion and electron temperatures in Alcator vary over quite a large range, $\sim$600 — 3000 eV, depending on the density, toroidal field, plasma current, fill gas, impurity concentrations, etc.; so at first glance it may seem preposterous to even consider that $T_o$ could be constant at the start of MHD activity over the entire explored parameter range. But it turns out that in general, temperatures rise with increasing $B_t$ but fall with increasing $\overline{n}_c$, so it is at least conceivable to have a constant $\beta(0)$ at the start of

Table 5

Ion and electron temperatures at MHD threshold

| $B$-field (kG) | Gas | $\overline{n}_e$ ($10^{14}$ cm$^{-3}$) | $T_{io}$ (eV) | $T_{eo}$ (ev) |
|---|---|---|---|---|
| 40 | $H_2$ | 1.3 | 740 | ~775 |
| 55 | $H_2$ | 2.4 | 750 | 950 |
| 55 | $D_2$ | 2.4 | 860 | 1050 |
| 78 | $D_2$ | 4.8 | 900 | 1100 |
| 95 | $D_2$ | 6.3 | 875 | 1250 |

MHD activity. Unfortunately most of the ion and electron temperature data were measured and tabulated before the $m$-spectrum analyzer was built and installed on the tokamak. Consequently $\beta$ cannot be calculated for each shot represented in Fig. 44. Rather an average value must be inferred from the compiled graphs of $T_{io}$ and $T_{eo}$ at 40, 55, 78, and 95 kG in deuterium and hydrogen. (For example, the 55 kG $D_2$ data is exhibited in Fig. 31.) Table 5 lists the mean temperatures from the available data at the proper value of $\overline{n}_e$ for each field. Substituting these values into equation (79) along with $\overline{n}_e/B^2$ from equation (74) yields the following $\beta_c(0)$'s:

| | | | |
|---|---|---|---|
| | $\beta_c(0)\|_{40} = 0.63\%$ | | — |
| Hydrogen: | $\beta_c(0)\|_{55} = 0.70\%$ | Deuterium: | $\beta_c(0)\|_{55} = 0.79\%$ |
| | — | | $\beta_c(0)\|_{78} = 0.83\%$ |
| | — | | $\beta_c(0)\|_{95} = 0.88\%$ |

The variation in $\beta_c(0)$ at different fields and in different isotopes is only about a factor of ~1.4, but this is considerably more that the standard deviation of $\overline{n}_e/B^2$. Hence, the hypothesis that a critical value of $\beta$ triggers the onset of resistive modes in Alcator C can probably be ruled out. Although only the peak value of $\beta$ has been looked at so far, it is unlikely that a local value of $\beta$ (at the singular surface, for example) or volume average would yield more consistent results, since the density and temperature profile *shapes* don't show much change over the large parameter space scanned for MHD activity.

The poloidal beta can be expressed in terms of total $\beta$:

$$\beta_p = \beta(0)\frac{B_t^2}{B_\theta^2(a)}$$
$$\beta_p = \beta_o\left(\frac{R}{a}\right)^2 q^2(a) \tag{80}$$

As mentioned previously, during the program of study leading to the data in Fig. 44, the limiter $q$ was held at a nearly constant value of 3.4 (except at 55 kG) and so $\beta_p$ was simply a constant multiple of $\beta(0)$. Therefore it also varies by the same amount as $\beta(0)$ does at the start of MHD activity. These findings lead to the conclusion that the physical mechanism responsible for the MHD threshold effect is truly density, and not the plasma pressure or beta.

IV.5 MHD activity and marfes

High on the list of unusual phenomena exhibited in Alcator C is the so-called "marfe"[69]. These events are characterized by a sudden increase in the visible emission from the inside edge of the plasma. The enhancement is typically a factor of 2 to 10 and can last from 10's of milliseconds to most of the discharge. Simultaneously the signal from the innermost chord of the density interferometer frequently breaks up, rendering the diagnostic useless over the inside region of the plasma. This problem is thought to be due to a very large density gradient associated with the marfe which refracts the laser beam out of the acceptance angle of the interference detector. During the very worst marfes, even the central density chord may be affected and the temperature profile may actually shrink a few centimeters. Bolometric and spectroscopic analysis from several different viewing angles has revealed a more detailed picture of this enhanced emission. It is localized in the poloidal plane to the inside edge of the plasma and usually above the midplane, although it is not clear yet whether the marfe actually extends into the plasma or is just in the shadow of the limiter. The enhanced emission is seen simultaneously in ports at several different toroidal locations and it does not appear to follow the rotational transform of the magnetic field. The emission most likely comes from low-$Z$ impurities such at nitrogen, carbon, and oxygen. No consistent theoretical explanation has been advanced yet, but preliminary speculations invoke some kind of interaction between the edge plasma and the limiter. As far as MHD activity is

concerned, a very important observation is that marfes *invariably* occur at high densities and are also occasionally seen at lower densities and during the current rise. Given that the plasma current profile may be affected by marfe activity, at least at the edge, is there a correlation between this phenomena and the magnetic islands detected by the $m$-spectrum analyzer? After all, they both are characteristically seen at high densities.

The answer is yes and no. The marfe phenomenon does not exhibit any consistent toroidal field dependence and its density dependence is not as repeatable as the MHD effect. By the time magnetic islands are picked up on the $m$-spectrum analyzer during the steady state current plateau, a marfe almost always exists. But the opposite is not true; there are many examples of intense marfe emission with absolutely no magnetic perturbations above the noise level. So in general the two phenomena are not strongly correlated. However there are a number of discharges in which the timing between the marfe and MHD activity indicates a definite coupling. Usually this type of event is associated with a gross change in the plasma, due to impurity injection, for example. Figure 50 shows an extreme example of this coupling. After reaching a peak density somewhat below $\overline{n}_c$ in a hydrogen plasma, a large puff of nitrogen gas was injected at $t = 260$ msec. The central-chord soft x-ray signal rose dramatically, indicating an increase in $Z_{eff}$ and $T_e(0)$. The line average electron density actually decreased slightly. At the same time, $m = 2$ and $m = 3$ modes grow from non-existent to large amplitudes, closely mirroring the soft x-ray behavior, even though the line average density is below $\overline{n}_c$. Simultaneously a large enhancement in the visible plasma emission, displayed in Fig. 51, attests to a marfe event. This shot is obviously an unusual case, but other more "reasonable" examples of a correlation between MHD and marfes exist. However I believe that after examining all the data accumulated to date, there is no solid evidence of a cause-and-effect relationship between these two phenomenon.

### IV.6 MHD activity in helium

Helium discharges have been run in Alcator at 55 kG and qualitative differences are found in several macroscopic characteristics, as well as in the tearing mode activity. Primarily the density profiles in helium plasmas are considerably more peaked than in either

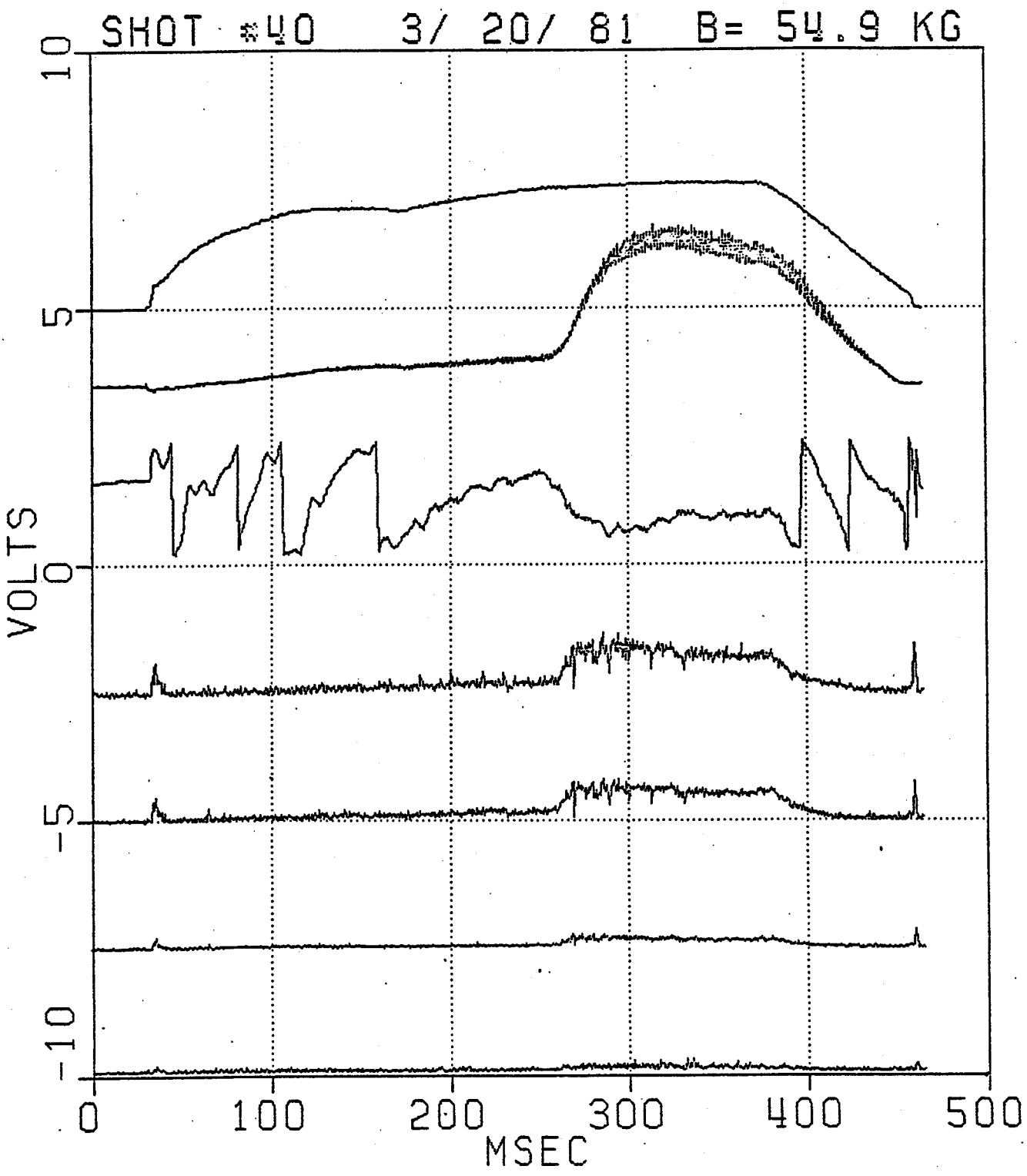


Fig. 50 — A hydrogen plasma into which nitrogen gas was injected at $t = 260$ msec. Gross changes are observed on the soft x-rays and magnetic pickup signals and to a lesser extent on the density.

hydrogen or deuterium. Even though the details have not been explained yet, several possible reasons for this difference can be enumerated; for one thing, helium plasmas have $Z_{eff} > 2$ whereas H and D typically have $1.1 \leq Z_{eff} \leq 1.4$. This affects both the radiation losses and also the ohmic power input rate through the $Z_{eff}$ dependence of the resistivity, $\eta$. In addition the kinetic pressure is no longer $n_e k(T_e + T_i)$ but rather $p_{He} = n_e k(T_e + \frac{1}{2}T_i)$ since the ions number only half of the electrons. Finally, neutral helium atoms at the vacuum wall interface form a noble gas, and the interactions and recycling going on in the limiter shadow are probably different than the corresponding processes in hydrogen isotopes, which are chemically active. Thus the edge density and particle influx rates could be substantially different. Considering all these facts, it is not surprising to find qualitatively different density profiles. Presumably the temperature and current profiles could also be qualitatively different, although the limited experimental data which has been gathered so far does not

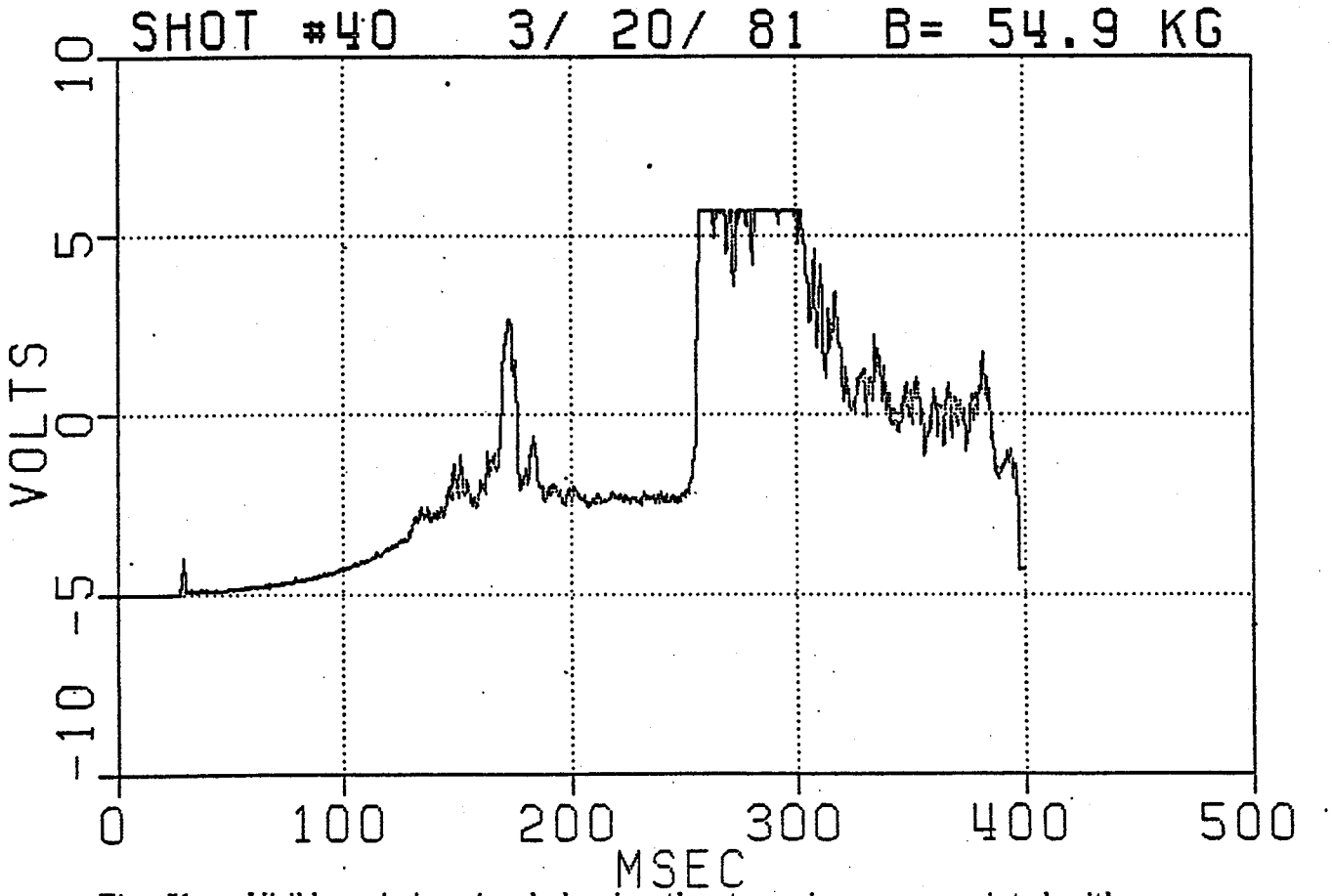


Fig. 51 — Visible emission signal showing the strong increase associated with a "marfe" event, apparently caused by the $N_2$ injection.

resolve any difference in the time-average profiles. However the sawtooth perturbations are markedly changed, with twice the amplitude and half the frequency of those in hydrogen or deuterium[37].

All of these distinctions were known to exist before the study of magnetic perturbations began with the $m$-spectrum analyzer. Clearly one should not expect the same MHD instability behavior in helium. Perhaps the value of $\overline{n}_c$ might be different, or there might not even be a threshold effect. This is one of the few instances where prior intuition proved to be correct. The $m = 2$ and 3 modes typically begin during the initial current rise and continue throughout the entire steady state portion of a helium discharge. Figure 52 illustrates this behavior. Although the sharp threshold phenomenon is gone, the rise in density above the 4-4$\frac{1}{2}$ fringe level still seems to coincide with a rapid increase in mode amplitude. This is admittedly somewhat subjective but it could hint that the underlying physical mechanism responsible for the threshold in H and D might even be operating in helium, even though it may no longer be the dominant term. High density disruptions in helium show the same characteristic behavior as those above $\overline{n}_c$ in H or D. Large, growing $m = 2$ and $m = 3$ signals follow the increasing line average density right up to the disruption.

One of the most intriguing results in helium is the correlation of MHD amplitude with decreased central confinement time of injected aluminum impurities. Using the laser blowoff technique[70] to introduce a short burst of several different types of impurity atoms into the edge plasma, Marmar and Rice have measured impurity confinement properties for many different elements, working gases, densities, plasma currents, etc.[71]. The technique relies on measurements of the time decay of characteristic radiation lines with an x-ray crystal spectrometer. The wavelengths are chosen to be representative of impurity charge states occurring predominantly at the center of the plasma. Because this yields an impurity confinement time for the central region of the discharge, it is unclear a priori whether or not tearing modes should appreciably alter the measurements, since the magnetic islands detected by the $m$-spectrum analyzer occur outside the $q = 1$ surface. Measurements of aluminum confinement in helium plasmas reveals a precipitous drop in $\tau_{Al}$ as the $m = 2$

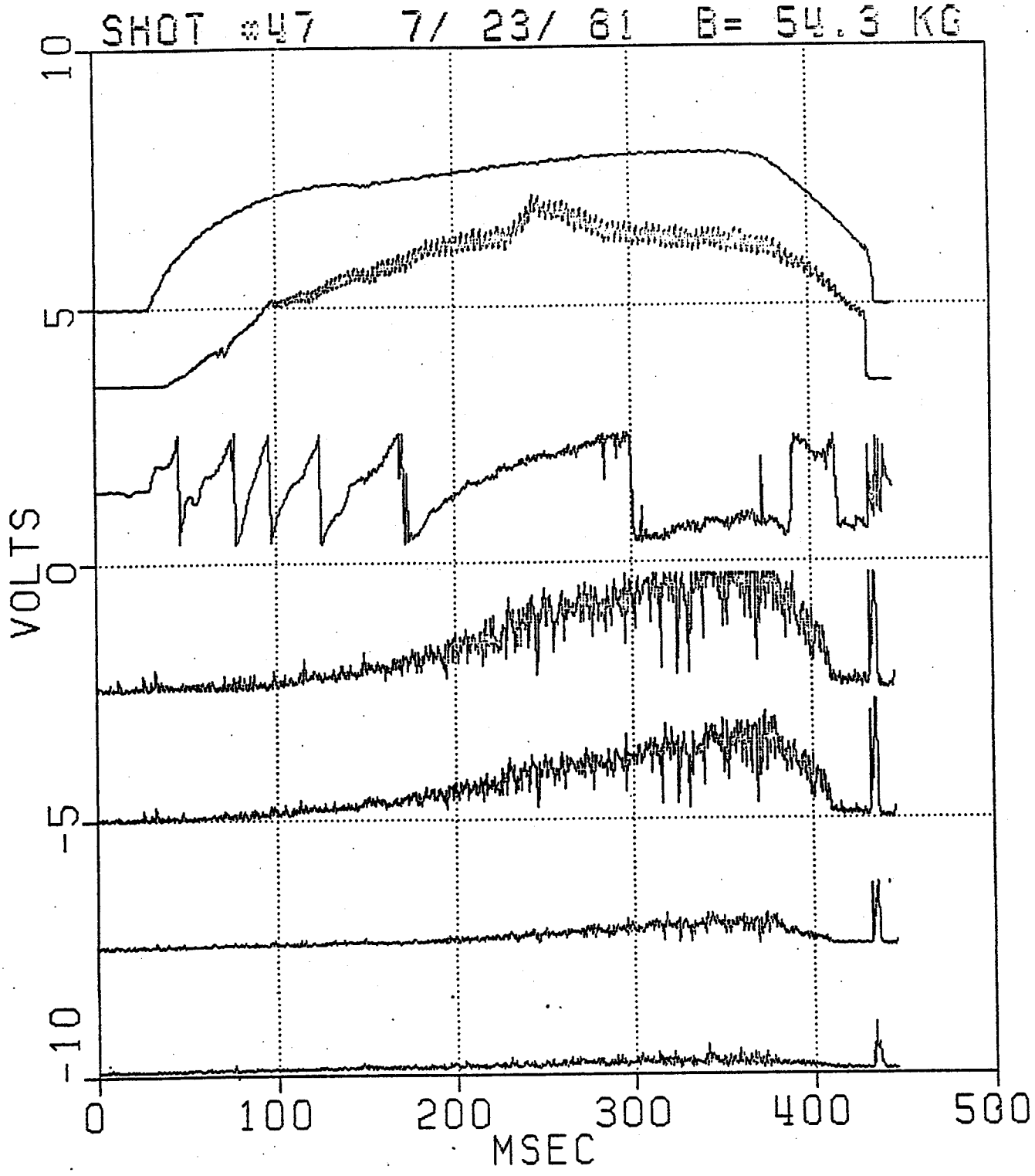


Fig. 52 — MHD activity in helium plasmas. The sharp MHD threshold with density is not evident, although the perturbation amplitude still increases with density.

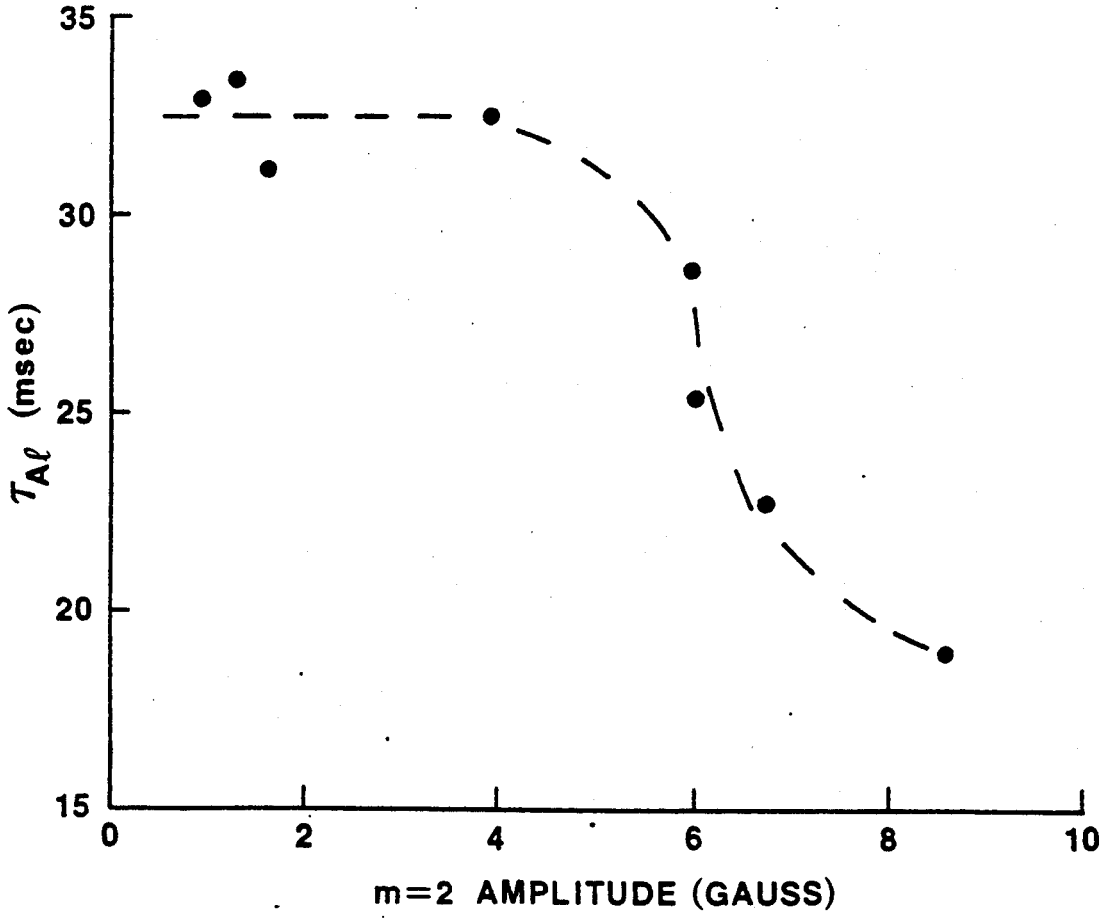


Fig. 53 — Confinement time of aluminum impurity ions in helium versus $m = 2$ amplitude. No such effect is seen in deuterium.

amplitude rises with increasing density. Figure 53 illustrates the factor of 2 decrease in confinement time. Higher densities could not be reached due to the disruption limit. These results are particularly surprising in light of the findings in deuterium. The same measurements were carried out twice in that gas with no discernible correlation between $\tau_{Al}$ and $m = 2$ or $\overline{n}_c$. Because of these inconsistencies, I doubt that MHD activity is directly responsible for the observed decrease in the impurity confinement time. Instead I would attribute this effect to the previously mentioned differences in the sawteeth oscillations. Since their amplitudes are twice that in deuterium, these internal disruptions could be playing a major

role in particle transport and energy confinement within the $q = 1$ surface.

# V. THEORETICAL HYPOTHESES FOR THE THRESHOLD EFFECT

## V.1 Possible explanations

In this section several possible theories will be discussed in an attempt to resolve the novel MHD density threshold and its simple scaling with toroidal field. The important point to remember is that resistive MHD theory, with the finite beta and/or diffusion modifications included, predicts that tearing modes should be stable in Alcator C, assuming the current profile is really Gaussian. Furthermore, the finite beta effects, if true, should become even more stabilizing as the density is raised. The data presented in the previous section agree with the modified theory at low densities, and this could be interpreted as experimental evidence supporting the modifications, since the elementary theory by itself predicts an unstable $m = 2/n = 1$ island. However, the high density destabilization and the threshold scaling with $B_t$ and $I_p$ can not be explained by the theory presented in section II.

Several distinctly different phenomena may be hypothesized in an attempt to understand the discrepancies with resistive MHD. The first is that magnetic fluctuations which are seen during the steady state are not due to tearing modes at all. Resistive interchange and ballooning modes are driven by the plasma pressure in conjunction with the curvature of the magnetic field lines, and as such would be density dependent and not a strong function of the current profile. But two fundamental discrepancies arise with this hypothesis. First of all, these pressure-driven modes theoretically become unstable at volume average beta's of several percent. In Alcator C the *peak* value of $\beta$ at the start of MHD activity is 0.6-0.9% and the volume average, $\langle\beta\rangle$, is about $\frac{1}{20}$ of the critical values typically required for interchange instability. Secondly, the original dilemma of explaining the absence of current-driven tearing modes has not been resolved. For these reasons, interchange and/or ballooning modes are not seriously considered as the cause of the observed signals on the pickup loops.

## V.2 Indirect coupling to the current profile

An obvious hypothetical explanation for the measured dependence of $m = 2$ and 3

activity on density which hasn't been ruled out yet is a coupling of the line average density to the plasma current profile. In sections II.2-II.5, the theory and methods of calculating the stability of any current profile to tearing modes was explained in detail. The crucial parameter, $\Delta'$, is determined from the sharp change in slope of $\tilde{B}_r$, or $\tilde{\psi}$, across the width of the magnetic island. The perturbed flux function is found by solving equation (51) subject to the proper boundary conditions. Because the denominator of the right hand side of equation (51) vanishes at the resonant surface, the form of $\tilde{\psi}$ near $r_s$, and consequently $\Delta'$, should depend very delicately on $\partial J_z/\partial r$ near the singularity. In order to get a feel for the degree of sensitivity, it is useful to make small changes in the standard Gaussian temperature profiles used to fit the Alcator C data, and see what magnitude of variation in $\Delta'$ results. Several different perturbations were added near the singular surface and the $\Delta'$ parameter was calculated numerically for each case. Two examples are shown in Figs. 54 and 55. These should be compared with the result in Fig. 8. Obviously these small deviations can drastically effect the stability of the $m = 2/n = 1$ tearing modes. Unfortunately, due to the inherent difficulties involved in making the $T_e(r)$ measurement from the electron cyclotron emission, such small amplitude and small scale features on the temperature profile cannot be detected with the present apparatus. There are experimental difficulties, such as the fact that the third harmonic, non-blackbody emission from the outside of the plasma begins to interfere with second harmonic radiation from the inner region, and there are more fundamental problems, such as the questionable assumption of a blackbody level of emission in the second harmonic from the outer annulus of the plasma. Even if these obstacles could be overcome, there is still the matter of in/out plasma motion, which given its present amplitude, is more than enough to obscure the desired refinements.

To get an idea of the relative insensitivity of the ECE diagnostic to small changes in $T_e(r)$, it is instructive to refer to Fig. 50, which documents a very unusual hydrogen discharge into which a strong pulse of nitrogen gas was injected. As is clearly evident, drastic changes occurred in the $m = 2$ and $m = 3$ tearing modes along with obvious changes in density and soft x-rays. But the ECE temperature profiles for this shot are displayed in

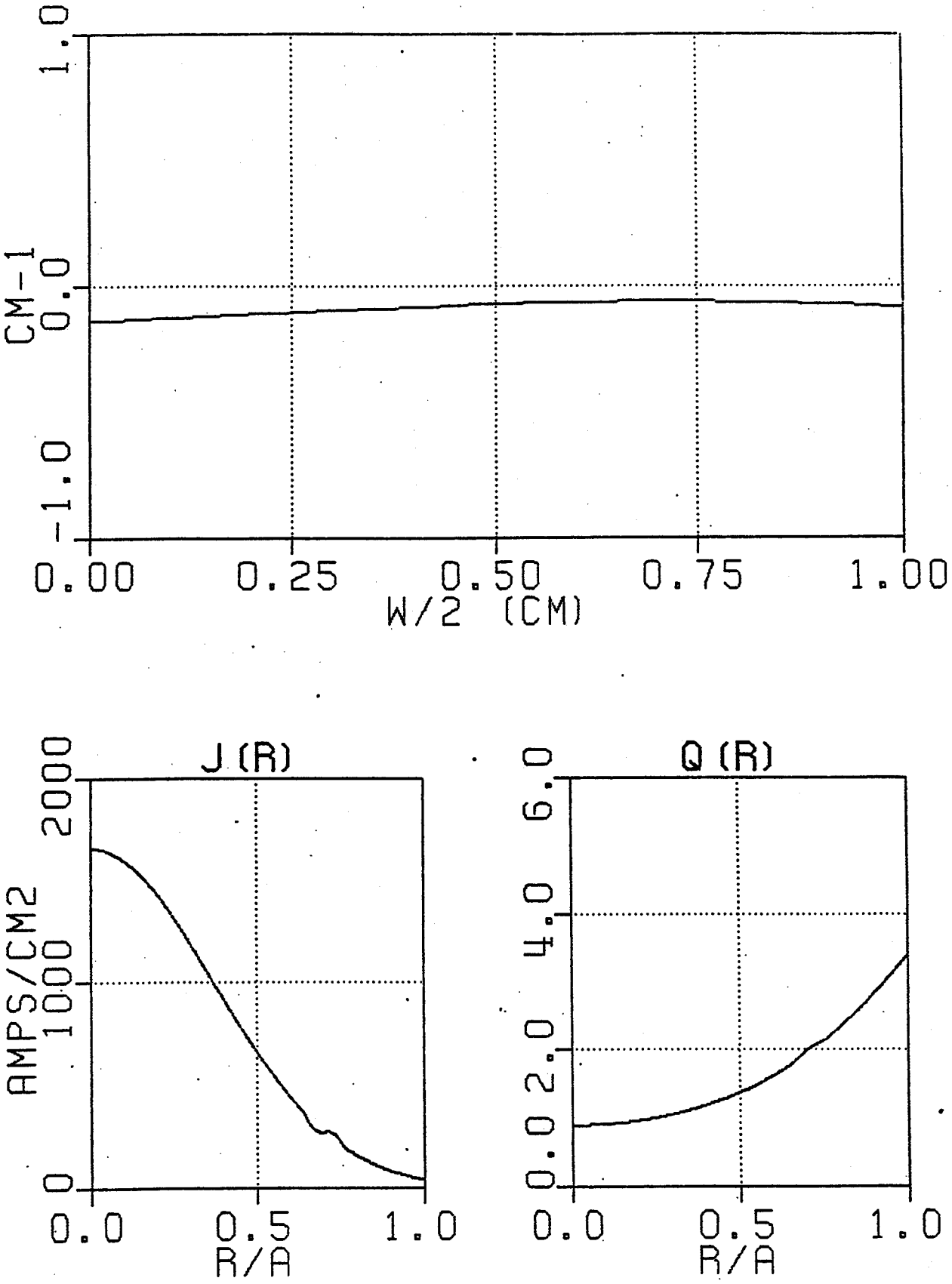


Fig. 54 — Graph of $\Delta'(W)$ showing the stabilization produced by a small deviation of the current profile which flattens the gradient near the singular surface.

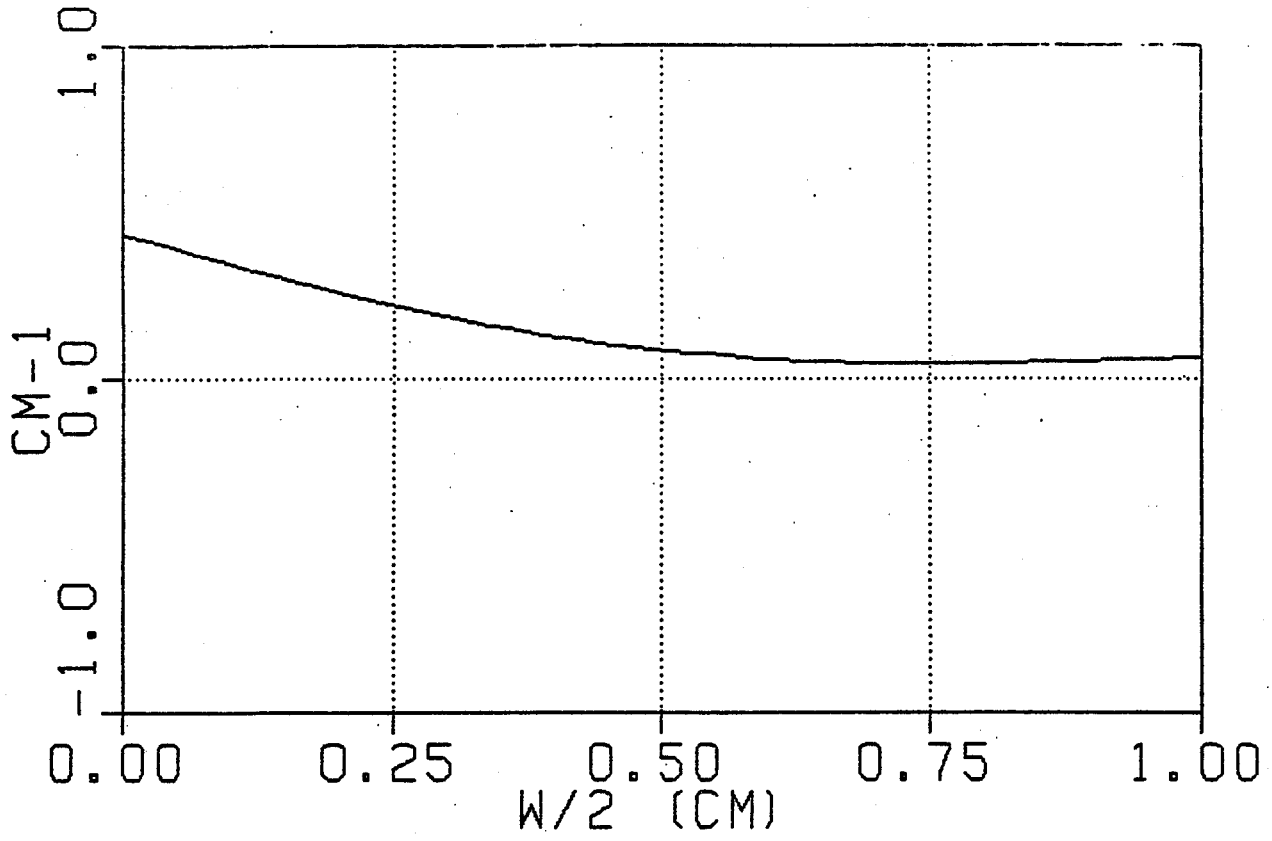


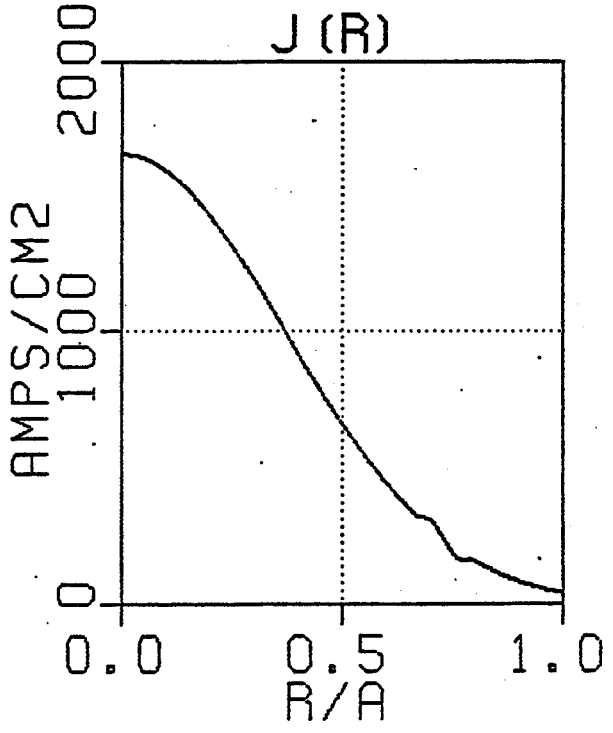


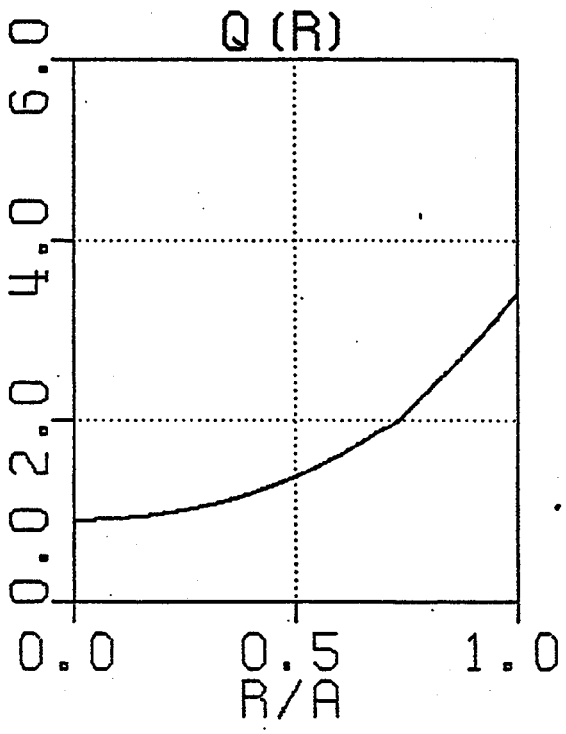


Fig. 55 — Graph of $\Delta'(W)$ showing the destabilization produced by a small deviation of the current profile which steepens the gradient near the singular surface.

Fig. 56 and the approximate time of the beginning of the impurity injection is marked by the arrow. Only a small change is measured—perhaps a 10% increase in the central temperature but no easily discernible variation in the profile shape. Still, this apparently miniscule difference translates into a current profile which must suddenly result in a positive $\Delta'$ in order to explain the $m$-spectrum analyzer signals. This example should give one a good feeling for the subtle effects which may be involved in triggering resistive perturbations. (In this particular example, $Z_{eff}$ also probably played an important role.) It becomes apparent that this hypothesis of an indirect coupling of the line average density to the temperature cannot be ruled out by direct experimental measurement.

However, the combination of several factors, most notably the excellent reproducibility of the threshold value and its scaling with $B^2$, makes such an explanation most implausible. The diagnostics operating on Alcator C indicate that there is no gross change in the temperature profile shape as the density is increased slowly, although minute variations cannot be ruled out given experimental uncertainties. The same thing can be said about the $Z_{eff}$ profile, which remains approximately flat, at least on the outer side of the major radius[36]. (The inside edge measurements are obscured with marfes by the time $\overline{n}_c$ is reached. See section IV.5) Under these conditions, there is no reason to expect a repeatable, predictable, subtle variation in $J_z(r)$ which scales correctly with $B_t$ and $I_p$ to produce the observed MHD behavior.

Several important points can be summarized from the discussion presented in this section:

(1) Measurements of $T_e(r)$ and $Z_{eff}(r)$ indicate that the gross profile shapes do not change with line average density within the operating range of interest here. However, subtle variations which are less than the experimental uncertainties cannot be ruled out.

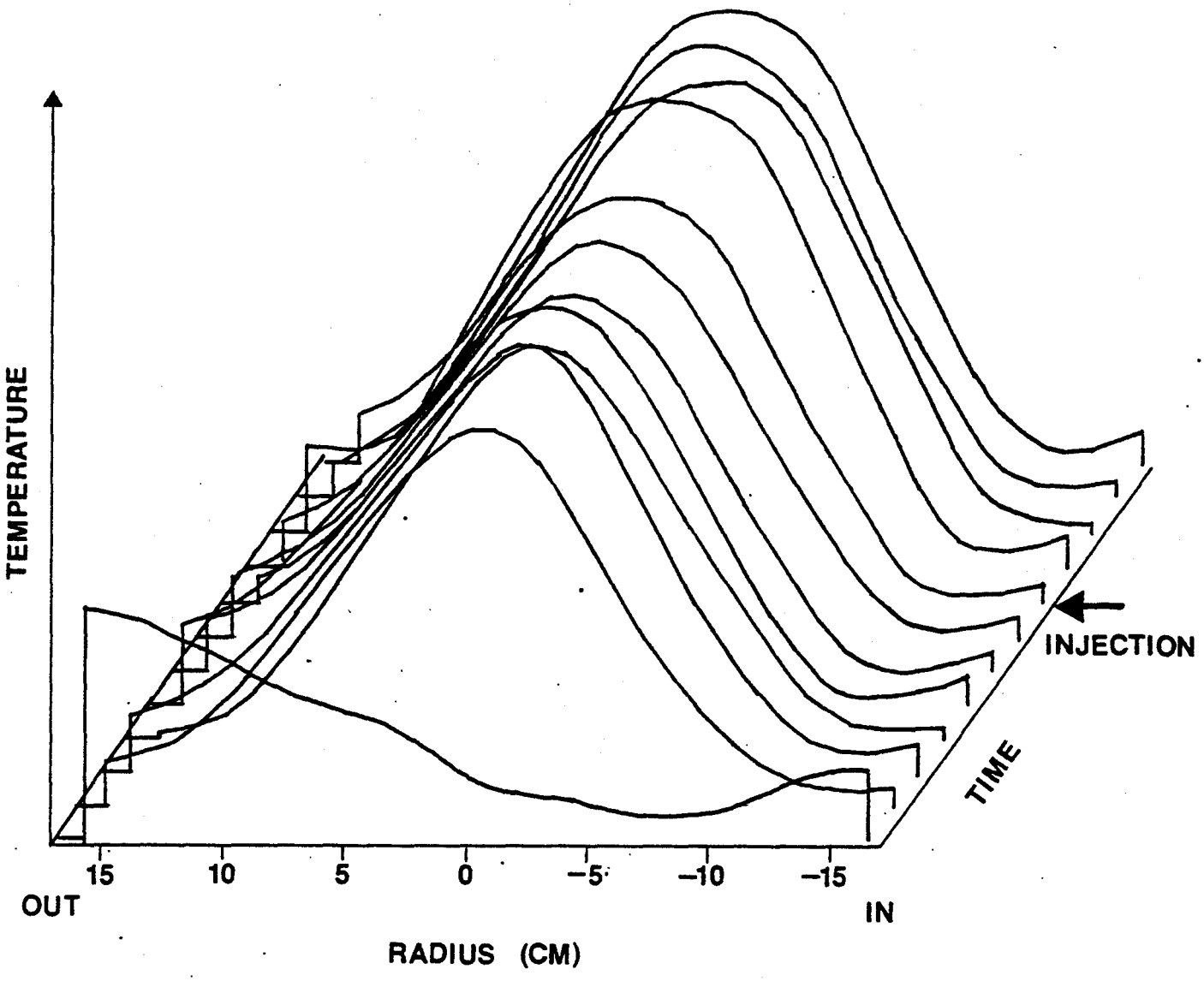


Fig. 56 — Evolution of electron temperature profile for shot into which nitrogen gas was injected. The arrow indicates the approximate time of injection. Courtesy of Dr. S. Kissel

(2) Such subtle variations in $J_z(r)$ could affect tearing mode stability according to elementary resistive MHD theory. But it is extremely unlikely that such minute dependence on $\overline{n}$ and $B$ could be responsible for the very repeatable threshold phenomenon and the clear scaling with toroidal field. The fact that $\overline{n}_c/B^2$ is independent of plasma current cannot be explained by this model.

(3) Under special circumstances profile effects on MHD activity certainly are seen when dramatic changes occur in macroscopic plasma properties. Examples of this occur during the current rise phase, during impurity injection, and when the working gas is switched to helium.

(4) Given the three previous points, it seems that the hypothetical explanations presented so far in this chapter cannot provide a believable explanation of the threshold effect. However, a coupling of the density to small changes in the current profile cannot be absolutely ruled out without more detailed measurements of the electron temperature profile in the neighborhood of the resonant surface.

None of the published literature, examined to date, dealing with the modifications to the tearing mode dispersion relation due to non-ideal physics (or other normally neglected terms) satisfactorily explains the MHD density threshold.

## V.3 Modification of the resistive MHD equations

Since no theory at present adequately accounts for the experimental findings, I shall speculate that perhaps the addition of an extra force, of unknown origin, to the MHD model is warranted. By examining the momentum balance equation, one can determine the basic form of this extra force term required to explain the threshold effect and its $B^2$ scaling.

The following argument is *not* a proper derivation of the linearized instability equations—it uses only the equilibrium relations, but this suffices when the plasma is at the marginal stability point. Suppose that:

$$\rho\frac{dv}{dt} = J \times B - \nabla p - F_? \tag{81}$$

Assume the pressure term is always negligible (the usual assumption in elementary resistive tearing theory). Substitute in equation (9) for $J$ to get:

$$\rho\frac{dv}{dt} \simeq \frac{1}{\mu_o}(\nabla \times B) \times B - F_? \tag{82}$$

As an educated guess, I will choose $F_?$ to be proportional to density and independent of magnetic field. The terms on the right can be thought of as two generalized forces:

$$\begin{aligned} F_{kink} &\equiv \frac{1}{\mu_o}(\nabla \times B) \times B \sim B^2 \\ F_? &\equiv n \end{aligned} \tag{83}$$

In static equilibrium these two forces would have to balance, $F_{kink} = F_?$. This condition can also be thought of as the criterion for marginal stability to MHD modes, and the scaling of the marginal stability point is:

$$\begin{aligned} F_{kink} &= F_? \\ \text{or} \quad B^2 &\sim n \end{aligned} \tag{84}$$

The phenomenon of a density threshold for MHD activity can be considered to be the physical realization of the theoretical concept of marginal stability. In that light, equation (84) specifies the density scaling of $n_c$:

$$n_c \sim B^2$$

This is exactly what is measured by the $m$-spectrum analyzer and the derivation depends only on the assumption that $F_? \sim n$ and independent of magnetic field. Ideally $F_?$ should

also be independent of ion mass in order to agree with the experimental finding of no difference for $\overline{n}_c$ in hydrogen and deuterium.

In this handwaving argument, many complicating details have been ignored, and the result should not be believed without a rigorous derivation. For example, in an equilibrium solution in the straight cylindrical model, the $J \times B$ force is actually a function of $B_\theta^2$, which is proportional to $B^2/q^2(a)$, not just $B^2$. However, the threshold in Alcator C does not show any independent variation with $q(a)$, as detailed in Fig. 34. Another mistake would be to use equation (82), which is applicable to the equilibrium, for the qualitative prediction of instability behavior without first doing a proper expansion for small linear perturbations. The rest of the MHD equations couple together fluctuations in velocity, pressure, fields, etc. so that the perturbed form of the force terms in equation (83) may be out of phase by $\pm 90°$ or $180°$ with each other and/or with the perturbed velocity. The real importance of this handwaving argument is that it specifies the form of a postulated force term which, when added to the usual MHD forces, may account for the threshold phenomenon and the scaling with $B$, and it confirms that a detailed calculation is indeed warranted.

Are there any familiar forces which have the required form of $F_?$? Yes, both gravity and centripetal acceleration produce forces which are linearly proportional to $n$ and independent of $B$. True gravitational effects are quite negligible in fusion plasmas, not to mention the fact that the ion mass dependence cannot be factored out. However centripetal acceleration remains a viable candidate. The reason this effect is not contained in the elementary resistive theory is because the plasma is always assumed to be in a static equilibrium, i.e. $v_o = 0$. In order to have a centripetal force, one must postulate that the plasma has a non-zero equilibrium fluid flow.

For linear instability theory to be most useful, the perturbed centripetal term must be expressible in the form $e^{i(m\theta - nz/R)}$. In a torus, a poloidal fluid rotation will produce a radial centripetal force which can be analyzed in this way. But a toroidal rotation will only yield a $\cos(\theta)$ variation, which is much more difficult to deal with in the linear theory. For this reason, the theoretical analysis which follows will be done in cylindrical geometry.

Several serious complications arise when a straight plasma with poloidal rotation is bent into a torus. These effects and their implications will be discussed at the end of this section.

If a finite equilibrium velocity is assumed then the cylindrical MHD equations require that it be a function of $r$ only. In addition, if the fluid is incompressible (a good approximation for the timescales of interest), $\nabla \cdot \boldsymbol{v} = 0$, and therefore $v_{ro}$ must be zero. In general,

$$\boldsymbol{v}_o(r,\theta,z) = v_{\theta o}(r)\hat{\theta} + v_{zo}(r)\hat{z} \tag{85}$$

Both the toroidal velocity and poloidal angular frequency,

$$\Omega(r) \equiv \frac{v_{\theta o}(r)}{r}$$

might reasonably be assumed constant, since the finite viscosity of a real plasma would tend to damp out sheared velocity flows. However, rigid motion is not required in the derivation that follows, but will be employed here for simplicity.

The centripetal perturbed forces are embodied in the convective part of the total time derivative on the left-hand side of the momentum equation:

$$\rho\frac{d\boldsymbol{v}}{dt} \equiv \rho\frac{\partial \boldsymbol{v}}{\partial t} + \rho(\boldsymbol{v}\cdot\nabla)\boldsymbol{v} \tag{86}$$

Equation (11) can then be rewritten as:

$$\rho\frac{\partial \boldsymbol{v}}{\partial t} = \boldsymbol{J}\times\boldsymbol{B} - \nabla p - \rho(\boldsymbol{v}\cdot\nabla)\boldsymbol{v} \tag{87}$$

which is now in the form of equation (81). Note that this extra force term is proportional to density and independent of $B$, as specified in the handwaving analysis. Linearizing this expression for arbitrarily small perturbations yields three separate terms which would not be present to first order without a zero-order velocity:

$$\tilde{\rho}(\boldsymbol{v}_o\cdot\nabla)\boldsymbol{v}_o, \qquad \rho_o(\tilde{\boldsymbol{v}}\cdot\nabla)\boldsymbol{v}_o, \qquad \text{and} \qquad \rho_o(\boldsymbol{v}_o\cdot\nabla)\tilde{\boldsymbol{v}}$$

The first term is purely radial for $v$ of the form given by equation (85). It simplifies to:

$$\tilde{\rho}(v_o \cdot \nabla)v_o = -\tilde{\rho}\frac{v_{\theta_o}^2}{r}\hat{r} = -\tilde{\rho}r\Omega^2\hat{r}$$

and represents the centripetal force on a perturbed mass element. The other two terms have components in all three orthogonal directions and include more complicated effects such as the Coriolis force. The linearized form of equation (87) is most easily handled by introducing the poloidal flux function, $\tilde{\psi}(r)$, and the velocity stream function, $\tilde{\phi}(r)$, which were defined and used previously in section II.1 (see equation 32). Operating with "$\hat{z}\cdot\nabla\times$" on the linearized expression gives:

$$\begin{aligned}-\rho_o\frac{\partial}{\partial t}\nabla_\perp^2\tilde{\phi} - \rho_o'\frac{\partial}{\partial t}\left(\frac{\partial\tilde{\phi}}{\partial r}\right) &= -\frac{i}{\mu_o}(k\cdot B)\nabla_\perp^2\tilde{\psi} + \frac{im}{r}J_{z_o}'\tilde{\psi} \\ &- im\Omega^2\tilde{\rho} - \frac{im}{r}\frac{\partial}{\partial r}\left[\rho_o(r\Omega)'\tilde{\phi}\right] + \frac{im}{r}\rho_o\Omega\frac{\partial\tilde{\phi}}{\partial r} \\ &+ \frac{i}{r}\frac{\partial}{\partial r}\left[\rho_o(k\cdot v_o)r\frac{\partial\tilde{\phi}}{\partial r}\right] - \frac{im}{r}(\rho_o\Omega)'\tilde{\phi} - \frac{im^2}{r^2}\rho_o(k\cdot v_o)\tilde{\phi}\end{aligned} \tag{88}$$

This formula contains three unknown perturbed quantities: $\tilde{\psi}$, $\tilde{\phi}$, and $\tilde{\rho}$. In order to solve the general case, two more independent equations are needed. One is the linearized equation of mass conservation:

$$\begin{aligned}&\frac{\partial\tilde{\rho}}{\partial t} + v_o\cdot\nabla\tilde{\rho} + \tilde{v}\cdot\nabla\rho_o = 0 \\ \text{or}\qquad &\frac{\partial\tilde{\rho}}{\partial t} + i(k\cdot v_o)\tilde{\rho} + \frac{im}{r}\rho_o'\tilde{\phi} = 0\end{aligned} \tag{89}$$

The other comes from the $\hat{r}$-component of the magnetic induction law:

$$\begin{aligned}\frac{\partial\tilde{B}_r}{\partial t} = -\hat{r}\cdot\nabla\times\tilde{E} &= \hat{r}\cdot\nabla\times(\tilde{v}\times B_o) + \hat{r}\cdot\nabla\times(v_o\times\tilde{B}) \\ &+ \hat{r}\cdot\frac{\eta}{\mu_o}\nabla^2\tilde{B} - \hat{r}\cdot\frac{1}{\mu_o}\nabla\eta\times(\nabla\times\tilde{B})\end{aligned}$$

which simplifies to:

$$\begin{aligned}\frac{\partial\tilde{\psi}}{\partial t} &= i(k\cdot B_o)\tilde{\phi} - i(k\cdot v_o)\tilde{\psi} \\ &+ \frac{\eta}{\mu_o}\left[\frac{\partial^2\tilde{\psi}}{\partial r^2} + \frac{1}{r}\frac{\partial\tilde{\psi}}{\partial r} - k^2\tilde{\psi}\right]\end{aligned} \tag{90}$$

Equation (88), (89), and (90) constitute the set of reduced resistive MHD equations in linearized form, valid for a cylindrical plasma with finite equilibrium velocity. If $v_o$ is set equal to zero, these three relations compress down to the standard pair of reduced MHD equations described in section II.2 and used in much of the published work on tearing instabilities. (Equation 89 is not needed in this case since the $\tilde{\rho}\Omega^2$ term vanishes.) With finite $v_o$, this set can still be reduced to two equations by solving (89) for $\tilde{\rho}$ in terms of $\tilde{\phi}$ assuming that the mode grows like $e^{\gamma t}$, and substituting into (88). After some manipulation, the results for a rigidly rotating plasma can be written in a form which closely resembles that of other researchers[72] studying ideal rotating plasmas:

$$\nabla_\perp \cdot \left[\rho_o(\gamma + i\boldsymbol{k}\cdot\boldsymbol{v}_o)^2 \nabla_\perp \tilde{\phi}\right] - \left[\frac{2im(\gamma + i\boldsymbol{k}\cdot\boldsymbol{v}_o)\Omega}{r}\rho_o' + \frac{m^2\Omega^2}{r}\rho_o'\right]\tilde{\phi}$$
$$= i(\gamma + i\boldsymbol{k}\cdot\boldsymbol{v}_o)\left[(\boldsymbol{k}\cdot\boldsymbol{B}_o)\frac{1}{\mu_o}\nabla_\perp^2\tilde{\psi} - \frac{m}{r}J_{z_o}'\tilde{\psi}\right] \tag{91}$$

and:

$$(\gamma + i\boldsymbol{k}\cdot\boldsymbol{v}_o)\tilde{\psi} = i(\boldsymbol{k}\cdot\boldsymbol{B}_o)\tilde{\phi} + \frac{\eta}{\mu_o}\left[\frac{\partial^2\tilde{\psi}}{\partial r^2} + \frac{1}{r}\frac{\partial\tilde{\psi}}{\partial r} - k^2\tilde{\psi}\right] \tag{92}$$

This pair of coupled differential equations can be solved by brute force numerical methods on a computer, but that is not a feasible approach for this thesis study. An analytic solution can be attempted by using the boundary layer theory mentioned in section II, and that has been left for future work. In principle the centripetal acceleration should act like simple gravity in a slab, and this class of problems has already been solved in great detail by Furth, Killeen, and Rosenbluth[5]. Their solution shows that for this case the poloidal rotation should be destabilizing. This result should be accepted cautiously however, because the finite $\beta$ and radial diffusion effects were not included in the derivation. Obviously the theory must eventually be done in a consistent manner by including all three of these modifications.

## V.4 Drawbacks of the theoretical velocity correction

A radial electric field given by equation (2) is required in ideal MHD for a moving

plasma to be in equilibrium. The resulting potential difference between the center of the plasma and the edge would not be expected to be larger than the plasma temperature. This restricts the fluid rotation frequency to be no more than several kilohertz.

Poloidal rotation introduces other problems which arise when the straight cylindrical plasma used in this derivation is bent into a torus to better represent the tokamak geometry. Because an inherent symmetry is lost in this process, the fluid can not be expected to flow unimpeded in the poloidal direction. The plasma velocity can no longer be divergenceless; as a fluid element rotates toward the inside of the torus it must compress and heat up, then expand and cool down as it approaches the outside. This cyclic heating and cooling process could result in dissipation of energy due to finite thermal conductivity. Even so, if the poloidal rotation is sufficiently fast, the heat lost during a cycle may be negligible and the compression could be approximately adiabatic.

However there other damping processes which cannot be described by the MHD fluid model of a plasma; one example is viscous drag against the distribution of trapped particles. By definition this population is located in the magnetic well on the outer side of the torus and therefore the trapped component of the plasma cannot rotate poloidally. The collisional friction with the bulk plasma should slow the $\hat{\theta}$-velocity and decrease the electric field on the timescale of the ion-ion collision rate, which is just a small fraction of a millisecond[73]. Therefore in order to sustain an equilibrium rotation, the electric potential must be continuously charged up, perhaps by a non-ambipolar loss of ions or electrons. In Alcator C, the collision frequency is high enough so that well-formed trapped banana orbits probably are insignificant, thereby rendering this process questionable in this particular experiment.

One final note concerns the toroidal velocity. This component drops out of the instability criterion in a cylinder because one can always jump to the frame moving with $v_{zo}$ (assuming rigid flow), which is Newtonian. Therefore $v_{zo}$ is completely arbitrary and certainly plausible even in a true toroidal geometry. The freedom in $v_{zo}$ permits decoupling of the poloidal rotation frequency from the measured magnetic perturbation frequency. Thus these two quantities need not be equal.

In conclusion, poloidal rotation in a torus is expected to be damped out on a collisional timescale unless a source of free energy can offset the dissipation of rotational kinetic energy. Since this cannot be ruled out at the present time, the inclusion of a finite equilibrium velocity remains a viable speculation for explaining the empirical findings.

# VI. SUMMARY AND RECOMMENDATIONS FOR FUTURE WORK

## VI.1 Principle experimental results

The $m$-spectrum analyzer has proven to be a valuable new instrument for the study of MHD instabilities in Alcator C. An important discovery is the marked occurrence of tearing mode activity at high plasma densities, in basic disagreement with resistive MHD theory. During the current plateau, no measurable magnetic perturbations are observed unless the line average density surpasses a threshold value, $\overline{n}_c$, which scales like the square of the toroidal magnetic field, $B_t^2$. This behavior is seen in both hydrogen and deuterium for virtually all sawtoothing discharges, and it is remarkably repeatable. Over the parameter ranges achieved so far in the experiment, the threshold phenomenon shows no discernible dependence on plasma current, $I_p$, or safety factor, $q(a)$—a finding which is also unexpected from the established theory.

Under normal operating conditions the $m = 2$ and $m = 3$ magnetic islands have no effect on any macroscopic plasma parameters. Specifically the energy confinement does not show a deleterious correlation with the onset of MHD activity. The single important consequence of these modes occurs at very high densities, where the perturbations reach large amplitudes and are associated with major disruptions. This behavior could certainly be in agreement with the present theoretical explanations of disruptions, but no direct measurement of magnetic island widths have been made and therefore island overlap cannot be proven. Apparently these tearing modes in Alcator C may limit the maximum attainable density at a given magnetic field. The limited quantity of data gathered so far suggests that the maximum density goes up faster than linear with $B_t$.

In helium discharges the MHD activity differs in some respects but also shows some similarities. A measurable perturbation level exists throughout the steady state portion of the shot, unlike the behavior in hydrogen or deuterium. However, a strong increase in $m = 2$ and $m = 3$ modes still occurs with increasing density.

Another surprising finding are low density disruptions, in which no tearing instabilities

are detected prior to the termination. Surprisingly these events are not rare. Detailed examination of the data shows no indication that magnetic islands are involved in causing the major disruption; in fact so far, no diagnostic experiment detects any hint of the impending trouble. This is rather disturbing from both the theoretical and experimental points of view since it could mean problems for feedback stabilization schemes aimed at preventing the major disruption.

Since the tearing mode stability criterion derived from the resistive MHD model contains no explicit destabilizing density term, this theory fails to account for the actual phenomena measured by the $m$-spectrum analyzer. In fact, if finite beta stabilization is truly correct, tearing modes should be more stable at higher densities. Two hypotheses can be thought of to resolve this dilemma—an implicit coupling between the line average density and the current profile, or a modification to the resistive model. The first explanation holds only for appreciable, rapid changes of the global plasma parameters. Such circumstances are rare and usually initiated "artificially", such as during impurity injection. However, during normal operation, the temperature profile shows no measurable dependence on the line average density and one would be forced to postulate that small, subtle variations on the current profile are responsible for the observed behavior. Even though minor changes in $J_z(r)$ can affect the tearing mode stability, the repeatability and small deviation in the threshold density as well as the basic scaling with $B^2$ renders any theory requiring "subtlety" most implausible.

Rather than giving up entirely on the resistive MHD tearing model, the previously neglected phenomenon of an equilibrium having a finite poloidal and toroidal flow velocity has been considered here. The convective part of the total time derivative must be included in the linear equations under these circumstances and the net effect is an extra radial force due to the centripetal acceleration caused by poloidal flow. This leads to an important destabilizing modification in the MHD equation for the perturbed magnetic field that perhaps may account for the density threshold observed in Alcator C, as well as the scaling of $\bar{n}_c$ with $B^2$. A consequence of the toroidal geometry is that any poloidal rotation should be

damped out on a $\tau_{ii}$ timescale and therefore a driving term for the $\hat{\theta}$ fluid flow is required. Appreciable charged particle losses, for example, could sustain a radial electric field which would drive the rotation.

## VI.2 Continuing studies and future experiments

Since the major consequence of MHD activity in Alcator C is to limit the maximum density, one is compelled to study high density disruptions in much more detail. In this thesis research, no scaling of maximum attainable density or disruptions with plasma current has been investigated yet and no data exists so far at toroidal magnetic fields greater than 80 kG. Does the peak density actually increase like $B^2$? Is the limit simply due to inefficient operation of the tokamak? Can the limit be exceeded by fine tuning the programming of plasma parameters? An important aid in these studies would be an x-ray tomography diagnostic. The question of whether or not the $m = 2$ and $m = 3$ islands are overlapping to cause the disruption, as present theory predicts, could probably only be answered by several arrays of soft x-ray detectors. The Alcator machine construction makes the necessary multi-angle views very difficult to obtain, however the payoff from such an experiment would certainly justify the effort.

Also of considerable importance are the low-density disruptions, which don't exhibit MHD activity. So far there is no known cause for these phenomena. Without a detailed understanding of the mechanisms leading to this type of current termination, there is little hope of predicting and/or avoiding the problem.

The $m$-spectrum analyzer itself could be improved by further reducing the pickup of power supply noise, thereby enabling the use of the $m = 1$ channel and improving the frequency measuring channels' resolution. For example, several clever techniques can be used to greatly reduce the interference generated by the vertical field supply. This system couples primarily to the cosine part of the loop signals, rather than the sine component. To eliminate this background without attenuating the magnetic island oscillations, the $m$-spectrum analyzer should not multiplex the Mirnov coils in the present cyclic pattern.

Instead two separate multiplexers controlled by common logic could each sample half the loops on each cycle, both starting on the midplane, but one going over the top of the liner while the other scans the bottom loops. The process would be repeated over and over, but now the two multiplexer signals, when added together properly, can eliminate the cosine pickup and leave only the sine signal[74].

As far as the theory goes, much more work is in order on the proposed modification to the resistive MHD model. A proper derivation of the full set of reduced resistive equations should be carried out with radial diffusive flow, finite plasma beta, and non-zero equilibrium velocity included together. (In order to get the proper stabilizing influence of $\beta$, it may be necessary to do this calculation in toroidal geometry.) Rigorous solutions describing the tearing instability evolution versus $\overline{n}/B^2$ should be generated, as well as a better estimate of the poloidal velocities needed to match the empirical behavior of the density threshold.

A test of the theoretical speculation of the threshold phenomenon being attributable to an equilibrium velocity is certainly warranted. A direct measurement of $v_{\theta o}$ and $v_{zo}$ should be carried out, probably by looking for a Doppler shift in an impurity radiation line. If the assumptions are made that the plasma rotates rigidly and the impurities move with the plasma, then a particular spectral line should be chosen which is emitted from the region of large minor radius for at least two reasons. First the $\hat{\theta}$-velocity increases with $r$ and second, the plasma is cooler and therefore the thermal Doppler spreading is less. As a quantitative example, suppose that an oxygen line is emitted from a radius of 14 cm where the temperature is 100 eV. If the poloidal rotation frequency is 10 kHz, then:

$$\frac{v_{\theta o}}{v_{thI}} = \frac{2\pi r \times 10 \text{ kHz}}{\sqrt{\frac{kT_I}{m_I}}} = \frac{0.88 \times 10^6 \text{ cm/sec}}{2.45 \times 10^6 \text{ cm/sec}} = 0.36$$

Thus the Doppler shift is $\frac{1}{3}$ of the Doppler width. However,

$$\frac{\Delta\lambda}{\lambda} \simeq \frac{v_{\theta o}}{c} \simeq 2.9 \times 10^{-5}$$

This requires very high resolution in the visible region of the spectrum, and therefore the measurement may only succeed in providing an upper limit on the rotation frequency.

Both poloidal and toroidal plasma velocities have already been measured by the Doppler method in at least one other ohmically heated tokamak, LT-3[75]. A value of 5 kHz was determined for the $\hat{\theta}$ rotation, and about three times that for the toroidal frequency. The experimental conditions were even more difficult, since for the LT-3 machine, $v_{0_o}/v_{th_I} \simeq 0.17$ and $\Delta\lambda/\lambda \simeq 5.3 \times 10^{-6}$.

Indirect methods of detecting equilibrium velocities may also be feasible. One possible suggestion is to measure the radial electric field and the plasma potential using a heavy ion beam probe[76]. This technique does have a fundamental drawback though—the inability to resolve the individual $\hat{\theta}$ and $\hat{z}$ velocity components. Another technique may be to measure shifts in the $k$-spectra of plasma fluctuations using a $CO_2$ laser scattering diagnostic[77].

Finally, if further study of the high-density disruption problem verifies the assertion that resistive tearing modes are responsible, then feedback stabilization experiments are recommended for future work. Unfortunately, because of Alcator's Bitter magnet construction and limited access, it would probably not be feasible to carry out this work on the present device.

## VII. ACKNOWLEDGMENT

I wish to express my appreciation to several people who played substantial roles in my graduate education and research.

-to Ron Parker, our project supervisor, for supporting this work academically and enabling me to accomplish it. I am especially grateful for the encouragement you offered prior to my first APS talk, where much of this research was presented.

-to Dave Overskei, my initial thesis advisor, for getting me interested in this field in the first place while still letting me do things my own way.

-to Pete Politzer and Jeff Freidberg, thesis advisors, for many helpful discussions on this work. Special thanks goes to Jeff for teaching me most of what I know about the ideal MHD model and its applications.

-and to the most important people of all, the Alcator staff. Your combination of scientific ability and unassuming friendship aided in both my professional and personal development. I always felt that I was part of the team.

## REFERENCES


[1]J.P. Freidberg, lecture notes (to be published in Rev. Mod. Phys.), MIT (1981).

[2]L. Spitzer and R. Härm, Phys. Rev. 89, 977 (1953).

[3]O.A.Anderson, W.R. Baker, S.A. Colgate, J. Ise, and R.V. Pyle, Phys. Rev. 110, 1375 (1958).

[4]V.D. Shafranov, Zh. Tekh. Fiz. 40, 241 (1970).

[5]H.P. Furth, J. Killeen, and M.N. Rosenbluth, Phys. Fluids 6, 459 (1963).

[6]J.D. Callen, B.V. Waddell, B. Carreras, M. Azumi, P.J. Catto, H.R. Hicks, J.A. Holmes, D.K. Lee, S.J. Lynch, J. Smith, M. Soler, K.T. Tsang, and J.C. Whitson, in *Plasma Physics and Controlled Nuclear Fusion Research* (Proc. 7$^{th}$ Int. Conf., Innsbruck, 1978) Vol. I, IAEA, Vienna 415 (1979).

[7]G.L. Jahns, M. Soler, B.V. Waddell, J.D Callen, and H.R. Hicks, Nucl. Fusion 18, 609 (1978).

[8]B. Carreras, H.R. Hicks, B.V. Waddell, "Tearing Mode Activity for Hollow Current Profiles," ORNL Report TM-6570 (1978).

[9]A.I. Morozov and L.S. Solov'er, "The Structure of Magnetic Fields," in *Reviews of Plasma Physics*, Vol. 2 (1966) pp. 60–78.

[10]B.V. Waddell, B. Carreras, H.R. Hicks, J.A. Holmes, and D.K. Lee, Phys. Rev. Lett. 41, 1386 (1978).

[11]H.R. Hicks, B. Carreras, J.A. Holmes, B.V. Waddell, "Interaction of Tearing Modes of Different Pitch in Cylindrical Geometry," ORNL Report TM-6096 (1977).

[12]R.B. White, D.A. Monticello, and M.N. Rosenbluth, Phys. Rev. Lett. 39, 1618 (1977).

[13]S.V. Mirnov and I.B. Semenov, in *Plasma Physics and Controlled Nuclear Fusion Research* (Proc. 4$^{th}$ Int. Conf., Madison, 1971) Vol. II, IAEA, Vienna 401 (1971).

[14]S. von Goeler, W. Stodiak, and N. Sauthoff, Phys. Rev. Lett. 33, 1201 (1974).

[15]J.C. Hosea, C. Bobeldijk, D.J. Grove, in *Plasma Physics and Controlled Nuclear Fusion Research* (Proc. 4$^{th}$ Int. Conf., Madison, 1971) Vol. II, IAEA, Vienna 425 (1972).

[16]R.S. Granetz, I.H. Hutchinson, and D.O. Overskei, Nucl. Fusion 19, 1587 (1979).

[17]B. Carreras, B.V. Waddell, H.R. Hicks, Nucl. Fusion 19, 1423 (1979).

[18]K. Toi, K. Sakurai, S. Tanahashi, S. Yasue, "Soft and Hard Major Disruptions in the Profile Control Experiment of the JIPP T-II Tokamak," Nagoya Univ. Inst. of Plasma Physics Report IPPJ-547 (1981).

[19]D.C. Robinson, K. McGuire, Nucl. Fusion 19, 115 (1979).

[20]Murakami *et al*, in *Plasma Physics and Controlled Nuclear Fusion Research* (Proc. 7$^{th}$ Int. Conf., Innsbruck, 1978) Vol. I, IAEA, Vienna 269 (1979).

[21]N.R. Sauthoff, S. Von Goeler, W. Stodiek, Nucl. Fusion 18, 1445 (1978).

[22]G.L. Jahns, N.H. Brooks, S. Ejima, R.D. Stambaugh, T.S. Taylor, "MHD Mode Observations in Doublet-III," Bull. Am. Phys. Soc. 26, 1029 (1981).

[23]T.P. Kochanski, P.E. Phillips, B. Richards, "MHD Phenomena and Disruptions in the TEXT," Bull. Am. Phys. Soc. 26, 1031 (1981).

[24]G. Hammett, K. McGuire, N. Sauthoff, "Identification of MHD Modes in PDX," Bull. Am. Phys. Soc. 26, 865 (1981).

[25]J.M. Finn, Phys. Fluids 20, 1749 (1977).

[26]G. Fussmann, B.J. Green, H.P. Zehrfeld, in *Plamsa Physics and Controlled Nuclear Fusion Research* (Proc. 8$^{th}$ Int. Conf., Brussels, 1980) Vol. I, IAEA, Vienna 353 (1981).

[27]G. Bateman, *MHD Instabilities*, MIT Press (1978), pp. 198–202.

[28]M.N. Rosenbluth, D.A. Monticello, H.R. Strauss, and R.B. White, Phys. Fluids 19, 1987 (1976).

[29]R.D. Hazeltine, D. Dobrott, and T.S. Wang, Phys. Fluids 18, 1778 (1975).

[30]P.H. Rutherford, Phys Fluids 16, 1903 (1973).

[31]R.B. White, D.A. Monticello, M.N. Rosenbluth, and B.V. Waddell, in *Plasma Physics and Controlled Nuclear Fusion Research* (Proc. 6$^{th}$ Int. Conf., Berchtesgaden, 1976) Vol. I, IAEA, Vienna 569 (1977).

[32]R.B. White, D.A. Monticello, M.N. Rosenbluth, and B.V. Waddell, Phys. Fluids 20, 800 (1977).

[33]B. Carreras, B.V. Waddell, and H.R. Hicks, Nucl. Fusion 19, 1423 (1979).

[34]H.P. Furth, *Propagation and Instabilities in Plasmas* (edited by W.I. Futterman), Stanford Univ. Press (1973), pp. 87–102.

[35]H.P. Furth, P.H. Rutherford, H. Selberg, Phys. Fluids 16, 1054 (1973).

[36]M.E. Foord, E.S. Marmar, J.L. Terry, "*Multichannel Light Detector System for Visible Continuum Measurements on Alcator C*," MIT Plasma Fusion Center Report JA-81-27 (submitted for publication in Rev. Sci. Inst.), (1981).

[37]S. Kissel, PhD thesis (unpublished), MIT Plasma Fusion Center, (June 1982).

[38]J.F. Drake and Y.C. Lee, Phys. Fluids 20, 1341 (1977).

[39]J.F. Drake and Y.C. Lee, Phys. Rev. Lett. 39, 453 (1977).

[40]D. Biskamp, Nucl. Fusion 19, 777 (1979).

[41]P.H. Rutherford and H.P. Furth, "Nonlinear Properties of Kink and Tearing Instabilities in Tokamaks," PPPL Report MATT-872 (1971).

[42]D.A. Monticello and R.B. White, Phys. Fluids 23, 366 (1980).

[43]D. Edery, R. Pellat, J.L. Soule, M. Frey, and J.P. Somon, in *Plasma Physics and Controlled Nuclear Fusion Research* (Proc. 8$^{th}$ Int. Conf., Brussels, 1980) Vol I, IAEA, Vienna 269 (1981).

[44]B.A. Carreras, M.N. Rosenbluth, and H.R. Hicks, Phys. Rev. Lett. 46, 1131 (1981).

[45]B.V. Waddell, B. Carreras, H.R. Hicks, and J.A. Holmes, Phys. Fluids 22, 896 (1979).

[46]B.A. Carreras, H.R. Hicks, J.A. Holmes, and B.V. Waddell, Phys. Fluids 23, 1811 (1980).

[47]R.K. Pollard and J.B. Taylor, Phys. Fluids 22, 126 (1979).

[48]D. Dobrott, S.C. Prager, J.B. Taylor, Phys. Fluids 20, 1850 (1977).

[49]A.H. Glasser, J.M. Greene, J.L. Johnson, Phys. Fluids 18, 875 (1975).

[50]A.H. Glasser, J.M. Greene, J.L. Johnson, Phys. Fluids 19, 567 (1976).

[51]R.J. Hastie, A. Sykes, M. Turner, J.A. Wesson, Nucl. Fusion 17, 515 (1977).

[52]J.A. Wesson, Nucl. Fusion 18, 87 (1978).

[53]J.A. Holmes, B. Carreras, H.R. Hicks, S.J. Lynch, B.V. Waddell, Nucl. Fusion 19, 1333 (1979).

[54]V.V. Arsenin *et al*, "Feedback Stabilization of Kink Instability in TO-1 Tokamak," PPPL Report TRANS-126 (translated by R.B. White) (1978).

[55]D.A. Monticello, R.B. White, and M.N. Rosenbluth, "Feedback Stabilization of Magnetic Islands in Tokamaks," PPPL Report MATT-1477 (1978).

[56]I.H. Hutchinson, private communication and lab notebook, (Dec. 1977).

[57]R.S. Granetz, Rev. Sci. Inst. 52, 1332 (1981).

[58]P. Besen and D. Grearson, $9^{th}$ *Symposium on Engineering Problems and Fusion Research*, Proceedings IEEE, Vol I, paper 4T-04 (1981).

[59]I.H. Hutchinson, Phys. Rev. Lett. 37, 338 (1976).

[60]R.S. Granetz, I.H. Hutchinson, D.O. Overskei, "Non-uniform Rotation of Magnetic Islands in Alcator," Bull. Am. Phys. Soc. 24, 997 (1979).

[61]E. Apgar *et al*, in Plasma Physics and Controlled Nuclear Fusion Research (Proc. $6^{th}$ Int. Conf., Berchtesgaden, 1976), Vol. I, IAEA, Vienna 247 (1977).

[62]D.S. Pappas, C.L. Fiore, A. Gondhalekar, M.J. Greenwald, S. Kissel, E.S. Marmar, J.E. Rice, "Parametric Studies of Electron and Ion Temperatures in Alcator C Ohmically Heated Discharges," Bull. Am. Phys. Soc. 26, 885 (1981).

[63]S. Fairfax *et al*, in Plasma Physics and Controlled Nuclear Fusion Research (Proc. $8^{th}$ Int. Conf., Brussels, 1980), Vol. I, IAEA, Vienna 439 (1981).

[64]M.M. Pickrell and B. Lipschultz, "Power Emission Profiles in the Alcator C Tokamak," Bull. Am. Phys. Soc. 26, 886 (1981).

[65]E.S. Marmar, private communication (1981).

[66]R.R. Parker, D. Gwinn, B. Lipschultz, D.O. Overskei, "Operating Regimes of the Alcator C Tokamak," Bull. Am. Phys. Soc. 26, 975 (1981).

[67]M. Murakami, J.D. Callen, L.A. Berry, Nucl. Fusion 16, 347 (1976).

[68]J. Castracane and H.W. Moos, "Impurity Emissions During Repetitive Disruptions on Alcator C," Bull. Am. Phys. Soc. 26, 886 (1981).

[69]J.L. Terry, E.S. Marmar, S.M. Wolfe, D. Gwinn, M. Pickrell, B. Lipschultz, M. Foord, "Strongly Enhanced Low Energy Continuum and Hydrogen Line Emission in Some Alcator C Discharges," Bull. Am. Phys. Soc. 26, 886 (1981).

[70]E.S. Marmar, J.L. Cecchi, S.A. Cohen, Rev. Sci. Inst. 46, 1149 (1975).

[71]J.E. Rice, J.L. Terry, E.S. Marmar, "Impurity Injections into the Alcator C Tokamak," Bull. Am. Phys. Soc. 26, 976 (1981).

[72]J.P. Freidberg and J.A. Wesson, Phys. Fluids 13, 1117 (1970).

[73]S.I. Braginskii, in *Reviews of Plamsa Physics*, Vol. I (Consultants Bureau, N.Y.) 205 (1965).

[74]G. Hammett, private communication (1981).

[75]M.G. Bell, Nucl. Fusion 19, 33 (1979).

[76]F.C. Jobes and R.L. Hickok, Nucl. Fusion 10, 195 (1970).

[77]R. Watterson, private communication (1982).

# PFC BASE LIST

## INTERNAL MAILINGS (MIT)

G. Bekefi
36-213

A. Bers
38-260

D. Cohn
NW16-250

B. Coppi
26-201

R.C. Davidson
NW16-202

T. Dupree
38-172

S. Foner
NW14-3117

J. Freidberg
38-160

M.O. Hoenig
NW16-176

M. Kazimi
NW12-209

L. Lidsky
38-174

E. Marmar
NW16-280

J. McCune
31-265

J. Meyer
24-208

D.B. Montgomery
NW16-140

J. Moses
NE43-514

D. Pappas
NW16-272

R.R. Parker
NW16-288

N.T. Pierce
NW16-186

P. Politzer
NW16-286

M. Porkolab
36-293

H. Praddaude
NW14-3101

D. Rose
24-210

J.C. Rose
NW16-189

R.M. Rose
4-132

B.B. Schwartz
NW14-5121

R.F. Post
NW21-203

L.D. Smullin
38-294

R. Temkin
NW16-254

N. Todreas
NW13-202

J.E.C. Williams
NW14-3210

P. Wolff
36-419

T.-F. Yang
NW16-164

Industrial Liaison Office
ATTN: Susan Shansky
Monthly List of Publications
39-513

MIT Libraries
Collection Development
ATTN: MIT Reports
14E-210

B. Colby
PFC Library
NW16-255

EXTERNAL MAILINGS

National

Argonne National Laboratory
Argonne, IL 60439
ATTN: Library Services Dept.

Battelle-Pacific Northwest Laboratory
P.O. Box 99
Richland, WA 99352
ATTN: Technical Information Center

Brookhaven National Laboratory
Upton, NY 11973
ATTN: Research Library

U.S. Dept. of Energy
Washington, D.C. 20545
ATTN: D.O.E. Library

Roger Derby
Oak Ridge National Lab.
ETF Design Center
Bldg. 9204-1
Oak Ridge, TN 37830

General Atomic Co.
P.O. Box 81608
San Diego, CA 92138
ATTN: Library

Lawrence Berkeley Laboratory
1 Cyclotron Rd.
Berkeley, CA 94720
ATTN: Library

Lawrence Livermore Laboratory
UCLA
P.O. Box 808
Livermore, CA 94550

Oak Ridge National Laboratory
Fusion Energy Div. Library
Bldg. 9201-2, ms/5
P.O. Box "Y"
Oak Ridge, TN 37830

Dr. D. Overskei
General Atomic Co.
P.O. Box 81608
San Diego, CA 92138

Princeton Plasma Physics Laboratory
Princeton University
P.O. Box 451
Princeton, NJ 08540
ATTN: Library

Plasma Dynamics Laboratory
Jonsson Engineering Center
Rensselaer Polytechnic Institute
Troy, NY 12181
ATTN: Ms. R. Reep

University of Wisconsin
Nuclear Engineering Dept.
1500 Johnson Drive
Madison, WI 53706
ATTN: UV Fusion Library

EXTERNAL MAILINGS

International

Professor M.H. Brennan
Willis Plasma Physics Dept.
School of Physics
University of Sydney
N.S.W. 2006, Australia

Division of Plasma Physics
Institute of Theoretical Physics
University of Innsbruck
A-6020 Innsbruck
Austria

c/o Physics Section
International Atomic Energy Agency
Wagramerstrasse 5
P.O. Box 100
A-1400 Vienna, Austria

Laboratoire de Physique des Plasmas
c/o H.W.H. Van Andel
Dept. de Physique
Universite de Montreal
C.P. 6128
Montreal, Que H3C 3J7
Canada

Plasma Physics Laboratory
Dept. of Physics
University of Saskatchewan
Saskatoon, Sask., Canada S7N OWO

The Library
Institute of Physics
Chinese Academy of Sciences
Beijing, China

Mrs. A. Wolff-Degives
Kernforschungsanlage Julich GmbH
Zentralbibliothek - Exchange Section
D-5170 Julich - Postfach 1913
Federal Republic of Germany

Preprint Library
Central Research Institute for Physics
H-1525 Budapest, P.O. Box 49
Hungary

Plasma Physics Dept.
Israel Atomic Energy Commission
Soreq Nuclear Research Center
Yavne 70600
Israel

The Librarian (Miss DePalo)
Associazione EURATOM - CNEN Fusione
C.P. 65-00044 Frascati (Rome)
Italy

Librarian
Research Information Center
Institute of Plasma Physics
Nagoya University
Nagoya, 464
Japan

Dr. A.J. Hazen
South African Atomic Energy Board
Private Bag X256
Pretoria 0001
South Africa